Engineering Journal

American Institute of Steel Construction

Second Quarter 2008 Volume 45, No. 2

97 Bending Strength of Steel Bracket and Splice Plates
M. Murray

107 Reduced Beam Section Spring Constants
bers and Tony C. Bartley

117 A Modified Equation for Expected Maximum Shear Strength of the Special Segment for Design of Special Truss Moment Frames
oel

127 Performance-Based Plastic Design of Special Truss Moment Frames
oel

151 Current Steel Structures Research

157 Suggested Reading from Other Publishers

www.aisc.org

ENGINEERING JOURNAL

AMERICAN INSTITUTE OF STEEL CONSTRUCTION

Dedicated to the development and improvement of steel construction, through the interchange of ideas, experiences and data.

Editorial Staff

Editor: Cynthia J. Duncan
Associate Editor: Bo Dowswell
Research Editor: Reidar Bjorhovde
Production Editor: Areti Carter

Officers

Rex I. Lewis, *Chairman*
Puma Steel, Cheyenne, WY

David Harwell, *Vice Chairman*
Central Texas Iron Works, Inc., Waco, TX

Stephen E. Porter, *Treasurer*
Indiana Steel Fabricating, Inc., Indianapolis, IN

Roger E. Ferch, *President*
American Institute of Steel Construction, Chicago

David B. Ratterman, *Secretary & General Counsel*
American Institute of Steel Construction, Chicago

John P. Cross, *Vice President*
AISC Marketing, LLC., Chicago

Charles J. Carter, *Vice President and Chief Structural Engineer*
American Institute of Steel Construction, Chicago

Scott L. Melnick, *Vice President*
American Institute of Steel Construction, Chicago

The articles contained herein are not intended to represent official attitudes, recommendations or policies of the Institute. The Institute is not responsible for any statements made or opinions expressed by contributors to this Journal.

The opinions of the authors herein do not represent an official position of the Institute, and in every case the officially adopted publications of the Institute will control and supersede any suggestions or modifications contained in any articles herein.

The information presented herein is based on recognized engineering principles and is for general information only. While it is believed to be accurate, this information should not be applied to any specific application without competent professional examination and verification by a licensed professional engineer. Anyone making use of this information assumes all liability arising from such use.

Manuscripts are welcomed, but publication cannot be guaranteed. All manuscripts should be submitted in duplicate. Authors do not receive a remuneration. A "Guide for Authors" is printed on the inside back cover.

ENGINEERING JOURNAL (ISSN 0013-8029) is published quarterly. Subscriptions: Members: one subscription, $20 per year, included in dues; Additional Member Subscriptions: $15 per year. Non-Members U.S., Canada, and Mexico: $40 per year, $110 for three years, single copy $15. International Members and Non-Members: $90 per year; $250 for three years; single copy $25. Published by the American Institute of Steel Construction at One East Wacker Drive, Suite 700, Chicago, IL 60601.

Periodicals postage paid at Chicago, IL and additional mailing offices. **Postmaster:** Send address changes to ENGINEERING JOURNAL in care of the American Institute of Steel Construction, One East Wacker Drive, Suite 700, Chicago, IL 60601.

Copyright 2008 by the American Institute of Steel Construction. All rights reserved. No part of this publication may be reproduced without written permission.

Subscribe to *Engineering Journal* by visiting our web site **www.aisc.org** or by calling 312.670.5444.

Copies of current and past *Engineering Journal* articles are available free to members online at **www.aisc.org/epubs.**

Non-members may purchase *Engineering Journal* article downloads at the AISC Bookstore at **www.aisc.org/bookstore** for $10 each. Starting with the First Quarter 2008, complete issue downloads of *Engineering Journal* are available for $15 each at **www.aisc.org/bookstore.**

An archival CD-ROM of past issues of *Engineering Journal* is available by calling 800.644.2400.

Bending Strength of Steel Bracket and Splice Plates

BENJAMIN A. MOHR and THOMAS M. MURRAY

Bracket plates typically support spandrel beams, or crane rails for industrial applications as shown in Figure 1. Often, these plates are bolted to the column flanges. A similar connection is the bolted web splice connection shown in Figure 2, which is typically used in cantilever construction to control the location of inflection points and reduce the required moment strength of the beams. The primary purpose of this study was to determine the ultimate behavior of bracket and splice plates and to compare the results with various design models.

CURRENT DESIGN MODELS

The required flexural strength, M_r, for the bracket plate shown in Figure 1 is simply the required vertical load, P_r, times the distance from its point of application to the first column of bolts, e. Likewise, the commonly assumed required flexural strength of the web splice plate shown in Figure 2 is the required beam shear, V_r, times the distance from the centerline of the connection to the first column of bolts, e. The required flexural strength must be less than the design strength ϕM_n in LRFD and M_n/Ω in ASD, according to the AISC *Specification for Structural Steel Buildings* (AISC, 2005a), where M_n is the nominal flexural strength, ϕ is the LRFD resistance factor, and Ω is the ASD safety factor.

The 3rd Edition of the AISC *Manual of Steel Construction, Load and Resistance Factor Design* (AISC, 2001), gives two limit states: flexural yielding and flexural rupture, in the design example on pages 15–13. The nominal flexural strength for yielding is determined from

$$M_n = F_y S_{gross} \tag{1}$$

where F_y is the specified minimum yield stress, and S_{gross} is the gross elastic section modulus of the plate. The nominal flexural strength for rupture is given by

$$M_n = F_u S_{net} \tag{2}$$

where

F_u = specified minimum tensile strength
S_{net} = net elastic section modulus of the plate

However, no literature is cited to support these relationships, nor has any been found by the writers. Conceptually, the behavior assumed by Equation 2 should never occur, since S_{net} assumes an elastic stress distribution, whereas F_u only occurs after plastic behavior.

The 13th Edition of the AISC *Steel Construction Manual* (AISC, 2005b) also uses two limit states to check flexural strength. The nominal flexural yielding strength is determined from

$$M_n = F_y Z_{gross} \tag{3}$$

where

Z_{gross} = gross plastic section modulus

However, the design examples for bracket plates and coped beams use $F_y S_{gross}$ for this limit state (AISC, 2005c).

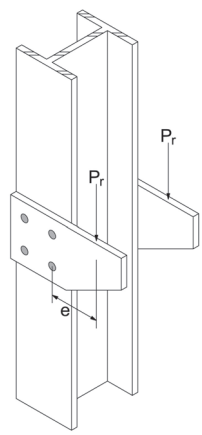

Fig. 1. Bracket plate connection.

Benjamin A. Mohr is a graduate assistant, Via Department of Civil and Environmental Engineering, Virginia Polytechnic Institute and State University, Blacksburg, VA.

Thomas M. Murray is Montague-Betts Professor of Structural Steel Design, Via Department of Civil and Environmental Engineering, Virginia Polytechnic Institute and State University, Blacksburg, VA.

The nominal flexural rupture strength is determined from

$$M_n = F_u Z_{net} \quad (4)$$

where

Z_{net} = net plastic section modulus

In an example for the design of a bolted beam web splice in *Analysis and Design of Connections* (Thornton and Kane, 1999), Equation 2 was used to determine the plate flexural rupture strength and Equation 3 was used for flexural yielding.

OVERVIEW OF STUDY

This study consisted of experimental testing and comparison of test results with various design methods. The experimental testing consisted of connecting two beams together with web splice plates to form a simple span, then loading the span symmetrically to induce pure moment at the location of the splice with the goal of achieving plate flexural rupture. The test setup is shown in Figure 3. The test results were compared to the predicted values from Equations 1 through 4, as well as a proposed design model.

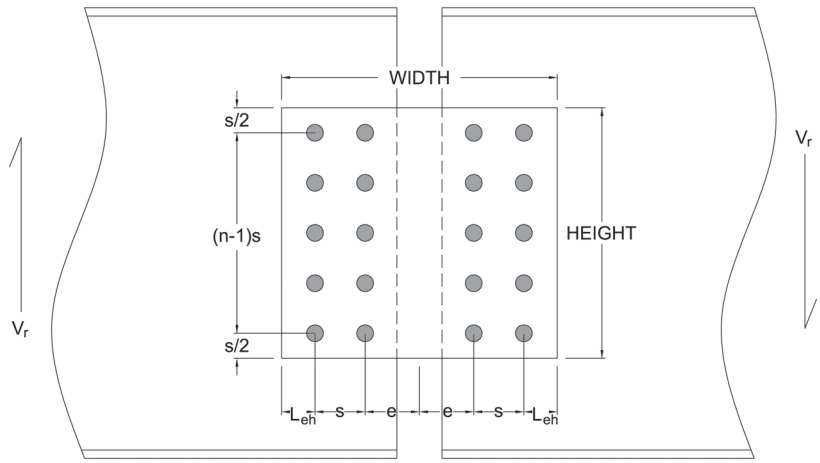

Fig. 2. Schematic representation of web splice plate.

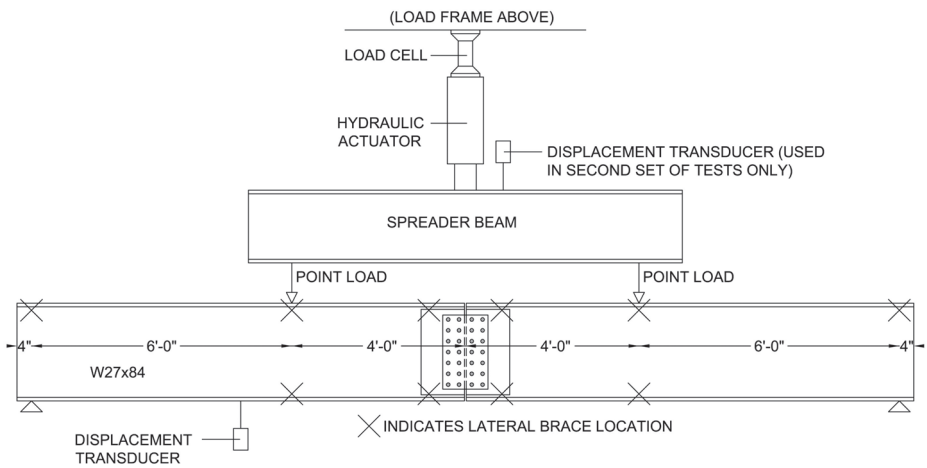

Fig. 3. Schematic diagram of test setup.

EXPERIMENTAL INVESTIGATION

Two series of splice plate tests were conducted. The first series consisted of six tests using three different bolt patterns with ⅜-in. plates and ¾-in.-diameter grade A490 bolts. The second series consisted of eight tests using both ⅜-in. and ⅝-in. plates and 1-in.-diameter grade A490 bolts. (Grade A490 bolts were used to eliminate the limit state of bolt shear.) For all tests, a plate was bolted to each side of the beam web.

The test setup (Figure 3) is not typical of standard construction. The large gap between the beams was required to accommodate the large deflections that occur prior to development of the plastic moment for the plates. If a smaller gap had been used, the top flanges of the beams would touch prior to plate rupture. Because of this large gap, the test setup experienced problems with stability, which are discussed below.

The test plates were checked for lateral-torsional buckling in accordance with the 2005 AISC Specification, Section F11.2 (AISC, 2005a). Using an unbraced length of 6.5 in. (the center-to-center distance between the innermost rows of bolts), lateral-torsional buckling was found not to be a controlling limit state for these tests.

Test Setup, Instrumentation and Procedures

The test setup consisted of two W27×84, A992 steel, beams, spliced together to form a simply supported 20-ft. span as shown in Figure 3. Two-point loading was used to create pure moment at midspan, and the connections were designed to ensure that the governing limit state would be flexural rupture of the plates.

The connection bolts were tightened with an impact wrench, except for two tests, where the bolts were snug-tightened using a spud wrench. No bolts were fully tightened.

Ten lateral braces were used, at the locations shown in Figure 3. Despite the braces, some out-of-plane movement of the beam compression flanges was observed at midspan during initial testing. To eliminate this movement, a channel, which fit tightly over the top flanges of both beams, was used to prevent the beams from rotating relative to each other. Also, during initial testing, lateral movement of the connection plates occurred. After some trial and error, an additional hole was punched at the centerline of the plate in line with the top row of bolts as shown in Figure 4. A bolt was passed through this hole, with washers inserted between the plates. The washers effectively prevented the plates from moving inward, and a snug-tight nut on the end of the bolt prevented outward movement.

Vertical deflections were measured for all tests using displacement transducers at the locations shown in Figure 3.

Test Specimens

Figure 4 shows the layout and dimensions for the splice plates. Each plate had either 3, 5 or 7 bolt rows, with all bolts spaced 3 in. on center. All vertical edge distances were 1½ in., and all horizontal edge distances were 2 in. The beam webs were punched for the seven row tests, and all plates were aligned with the beam centerline.

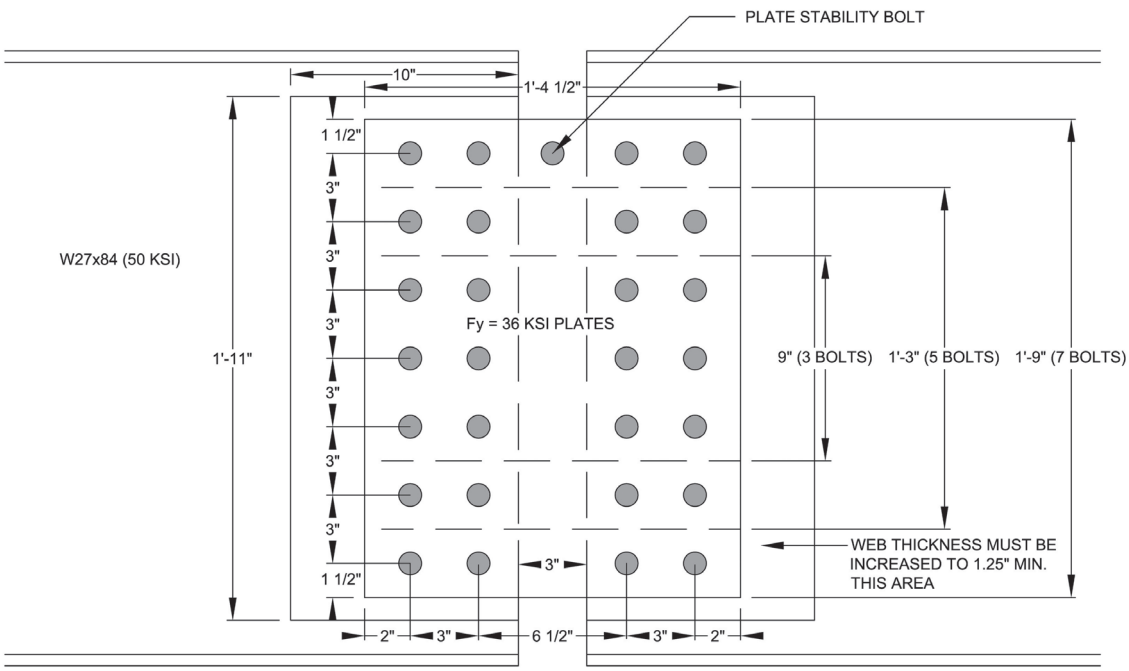

Fig. 4. Splice plate geometry.

Table 1. Measured Splice Plate Material Properties			
Heat	**F_y (ksi)**	**F_u (ksi)**	**Elongation**
1	49.5	72.1	N/A
2	48.4	63.7	47%
3	71.8	88.1	N/A

Table 2. Specimen Matrix

	Test No.	Bolt Rows (A90 Bolts)	Bolt Diameter (in.)	Measured Plate Thickness (in.)	Height (in.)	Width (in.)	Tightening Method
Heat 1	3-3/4-H1-3/8-A	3	¾	0.370	9	16.5	Impact Wrench
	3-3/4-H1-3/8-B	3	¾	0.370	9	16.5	Spud Wrench
	5-3/4-H1-3/8-A	5	¾	0.370	15	16.5	Impact Wrench
	5-3/4-H1-3/8-B	5	¾	0.370	15	16.5	Impact Wrench
	7-3/4-H1-3/8-A	7	¾	0.370	21	16.5	Impact Wrench
	7-3/4-H1-3/8-B	7	¾	0.370	21	16.5	Impact Wrench
Heat 2	3-1-H2-5/8-A	3	1	0.620	9	16.5	Impact Wrench
	3-1-H2-5/8-B	3	1	0.620	9	16.5	Impact Wrench
	3-1-H2-5/8-C	3	1	0.620	9	16.5	Impact Wrench
	5-1-H2-5/8-A	5	1	0.620	15	16.5	Impact Wrench
	5-1-H2-5/8-B	5	1	0.620	15	16.5	Impact Wrench
	5-1-H2-5/8-C	5	1	0.620	15	16.5	Impact Wrench
Heat 3	5-1-H3-3/8-A	5	1	0.381	15	16.5	Spud Wrench
	5-1-H3-3/8-B	5	1	0.381	15	16.5	Impact Wrench

Steel from three heats was used for the specimens. The first heat was a sheet of A36 steel, ⅜ in. × 18 in. × 20 ft. The second heat was also A36 steel, ⅝ in. × 18 in. × 20 ft. These are referred to as Heats 1 and 2, respectively. All plates fabricated from this material were cut with a standard steel bandsaw and all holes were punched using laboratory equipment. The plates from the third heat consisted of ⅜-in. fabricated plates with 13⁄16-in. punched holes and were provided by the sponsor. It was found through tensile testing that these plates had a very high strength, and therefore, bolt shear would be the governing limit state if ¾-in.-diameter bolts were used. Therefore, 1 1⁄16-in.-diameter holes were drilled to accommodate 1-in. A490 bolts, eliminating bolt shear as the controlling limit state. This material is referred to as Heat 3. Table 1 is a summary of tensile coupon test results for the steel from the three heats.

Connection geometry, measured splice plate thickness, and method of tightening are shown in Table 2. The tests are organized by heat number, then by number of bolts and are designated by number of bolts, bolt size, heat number, and nominal plate thickness. For instance, Test 3-3/4-H1-3/8-A has three bolt rows, ¾-in.-diameter bolts, and steel from Heat 1 of ⅜-in. thickness. The A at the end signifies that this is the first test of this type.

Test Results

Table 3 is a summary of the test results. The failure mode for all tests was either flexural rupture of the splice plate or when the mid-span beam deflection reached the limit of the test setup, approximately 8 in. The tests with ⅜-in. plates from Heat 1 all failed by flexural rupture. The tests with ⅝-in. plate from Heat 2 were stopped due to excessive deflection prior to flexure rupture, except for Tests 5-1-H2-5/8-A and 5-1-H2-5/8-C, which failed by flexural rupture. Tests 5-1-H3-3/8-A and 5-1-H3-3/8-B were conducted with higher yield stress material, Heat 3. Test 5-1-H3-3/8-A was stopped due to excessive deflection, and Test 5-1-H3-3/8-B

Table 3. Test Results					
	Test No.	No. of Bolt Rows	Observed First Yield Moment M_{ye} (kip-ft)	Maximum Applied Moment M_{ue} (kip-ft)	Failure Mode
Heat 1	3-3/4-H1-3/8-A	3	23	34.2	Flexural Rupture
	3-3/4-H1-3/8-B	3	22	31.5	Flexural Rupture
	5-3/4-H1-3/8-A	5	67	91.7	Flexural Rupture
	5-3/4-H1-3/8-B	5	70	88.8	Flexural Rupture
	7-3/4-H1-3/8-A	7	118	167.1	Flexural Rupture
	7-3/4-H1-3/8-B	7	122	175.4	Flexural Rupture
Heat 2	3-1-H2-5/8-A	3	39	48.3	Excessive Deflection
	3-1-H2-5/8-B	3	37	53.6	Excessive Deflection
	3-1-H2-5/8-C	3	35	51.5	Excessive Deflection
	5-1-H2-5/8-A	5	106	169.5	Flexural Rupture
	5-1-H2-5/8-B	5	107	134.4	Excessive Deflection
	5-1-H2-5/8-C	5	100	152.1	Flexural Rupture
Heat 3	5-1-H3-3/8-A	5	70	107.3	Excessive Deflection
	5-1-H3-3/8-B	5	84	117.8	Flexural Rupture

Table 4. Comparison of Test Data with Predicted First Yield Moment Values						
	Test No.	First Yield Moment M_{ye} (kip-ft)	F_y (ksi)	S_{gross} (in.^{3})	F_yS_{gross} (kip-ft)	$\frac{F_yS_{gross}}{M_{ye}}$
Heat 1	3-3/4-H1-3/8-A	23	49.5	5.00	20.6	0.89
	3-3/4-H1-3/8-B	22	49.5	5.00	20.6	0.93
	5-3/4-H1-3/8-A	67	49.5	13.88	57.3	0.85
	5-3/4-H1-3/8-B	70	49.5	13.88	57.3	0.82
	7-3/4-H1-3/8-A	118	49.5	27.20	112	0.95
	7-3/4-H1-3/8-B	122	49.5	27.20	112	0.92
Heat 2	3-1-H2-5/8-A	39	48.4	8.37	33.8	0.86
	3-1-H2-5/8-B	37	48.4	8.37	33.8	0.91
	3-1-H2-5/8-C	35	48.4	8.37	33.8	0.96
	5-1-H2-5/8-A	106	48.4	23.25	93.8	0.88
	5-1-H2-5/8-B	107	48.4	23.25	93.8	0.88
	5-1-H2-5/8-C	100	48.4	23.25	93.8	0.93
Heat 3	5-1-H3-3/8-A	70	71.8	14.29	85.5	1.22
	5-1-H3-3/8-B	84	71.8	14.29	85.5	1.02

failed by flexural rupture. Photographs of tested plates are shown in Figure 5.

Two representative moment at the bolt line vs. vertical deflection plots are shown in Figure 6. Test 3-3/4-H1-3/8-A failed by flexural rupture and Test 3-1-H2-5/8-A was stopped because of excessive deflection. The nonlinear response up to approximately 10 kip-ft is attributed to movement at the bolt holes since the bolts were only snug tight. The experimental yield point is defined as the intersection of the elastic and strain hardening slopes of the curves, as shown in Figure 6. Also shown in the figure are the predicted plate yield moments for each test, F_yS_{gross}, using measured material properties.

Table 4 compares the experimental first yield moments, M_{ye}, to the predicted first yield moments determined using measured plate properties for all tests. All moments shown are per splice plate. A value of the ratio of the experimental first yield moment-to-predicted first yield moment less than 1.0 indicates that the prediction is conservative. Overall, the test results show good agreement with the predicted first yield moment, F_yS_{gross}. The results are somewhat conservative for Heats 1 and 2 (mean ratio = 0.90). For Heat 3, the experimental yield moment of Test 5-1-H3-3/8-A is 122% of the predicted first yield moment. However, the same plate material was used in Test 5-1-H3-3/8-B and the ratio is 1.02. Excluding Test 5-1-H3-3/8-A, the mean ratio for the remaining 13 tests is 0.91 or approximately 9% conservative.

COMPARISON OF EXPERIMENTAL MOMENT WITH CURRENT DESIGN MODELS

Comparisons of predicted moments, F_uS_{net}, F_yZ_{gross}, and F_uZ_{net}, from current design models with the maximum applied experimental moment, M_{ue}, are shown in Table 5. All moments are per plate, and all predicated moments were determined using measured material properties.

The net elastic section modulus, S_{net}, was determined from:

$$S_{net} = \frac{t}{6}\left[d^2 - \frac{s^2 n\left(n^2-1\right)\left(d_h'\right)}{d}\right] \quad (5)$$

where

d = depth of the plate
s = bolt spacing
n = number of bolts in one vertical row
d_h' = effective diameter of the bolt hole

The vertical edge distances are assumed to be $s/2$, and the vertical dimension of the plate is then $d = ns$. Because standard size holes were used, d_h' was taken as the bolt diameter plus ⅛ in. The gross plastic section modulus, Z_{gross}, was calculated using:

$$Z_{gross} = \frac{td^2}{4} \quad (6)$$

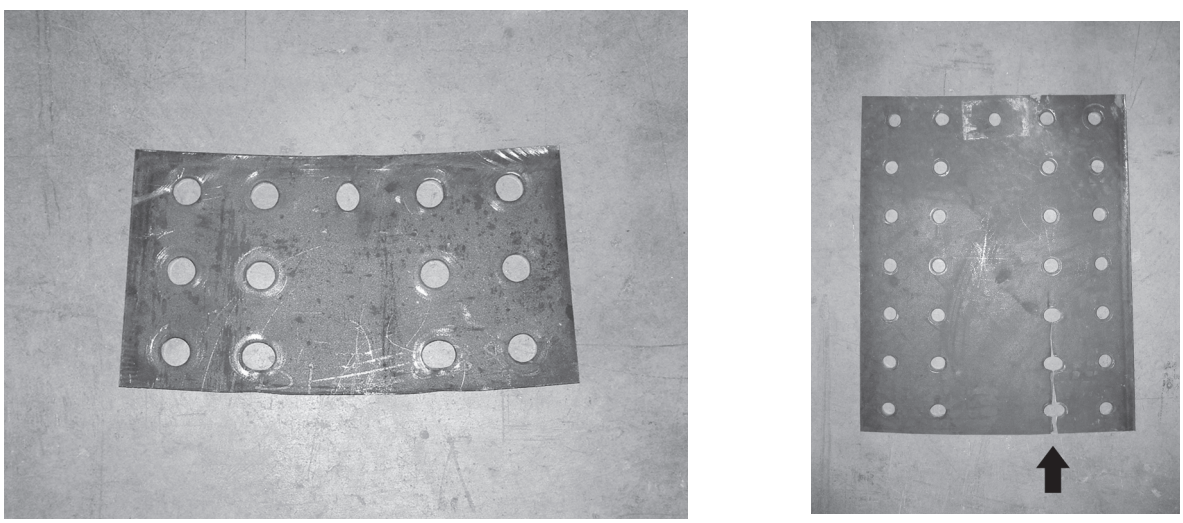

(a) (b)

Fig. 5. Photographs of tested plates.

The net plastic section modulus, Z_{net}, for an odd number of bolt rows is

$$Z_{net} = \frac{1}{4}t\left(s - d_h'\right)\left(n^2 s + d_h'\right) \quad (7)$$

and, for an even number of bolt rows

$$Z_{net} = \frac{1}{4}t\left(s - d_h'\right)n^2 s \quad (8)$$

For both equations, the vertical edge distances are assumed to be $s/2$ with a plate depth of ns.

Also shown in Table 5 are the ratios of the predicted moments (F_uS_{net}, F_yZ_{gross}, and F_uZ_{net}) to the maximum experimental moments using measured plate properties. The predicted strength using F_uS_{net} gives very conservative results with significant scatter.

For Heat 1, the predicted strengths, F_yZ_{gross} and F_uZ_{net}, are within 5% of each other. The minimum predicted strength for all six Heat 1 tests is F_yZ_{gross}; however, the experimental failure mode for all tests was flexural rupture. The mean value of the minimum predicted strength-to-maximum experimental moment ratios, F_yZ_{gross}/M_{ue}, is 0.96, or approximately 4% conservative.

For Heat 2, the predicted limit state strengths are flexural rupture for all six tests. Four of the six tests were terminated before flexural rupture because of excessive deflection; continued loading may have caused rupture. The mean value of the minimum predicted strength-to-maximum experiment moment ratios, F_uZ_{net}/M_{ue}, is 0.83, or approximately 17% conservative.

The predicted strengths for the two Heat 3 tests are flexural rupture. One test was terminated because of excessive deflection and the other failed by flexural rupture. The mean value of the minimum predicted strength-to-maximum experimental moment ratios, F_uZ_{net}/M_{ue}, is 0.89, or approximately 11% conservative.

The mean value of the predicted controlling limit state moment to the maximum experimental moment ratios for all 14 tests is 0.89 with no value exceeding 1.0, but with some scatter.

ALTERNATIVE NEW DESIGN MODEL

An alternative design model for flexural rupture is to assume that bolt holes in the compression region of the plate can be neglected when computing the net plastic section modulus (as is done, for instance, in columns), resulting in a modified section modulus, Z'_{net}. Thus,

$$M_n = F_uZ'_{net} \quad (9)$$

with

$$Z'_{net} = \sum |A_i d_i| \quad (10)$$

where

A_i = area of plate section i

d_i = distance from the center of section i to the plastic neutral axis, as explained in Figure 7

The plastic neutral axis is located by setting the area of the plate in compression equal to the area of the plate in tension.

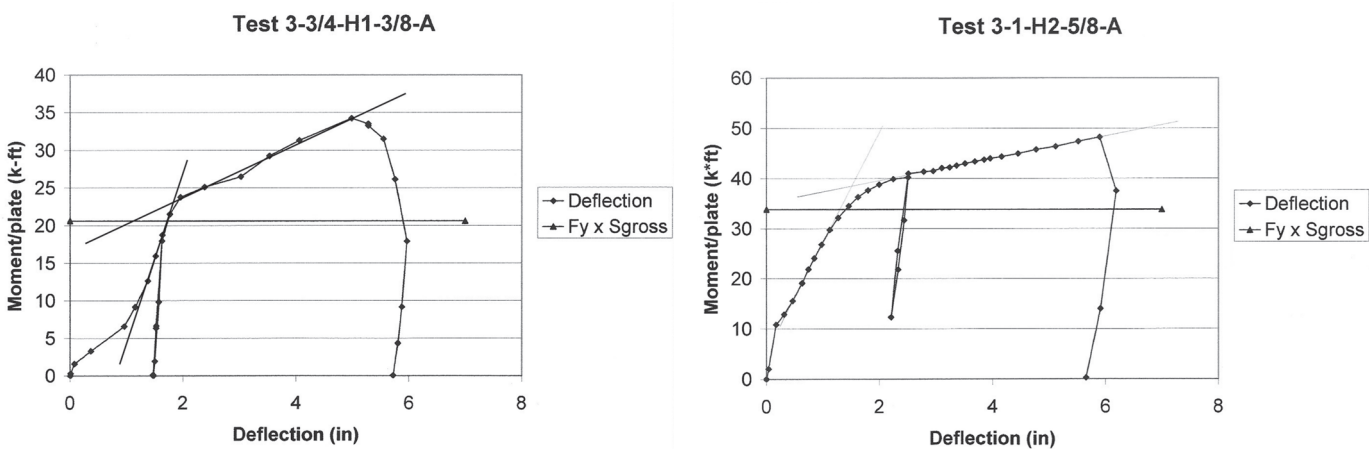

(a) (b)

Fig. 6. Representative moment vs. deflection plots.

Table 5. Comparison of Test Data with Existing Design Models												
	Test No.	M_{ue} (kip-ft)	F_y (ksi)	F_u (ksi)	S_{net} (in.^{3})	Z_{gross} (in.^{3})	Z_{net} (in.^{3})	Z'_{net} (in.^{3})	$\frac{F_uS_{net}}{M_{ue}}$	$\frac{F_yZ_{gross}}{M_{ue}}$	$\frac{F_uZ_{net}}{M_{ue}}$	$\frac{F_uZ'_{net}}{M_{ue}}$
Heat 1	3-3/4-H1-3/8-A	34.2	49.5	72.1	3.70	7.49	5.48	6.24	0.65	0.90	0.96	1.10
	3-3/4-H1-3/8-B	31.5	49.5	72.1	3.70	7.49	5.48	6.24	0.70	0.98	1.04	1.19
	5-3/4-H1-3/8-A	91.7	49.5	72.1	9.97	20.81	14.91	17.26	0.65	0.94	0.98	1.13
	5-3/4-H1-3/8-B	88.8	49.5	72.1	9.97	20.81	14.91	17.26	0.67	0.97	1.01	1.17
	7-3/4-H1-3/8-A	167.1	49.5	72.1	19.42	40.79	29.07	33.83	0.70	1.00	1.05	1.21
	7-3/4-H1-3/8-B	175.4	49.5	72.1	19.42	40.79	29.07	33.83	0.66	0.96	1.00	1.16
Heat 2	3-1-H2-5/8-A	48.3[1]	48.4	63.7	5.58	12.56	8.17	9.68	0.61	1.05	0.90	1.06
	3-1-H2-5/8-B	53.6[1]	48.4	63.7	5.58	12.56	8.17	9.68	0.55	0.95	0.89	0.96
	3-1-H2-5/8-C	51.5[1]	48.4	63.7	5.58	12.56	8.17	9.68	0.57	0.98	0.84	1.00
	5-1-H2-5/8-A	169.5	48.4	63.7	14.88	34.88	22.12	26.83	0.47	0.83	0.69	0.84
	5-1-H2-5/8-B	134.4[1]	48.4	63.7	14.88	34.88	22.12	26.83	0.59	1.05	0.87	1.06
	5-1-H2-5/8-C	152.1	48.4	63.7	14.88	34.88	22.12	26.83	0.52	0.93	0.77	0.94
Heat 3	5-1-H3-3/8-A	107.3[1]	71.8	88.1	9.14	21.43	13.60	16.49	0.63	1.19	0.93	1.13
	5-1-H3-3/8-B	117.8	71.8	88.1	9.14	21.43	13.60	16.49	0.57	1.09	0.85	1.03

[1]Test terminated due to excessive deflection.

The ratio of the predicted moment from Equation 9 using measured material properties to the maximum experimental moment for each test is given in Table 5. The ratios are larger (less conservative) than those using F_uZ_{net} for all 14 tests. For Heats 2 and 3, the ratios using the moment from Equation 9 are very near the ratios M_{ue}/F_yZ_{gross}. The mean ratio for the predicted controlling limit state (smaller of F_yZ_{gross} and $F_uZ'_{net}$) for the 14 tests is 0.98, with some values greater than 1.0.

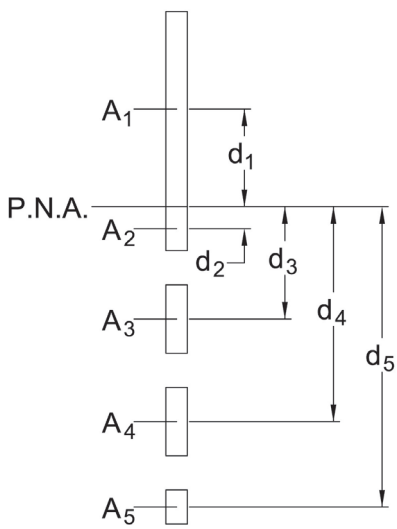

Fig. 7. Terms used in calculation of Z'_{net}.

OVERALL EVALUATION

From the results of the 14 tests, the minimum of the predicted moments F_yZ_{gross} and F_uZ_{net}, or F_yZ_{gross} and $F_uZ'_{net}$, matches the controlling experimental failure mode and generally provides an accurate prediction of the maximum experimental moment. However, the use of $F_uZ'_{net}$ resulted in unconservative predictions for all of the Heat 1 tests.

It is important to note that the maximum experimental moments were obtained only after very large deflections and that restraints were used to prevent compression flange movement at the connections as well as splice plate buckling as explained earlier.

A significant contribution to the deflection was movement of the bolts prior to application of load. When the erection supports were removed, the test setup frequently showed large initial deflections due to self-weight. This was especially evident in the plates with three rows of bolts and was caused by movement of the bolts within the standard-size holes. Initial stiffness was affected by the method used to tighten the bolts; impact wrench tightening resulted in a slightly stiffer connection. However, the maximum moment strengths were not affected.

Despite the precautions taken to prevent buckling, some local buckling was observed in the compression region of several plates. It is emphasized that to achieve the experimental moment strength in this study, it was necessary to use an additional bolt through the center of the plate in line with the top row of bolts as shown in Figure 4.

Table 6. Comparison of Available Moment Strengths F_yZ_{gross} and F_uZ_{net}					
No. of Bolts	Bolt Diameter (in.)	Nominal Moment Strength			
		F_y = 36 ksi	F_u = 58 ksi	F_y = 50 ksi	F_u = 65 ksi
		$0.9F_yZ_{gross}$ (kip-ft)	$0.75F_uZ_{net}$ (kip-ft)	$0.9F_yZ_{gross}$ (kip-ft)	$0.75F_uZ_{net}$ (kip-ft)
2	¾	24.3	23.1	33.8	25.9
	⅞	24.3	21.8	33.8	24.4
	1	24.3	20.4	33.8	22.9
3	¾	54.7	53.7	75.9	60.2
	⅞	54.7	50.8	75.9	56.9
	1	54.7	47.8	75.9	53.6
4	¾	97.2	92.4	135	103
	⅞	97.2	87.0	135	97.5
	1	97.2	81.6	135	91.4
5	¾	151	146	210	163
	⅞	151	137	210	154
	1	151	129	210	145
6	¾	218	208	303	233
	⅞	218	195	303	219
	1	218	183	303	205
7	¾	297	284	413	319
	⅞	297	268	413	300
	1	297	251	413	282
8	¾	388	369	540	414
	⅞	388	348	540	390
	1	388	326	540	365
9	¾	492	469	683	526
	⅞	492	442	683	495
	1	492	414	683	464
10	¾	607	577	843	647
	⅞	607	543	843	609
	1	607	509	843	571

COMPARISON OF NOMINAL MOMENT STRENGTHS

Table 6 shows available LFRD moment strengths using $0.9F_yZ_{gross}$ and $0.75F_uZ_{net}$ for connections with two to 10 bolts using nominal material properties, for A36 and A572 Grade 50 steels, s = 3 in., vertical edge distance $s/2$ = 1.5 in., plate thickness of 1 in., and bolt diameters of ¾, ⅞ and 1 in. The data show that for every connection, flexural rupture, F_uZ_{net}, is the controlling limit state. It is noted that these are relative values and actual connection strength may be governed by bolt shear or another limit state.

DESIGN RECOMMENDATIONS

This study indicates that design models used prior to the publication of the 13th Edition AISC *Steel Construction Manual* (AISC, 2005b) for determining bracket plate and web splice nominal moment strength are overly conservative. From the test results, the available moment strength in LRFD, ϕM_n, can safely be calculated as the minimum of $0.9F_yZ_{gross}$ and $0.75F_uZ_{net}$, or in ASD as the minimum of $F_yZ_{gross}/1.67$ and $F_uZ_{net}/2.0$, which are the current AISC Manual design models. Consequences of large deflections and supported member or plate instability must be considered when these values

are used. If deflection is a concern, the factored loads should also be checked against $0.9F_yS_{gross}$.

Lateral stability is extremely important to reach the maximum plastic moment; therefore, these results are not recommended for coped beams or unbraced bracket plates.

ACKNOWLEDGMENTS

Funding for this study was provided by Cives Steel Company. The contributions of William A. Thornton, Larry S. Muir, and Rob Kerr are greatly appreciated.

REFERENCES

AISC (2001), *Manual of Steel Construction, Load and Resistance Factor Design,* 3rd Edition, American Institute of Steel Construction, Chicago, IL.

AISC (2005a), *Specification for Structural Steel Buildings*, American Institute of Steel Construction, Chicago, IL, March 9.

AISC (2005b), *Steel Construction Manual*, 13th Edition, American Institute of Steel Construction, Chicago, IL.

AISC (2005c), *Design Examples V.13.0*, American Institute of Steel Construction, Chicago, IL.

Thornton, W.A. and Kane, T. (1999), *Handbook of Structural Steel Connection Design and Details*, McGraw-Hill Book Company, New York.

Reduced Beam Section Spring Constants

BART MORTENSEN, JANICE J. CHAMBERS
and TONY C. BARTLEY

A moment connection that includes a wide flange beam with trimmed flanges is commonly known as a reduced beam section (RBS) connection, and the beam of this connection is known as an RBS beam. RBS connections are widely used in steel buildings throughout the developed world, and those with radius cuts (Figure 1) have been designated a *prequalified* moment connection for special and intermediate moment frames by the American Institute of Steel Construction (AISC) and the American National Standards Institute (ANSI) (AISC, 2005). The key analytical components of a structure's stiffness are its elements' stiffness matrices. Hence, knowledge of the stiffness matrices for RBS beams is fundamental to the quantification of both the elastic and inelastic performance of structures that incorporate these nonprismatic beams. For example, a pushover analysis of a moment frame that includes RBS connections requires both the elastic stiffness matrices and plastic moment capacities of its RBS beams. The design procedures for RBS connections specified in AISC's *Prequalified Connections for Special and Intermediate Steel Moment Frames for Seismic Applications* (RBS Design Procedures) states, "in lieu of specific calculations, effective elastic drifts may be calculated by multiplying elastic drifts based on gross beam sections by 1.1 for flange reductions up to 50% of the beam flange width. Linear interpolation may be used for lesser values of beam width reduction" (AISC, 2005). Incorporation of the closed-form solution of RBS frame elements' stiffness matrices (RBS-CFS stiffness matrices) into structural analysis will give a more precise estimate of the elastic component of the drift of a frame that includes RBS connections than that recommended by the RBS Design Procedures. However, it may be difficult or impossible for some structural design firms to integrate RBS-CFS stiffness matrices into their structural analysis software. Methods to capture the effect of RBS cuts on the stiffness of beams by adjusting the moment of inertia of prismatic beams have been derived from approximate numerical integration applied to a limited sample of RBS beams (Grubbs, 1997; Dumonteil, 2006). Chambers, Almudhafar and Stenger (2003) were the first to present the closed-form solution of the stiffness matrix of an RBS beam. Recently Kim and Engelhardt (2007) extended the work of Chambers et al. (2003) to include transverse shear deformations in the RBS stiffness matrix and also offer a method to adjust the moment of inertia of prismatic beams to capture the affect of RBS cuts. The adjusted moment of inertia is referred to as an effective moment of inertia. No research has been published to date that offers a spring constant for semi-rigid connections, which can be easily implemented into commercial structural analysis software, to simulate the effect of RBS cuts on the stiffness of moment frames (Figure 2). This paper presents the derivation of the formula for the spring constants of an RBS beam using the RBS-CFS stiffness matrix derived by Chambers et al. (2003) and validates it. Further, from a study of the spring constants for a plethora of RBS beams, it was found that a strong linear relationship exists between the minimum plastic section modulus of RBS beams and their spring constants. Thus, this paper has direct applicability to the practical and accurate determination of the elastic drift of a moment frame with RBS connections.

Bart Mortensen is a structural engineer, Reaveley Engineers, Inc., Salt Lake City, UT.

Janice J. Chambers is associate professor, department of civil and environmental engineering, University of Utah, Salt Lake City, UT.

Tony C. Bartley is a graduate student, department of civil and environmental engineering, University of Utah, Salt Lake City, UT.

DERIVATION OF THE SPRING CONSTANTS OF AN RBS BEAM

The derivation of the RBS-CFS stiffness matrix is presented in detail in Chambers et al. (2003). The paper presents the following relationship between end moments, m_i and m_j, and rotations θ_i and θ_j

$$\begin{Bmatrix} m_i \\ m_j \end{Bmatrix} = \frac{EI_g}{u(s+t)} \begin{bmatrix} t & -s \\ -s & t \end{bmatrix} \begin{Bmatrix} \theta_i \\ \theta_j \end{Bmatrix} \quad (1)$$

where

E = modulus of elasticity of the material
I_g = gross moment of inertia of the cross section about the major axis

and

$$s = \frac{2a^3}{3L} - a^2 - \frac{g^3}{6L} + ga\left(\frac{a}{L} - 1\right) - \frac{gb}{L}\left(b + g\right) - \frac{1}{2Ln}\left\{2\gamma\left(R^2 - ef\right) + 4\Omega\left[ef + R^2\left(\frac{1}{\omega^2} - 1\right)\right] - \lambda\right\} \quad (2)$$

$$t = \frac{2a^3}{3L} + \frac{g^3}{3L} + \frac{ga}{L}\left(g + a\right) + \frac{gb}{L}\left(L - b\right) + a\left(L - a\right) + \frac{1}{4Ln}\left\{-2\gamma\left(2R^2 + e^2 + f^2\right) + 4\Omega\left[e^2 + f^2 + 2R^2\left(1 - \frac{1}{\omega^2}\right)\right] + 2\lambda\right\} \quad (3)$$

$$u = a + \frac{g}{2} + \frac{1}{n}\left(\Omega - \frac{\gamma}{2}\right) \quad (4)$$

where

a = distance from the end of the beam to the start of the radius cut as shown in Figure 1

b = length of the radius cut along the length of the beam as shown in Figure 1

b_f = beam flange width

c = depth of the radius cut normal to the beam length as shown in Figure 1

d = beam depth

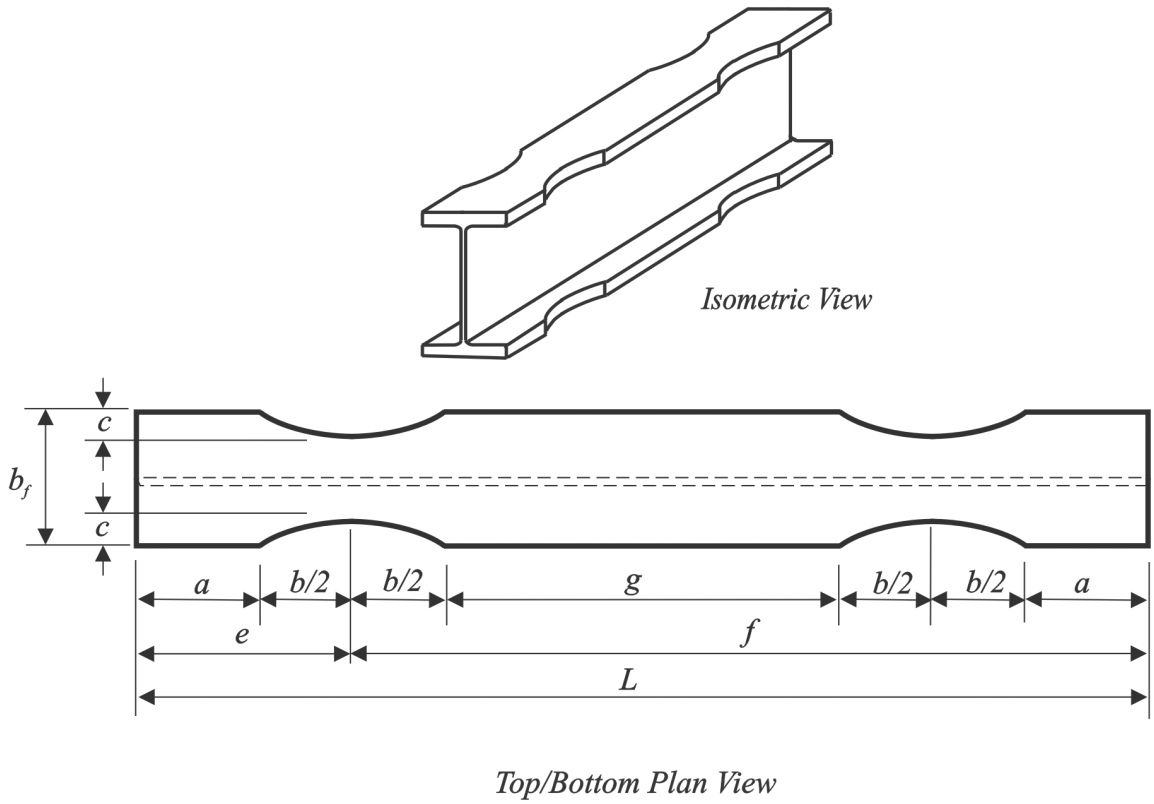

Fig. 1. RBS beam.

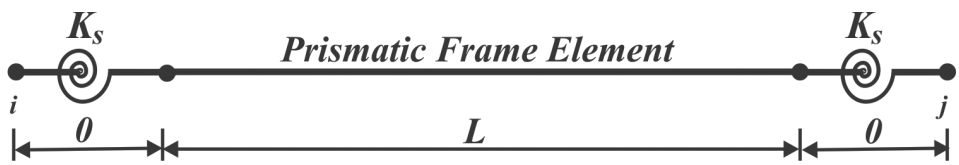

Fig. 2. Model of frame element with springs at its ends.

e = distance from the near end of the beam to the center of the radius cut as shown in Figure 1

f = distance from the far end of the beam to the center of the radius cut as shown in Figure 1

g = distance between the radius cuts at each end of the beam as shown in Figure 1

L = beam length

t_f = beam flange thickness

$$n = \frac{1}{I_g}\left[\frac{t_f^{\,3}}{12} + \left(\frac{d-t_f}{2}\right)^2 t_f\right]$$

$$R = \frac{c^2 + \frac{b^2}{4}}{2c}$$

$$\beta = 1 - 4n\left(c - R\right)$$

$$\gamma = \sin^{-1}\left($$

$$\lambda = R^2\left[\gamma + \frac{1}{2}\sin\left(2\gamma\right) + \frac{2}{\omega}\left(\sin\gamma + \frac{\gamma}{\omega}\right)\right]$$

$$\mu = 4Rn$$

$$\Omega = \frac{\tan^{-1}\left[\sqrt{\frac{1+\omega}{1-\omega}}\tan\left(\frac{\gamma}{2}\right)\right]}{\sqrt{1-\omega^2}}$$

$$\omega = \frac{\mu}{\beta}$$

Equation 1 may be abbreviated as

$$\begin{Bmatrix} m_i \\ m_j \end{Bmatrix} = \begin{bmatrix} S_{ii} & S_{ij} \\ S_{ij} & S_{ii} \end{bmatrix} \begin{Bmatrix} \theta_i \\ \theta_j \end{Bmatrix} \tag{5}$$

where

$$S_{ii} = EI_g\left[\frac{t}{u\left(s+t\right)}\right]$$

$$S_{ij} = EI_g\left[\frac{-s}{u\left(s+t\right)}\right]$$

Solving Equation 5 for the rotations

$$\begin{Bmatrix} \theta_i \\ \theta_j \end{Bmatrix} = \frac{1}{S_{ii}^{\,2} - S_{ij}^{\,2}} \begin{bmatrix} S_{ii} & -S_{ij} \\ -S_{ij} & S_{ii} \end{bmatrix} \begin{Bmatrix} m_i \\ m_j \end{Bmatrix} \tag{6}$$

Now, consider the relationship between Euler-Bernoulli beam end moments and rotations

$$\begin{Bmatrix} m_i \\ m_j \end{Bmatrix} = \begin{bmatrix} \frac{4EI_g}{L} & \frac{2EI_g}{L} \\ \frac{2EI_g}{L} & \frac{4EI_g}{L} \end{bmatrix} \begin{Bmatrix} \theta_i \\ \theta_j \end{Bmatrix} \tag{7}$$

Solving Equation 7 for the rotations

$$\begin{Bmatrix} \theta_i \\ \theta_j \end{Bmatrix} = \begin{bmatrix} \frac{L}{3EI_g} & -\frac{L}{6EI_g} \\ -\frac{L}{6EI_g} & \frac{L}{3EI_g} \end{bmatrix} \begin{Bmatrix} m_i \\ m_j \end{Bmatrix} \tag{8}$$

Referring to Figure 2, Equation 8 may be adjusted for an RBS beam by adding the flexibility of the rotational springs, $1/K_s$, at each end of the beam

$$\begin{Bmatrix} \theta_i \\ \theta_j \end{Bmatrix} = \begin{bmatrix} \frac{L}{3EI_g} + \frac{1}{K_s} & -\frac{L}{6EI_g} \\ -\frac{L}{6EI_g} & \frac{L}{3EI_g} + \frac{1}{K_s} \end{bmatrix} \begin{Bmatrix} m_i \\ m_j \end{Bmatrix} \tag{9}$$

Considering only the rotational stiffness of the joints, the value of the rotational spring constant for an RBS frame element can be found by equating the diagonal terms of Equations 6 and 9

$$\frac{L}{3EI_g} + \frac{1}{K_s} = \frac{S_{ii}}{S_{ii}^{\,2} - S_{ij}^{\,2}} \tag{10}$$

Thus, the spring constant for an RBS connection is

$$K_s = \frac{3EI_g\left(S_{ii}^{\,2} - S_{ij}^{\,2}\right)}{3EI_g S_{ii} - L\left(S_{ii}^{\,2} - S_{ij}^{\,2}\right)} \tag{11}$$

SPRING CONSTANT VALIDATION

The design process for seismic moment frames usually begins with a target elastic story drift coefficient of approximately 0.25% and the base seismic shear (ASCE, 2005). The frame used to validate Equation 11, "the validation frame" is shown in Figure 3. The stiffness method was used to analyze the structure without flange reductions. The shear deformations and P-Delta effects were neglected. Thus, Euler-Bernoulli frame stiffness matrices were employed. The cross-sectional properties of the members that were used in

the analysis are shown in Table 1. The modulus of elasticity was equal to 29,000 ksi. Due to axial deformations of the beams, the lateral displacement at the top of each column in a story of the validation frame was slightly different, and the average of these displacements was used to determine the story drift. The maximum story drift coefficient obtained from the frame analysis described earlier was 0.20%. The frame was then analyzed using RBS-CFS stiffness matrices for all the beams with $a = 0.5b_f$, $b = 0.85d$, and $c = 0.2b_f$, which are within the limits specified by the RBS Design Procedures. The frame was also analyzed using Euler-Bernoulli prismatic frame element stiffness matrices and rotational springs at each end of the frame elements (RBS-EBWS stiffness matrices). The moment-rotation spring constants of the springs were calculated from Equation 11 and are presented in Table 2. [The reader may refer to equation 13.31 of *Matrix Structural Analysis* (McGuire, Gallagher and Ziemian, 2000) to obtain the formula for stiffness matrix of a beam with rotational springs on each end.] A comparison between the analytical results for the validation frame is presented in Table 3. As can be seen from the table, the story drift coefficients using RBS-EBWS stiffness matrices range from 0.9% to 1.5% larger than the story drift coefficients obtained using RBS-CFS stiffness matrices. Differences exist because the spring constants only account for the RBS cuts' influence on the M/θ stiffness of the frame [i.e., compare Equation 1 with Equation 24 of Chambers et al. (2003)]. Thus, for practical purposes, Equation 11 is a valid equation for the rotational spring constants of an RBS beam.

TRANSVERSE SHEAR DEFORMATIONS

Because an industry-acceptable formula for the shear area, A_s, of a wide flange beam is not a function of the flange area ($A_s = dt_w$), spring stiffnesses obtained from Equation 11 may be used with prismatic frame elements that account for transverse shear deformations (i.e., Timoshenko beams) to obtain greater accuracy in the drifts of frames with RBS connections than that which would be obtained using Euler-Bernoulli beams.

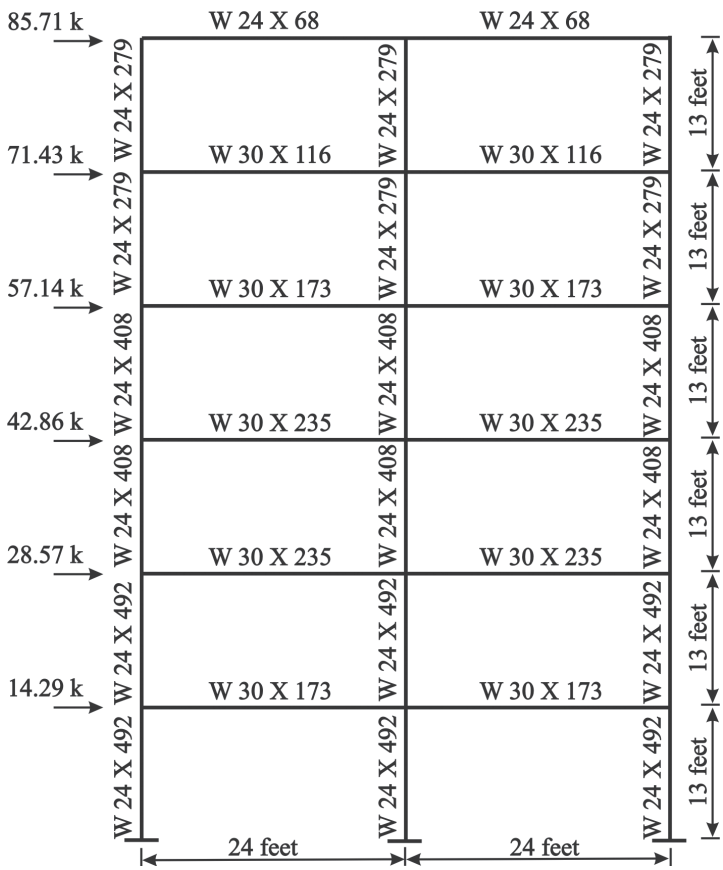

Fig. 3. Validation frame.

Table 1. Validation Frame Member Geometric Properties						
Section	d (in.)	b_f (in.)	t_f (in.)	t_w (in.)	A_g (in.^{2})	I_g (in.^{4})
W24×492	29.6	14.12	3.540	1.970	144.0	19100
W24×408	28.5	13.80	2.990	1.650	119.0	15100
W24×279	26.7	13.30	2.090	1.160	82.0	9600
W30×173	30.4	15.00	1.070	0.655	51.0	8230
W30×235	31.3	15.10	1.500	0.830	69.2	11700
W30×116	30.0	10.50	0.850	0.565	34.2	4930
W24×68	23.7	8.97	0.585	0.415	20.1	1830

Table 2. Validation Frame Beam Spring Constants for $a = 0.5b_f$, $b = 0.85d$, and $c = 0.2b_f$, (kip-in./rad)			
	S_{ii}	S_{ij}	K_s
W30×173	2996397.25	1426943.49	34025298.77
W30×235	4235845.34	2012390.79	45532313.05
W30×116	1812145.24	865520.46	23013555.73
W24×68	683142.46	328229.93	10610757.25

Table 3. Spring Constant Validation			
Story	% Drift		Relative Difference
	RBS Stiffness Matrix		
	CFS	EBWS	
1	0.12055	0.12168	0.94%
2	0.20625	0.20893	1.30%
3	0.21054	0.21367	1.49%
4	0.20481	0.20793	1.52%
5	0.21958	0.22242	1.29%
6	0.20566	0.20809	1.18%

RELATIONSHIP BETWEEN THE SPRING CONSTANT AND MINIMUM PLASTIC SECTION MODULUS OF RBS BEAMS

The minimum plastic section modulus of an RBS beam as defined in the RBS Design Procedures is

$$Z_e = Z_x - 2ct_f\left(d - t_f\right) \tag{12}$$

A strong linear relationship between K_s (Equation 11) and Z_e (Equation 12) was found from a study conducted on RBS beams. The wide flange shapes used for the study were obtained from the AISC Shapes Database v. 13.0. Only those RBS beams that satisfied criteria in the RBS Design Procedures were used. Beam lengths were limited to 25d. A plethora of data was generated—almost 200,000 springs (1,080 spring constant values for 177 wide flange shapes). Correlation coefficients squared (R^2) between K_s and Z_e for specific trim geometries (relative to the depth and flange width of the beam) and beam lengths (relative to the depth of the beam) were obtained for all the wide flange shapes used in the study. Figure 4 illustrates the exercises conducted. The maximum and minimum R^2 values were 0.9993 and 0.9966, respectively. Thus, in lieu of Equation 11, an excellent approximation for K_s may be found by multiplying Z_e by the slope of the best-fit line, m, for the given trim geometry and beam length

$$K_S = mZ_e \tag{13}$$

The values for m obtained from the study are presented in Table 4 (at the end of paper). Note that "% flange reduction" is equal to the total flange reduction, $2c/b_f$.

EXAMPLE

Consider a 30-ft **W**30×170 with $a = 0.7b_f$, $b = 0.75d$, and a 40% flange reduction. Pertinent geometric properties of a **W**30×170 are

$$d = 36.2 \text{ in.},\ b_f = 12.0 \text{ in.},\ t_f = 1.10 \text{ in.},$$
$$I_g = 10{,}500 \text{ in.}^4, \text{ and } Z_x = 668 \text{ in.}^3$$

Application of Equation 12

$$Z_e = 668 - \left(2\right)\left[\frac{\left(0.4\right)\left(12\right)}{2}\right]\left(1.10\right)\left(36.2 - 1.10\right) = 482.7 \text{ in.}^3$$

The length of the beam is 30(12)/36.2 = 9.945d. Linear interpolation within Table 4 gives

$$m = 90{,}932.9 \text{ kip/in.}^2\text{-rad}$$

Therefore, the spring constant for the beam is from Equation 13 approximately

$$K_S = mZ_e = \left(90{,}932.9\right)\left(482.7\right) = 43{,}893{,}214 \text{ kip-in./rad}$$

Equation 11 offers a more precise value of 45,449,330 kip-in./rad (3.5% larger than that value obtained using the table).

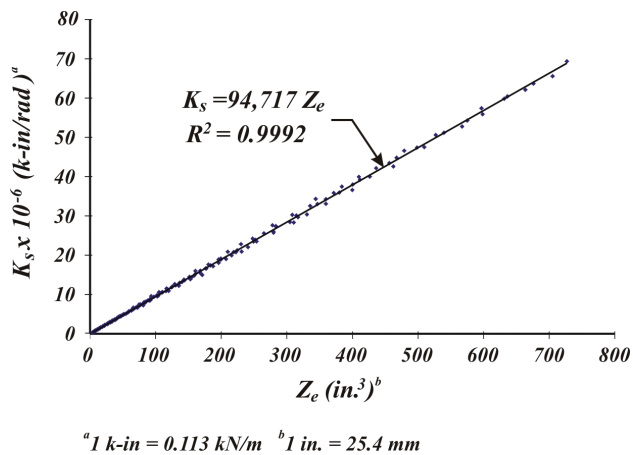

Fig. 4. Relationship between spring constants and minimum plastic section modulus of RBS beams (a = *0.75*b_f, b = *0.65*d, c = *0.25*b_f, L = *5*d).

CONCLUSION

Accurate analysis of frames incorporating RBS beams requires knowledge of the elastic stiffness matrix of RBS beams. This stiffness matrix is known. In lieu of using this stiffness matrix, an RBS beam can be modeled as an Euler-Bernoulli frame element with rotational springs at each end, which can be easily implemented in structural analysis software. The spring constants of these frame elements have been derived herein. The spring constants may also be added to prismatic frame elements that include transverse shear deformations for a more accurate analysis as shear deformations are predominantly a function of the web area. A strong linear relationship between the spring constants and the minimum plastic section modulus of RBS beams was found. Thus, to obtain a very accurate estimate of the rotational spring constant of an RBS beam, one may simply multiply the minimum plastic section modulus of an RBS beam by the coefficient provided in Table 4 of this paper.

REFERENCES

AISC (2005), *Prequalified Connections for Special and Intermediate Steel Moment Frames for Seismic Applications,* ANSI/AISC 358-05, American Institute of Steel Construction, Chicago, IL.

ASCE (2005), *Minimum Design Loads for Buildings and Other Structures,* ASCE/SEI 7-05, American Society of Civil Engineers, Reston, VA.

Chambers, J.J., Almudhafar, S. and Stenger, F. (2003), "Effect of Reduced Beam Section Frame Elements on Stiffness of Moment Frames," *Journal of Structural Engineering*, American Society of Civil Engineers, Vol. 129, No. 3, pp. 383–393.

Dumonteil, P. (2006), "In-Plane Properties and Modeling of Reduced Beam Sections," *Engineering Journal*, American Institute of Steel Construction, 2nd Quarter.

Grubbs, K.V. (1997), *The Effect of the Dogbone Connection on the Elastic Stiffness of Steel Moment Frames,* Master's Thesis, University of Texas, Austin, TX.

Kim, K.-D. and Engelhardt, M.D. (2007), "Nonprismatic Beam Elements for Beams with RBS Connections in Steel Moment Frames," *Journal of Structural Engineering*, American Society of Civil Engineers, Vol. 133, No. 2, pp. 176–184.

McGuire, W., Gallagher, R.H. and Ziemian, R.D. (2000), *Matrix Structural Analysis*, 2nd ed., John Wiley and Sons.

Table 4. Factors Relating the Minimum Plastic Section Modulus of RBS Beams to Their Rotational Spring Constants, *m* (kip/in.^{2}-rad)

			Beam Length								
		Flange Reduction	5*d*	7.5*d*	10*d*	12.5*d*	15*d*	17.5*d*	20*d*	22.5*d*	25*d*
$a = 0.5b_f$	$b = 0.65d$	20%	223231	207906	200517	196181	193334	191321	189823	188665	187743
		30%	149807	139537	134585	131680	129771	128423	127419	126643	126025
		40%	112944	105214	101488	99301	97865	96850	96095	95511	95046
		50%	90707	84512	81526	79774	78623	77810	77205	76737	76364
	$b = 0.70d$	20%	209359	194423	187223	183000	180227	178268	176811	175684	174788
		30%	140611	130591	125761	122929	121069	119755	118777	118022	117420
		40%	106128	98577	94938	92803	91402	90412	89675	89106	88652
		50%	85353	79292	76371	74657	73533	72738	72147	71690	71326
	$b = 0.75d$	20%	197320	182722	175684	171559	168851	166938	165515	164416	163541
		30%	132612	122810	118086	115316	113499	112215	111260	110522	109935
		40%	100182	92787	89223	87134	85763	84795	84074	83518	83075
		50%	80664	74720	71856	70177	69075	68296	67718	67270	66914
	$b = 0.80d$	20%	186774	172472	165576	161535	158883	157011	155619	154543	153687
		30%	125592	115983	111350	108636	106855	105597	104662	103940	103365
		40%	94951	87694	84197	82147	80802	79853	79147	78601	78167
		50%	76526	70686	67872	66223	65141	64377	63809	63370	63021
	$b = 0.85d$	20%	177461	163420	156649	152682	150080	148243	146877	145822	144983
		30%	119383	109945	105393	102727	100978	99744	98826	98117	97553
		40%	90315	83181	79741	77727	76406	75473	74780	74244	73818
		50%	72849	67102	64332	62710	61646	60894	60336	59905	59562
$a = 0.55b_f$	$b = 0.65d$	20%	225214	209162	201430	196897	193922	191820	190257	189048	188086
		30%	151133	140376	135195	132158	130165	128756	127709	126899	126255
		40%	113939	105844	101946	99660	98160	97100	96312	95703	95218
		50%	91500	85015	81892	80061	78859	78010	77378	76890	76501
	$b = 0.70d$	20%	211212	195596	188075	183668	180776	178734	177215	176041	175107
		30%	141851	131376	126331	123375	121436	120066	119047	118260	117634
		40%	107060	99166	95366	93139	91678	90645	89878	89285	88813
		50%	86097	79763	76713	74926	73753	72925	72309	71833	71454
	$b = 0.75d$	20%	199060	183822	176483	172184	169364	167374	165893	164750	163840
		30%	133776	123547	118621	115735	113843	112506	111513	110745	110135
		40%	101058	93341	89626	87449	86022	85014	84265	83686	83225
		50%	81365	75163	72178	70429	69282	68472	67870	67405	67035
	$b = 0.80d$	20%	188414	173509	166328	162124	159367	157421	155974	154857	153968
		30%	126690	116677	111854	109030	107179	105872	104900	104150	103553
		40%	95778	88217	84576	82444	81046	80059	79326	78760	78309
		50%	77189	71105	68176	66461	65336	64543	63953	63497	63134
	$b = 0.85d$	20%	179011	164401	157360	153238	150536	148630	147213	146118	145248
		30%	120423	110602	105870	103100	101284	100003	99051	98316	97731
		40%	91097	83676	80100	78008	76636	75668	74949	74393	73952
		50%	73477	67499	64620	62935	61830	61051	60472	60025	59669

Table 4 (cont'd.). Factors Relating the Minimum Plastic Section Modulus of RBS Beams to Their Rotational Spring Constants, *m* (kip/in.^{2}-rad)

			Beam Length								
		Flange Reduction	5*d*	7.5*d*	10*d*	12.5*d*	15*d*	17.5*d*	20*d*	22.5*d*	25*d*
$a = 0.6b_f$	$b = 0.65d$	20%	227209	210424	202347	197616	194512	192321	190691	189432	188430
		30%	152466	141220	135808	132639	130559	129091	127999	127156	126484
		40%	114939	106476	102405	100021	98456	97351	96530	95895	95390
		50%	92298	85520	82258	80348	79095	78210	77552	77044	76639
	$b = 0.70d$	20%	213076	196774	188930	184338	181326	179200	177619	176399	175427
		30%	143097	132164	126903	123824	121804	120378	119318	118499	117848
		40%	107996	99758	95796	93475	91954	90880	90081	89465	88974
		50%	86846	80236	77056	75195	73974	73112	72471	71977	71583
	$b = 0.75d$	20%	200808	184928	177285	172812	169880	167810	166272	165084	164139
		30%	134947	124287	119158	116156	114188	112799	111767	110969	110335
		40%	101938	93898	90029	87765	86281	85234	84455	83854	83376
		50%	82070	75609	72501	70682	69489	68648	68023	67540	67155
	$b = 0.80d$	20%	190061	174551	167084	162715	159851	157831	156330	155171	154249
		30%	127794	117375	112360	109426	107503	106147	105139	104360	103741
		40%	96608	88742	84956	82742	81290	80267	79506	78918	78451
		50%	77854	71526	68481	66699	65532	64709	64097	63624	63248
	$b = 0.85d$	20%	180569	165387	158074	153796	150994	149017	147549	146415	145514
		30%	121467	111262	106348	103474	101591	100263	99276	98514	97909
		40%	91884	84173	80461	78289	76867	75864	75119	74543	74086
		50%	74108	67898	64909	63161	62016	61208	60608	60145	59776
$a = 0.65b_f$	$b = 0.65d$	20%	229215	211692	203267	198337	195104	192823	191127	189817	188775
		30%	153807	142067	136423	133121	130955	129427	128290	127413	126715
		40%	115944	107112	102867	100382	98753	97603	96748	96088	95563
		50%	93101	86027	82627	80637	79332	78411	77726	77198	76777
	$b = 0.70d$	20%	214948	197958	189789	185010	181878	179668	178025	176757	175748
		30%	144350	132956	127478	124273	122173	120691	119590	118739	118063
		40%	108937	100353	96227	93813	92231	91115	90285	89645	89135
		50%	87598	80711	77401	75465	74196	73300	72634	72120	71712
	$b = 0.75d$	20%	202565	186039	178090	173442	170396	168248	166652	165420	164439
		30%	136123	125031	119697	116577	114534	113092	112021	111194	110536
		40%	102822	94457	90435	88082	86541	85454	84647	84023	83527
		50%	82778	76056	72825	70936	69698	68824	68176	67675	67276
	$b = 0.80d$	20%	191716	175597	167842	163307	160338	158243	156687	155486	154531
		30%	128903	118076	112868	109823	107829	106423	105378	104572	103930
		40%	97443	89270	85339	83041	81535	80474	79686	79077	78593
		50%	78523	71949	68787	66939	65728	64875	64241	63751	63362
	$b = 0.85d$	20%	182133	166377	158791	154356	151453	149406	147886	146712	145780
		30%	122515	111926	106829	103849	101899	100523	99502	98714	98087
		40%	92673	84673	80822	78572	77099	76060	75289	74693	74220
		50%	74741	68299	65199	63387	62201	61365	60744	60265	59884

Table 4 (cont'd.). Factors Relating the Minimum Plastic Section Modulus of RBS Beams to Their Rotational Spring Constants, m (kip/in.^{2}-rad)											
			Beam Length								
		Flange Reduction	5*d*	7.5*d*	10*d*	12.5*d*	15*d*	17.5*d*	20*d*	22.5*d*	25*d*
$a = 0.7b_f$	$b = 0.65d$	20%	231231	212966	204192	199060	195698	193326	191563	190202	189120
		30%	155154	142919	137041	133604	131352	129763	128582	127670	126945
		40%	116954	107751	103330	100745	99051	97855	96967	96281	95736
		50%	93907	86536	82996	80926	79570	78612	77901	77352	76915
	$b = 0.70d$	20%	216830	199148	190652	185685	182431	180137	178432	177116	176069
		30%	145609	133752	128055	124725	122543	121005	119862	118979	118277
		40%	109882	100951	96660	94152	92509	91350	90490	89825	89296
		50%	88354	81189	77747	75736	74418	73488	72798	72265	71841
	$b = 0.75d$	20%	204330	187155	178899	174074	170915	168687	167033	165755	164740
		30%	137305	125778	120238	117000	114881	113386	112276	111419	110737
		40%	103711	95018	90841	88400	86802	85675	84838	84192	83678
		50%	83489	76506	73151	71190	69906	69001	68329	67810	67397
	$b = 0.80d$	20%	193378	176649	168603	163902	160825	158656	157045	155802	154814
		30%	130016	118781	113378	110222	108156	106699	105618	104783	104119
		40%	98280	89800	85722	83340	81781	80682	79866	79236	78735
		50%	79194	72373	69094	67179	65925	65042	64385	63879	63476
	$b = 0.85d$	20%	183703	167371	159510	154918	151913	149796	148223	147010	146046
		30%	123568	112592	107311	104226	102207	100784	99728	98913	98265
		40%	93466	85174	81185	78856	77331	76257	75459	74844	74354
		50%	75377	68701	65490	63615	62388	61523	60881	60386	59992
$a = 0.75b_f$	$b = 0.65d$	20%	233256	214247	205120	199786	196294	193831	192001	190589	189465
		30%	156508	143774	137661	134089	131750	130100	128875	127929	127176
		40%	117970	108392	103795	101109	99349	98108	97187	96475	95909
		50%	94717	87048	83368	81217	79808	78814	78076	77507	77053
	$b = 0.70d$	20%	218720	200343	191517	186361	182986	180607	178839	177475	176391
		30%	146873	134551	128634	125177	122914	121319	120134	119220	118493
		40%	110832	101551	97095	94492	92788	91587	90694	90006	89458
		50%	89113	81669	78095	76007	74641	73677	72962	72409	71970
	$b = 0.75d$	20%	206102	188276	179711	174708	171435	169127	167414	166092	165041
		30%	138491	126529	120781	117425	115229	113681	112531	111644	110939
		40%	104603	95583	91250	88720	87064	85897	85030	84361	83830
		50%	84203	76957	73478	71446	70116	69179	68483	67946	67519
	$b = 0.80d$	20%	195046	177705	169367	164499	161314	159070	157404	156118	155097
		30%	131134	119488	113890	110621	108483	106976	105858	104995	104309
		40%	99121	90332	86108	83641	82028	80891	80047	79396	78878
		50%	79868	72800	69403	67420	66123	65209	64530	64007	63590
	$b = 0.85d$	20%	185279	168370	160232	155482	152375	150186	148562	147309	146313
		30%	124624	113262	107795	104604	102517	101046	99955	99113	98444
		40%	94262	85678	81550	79140	77564	76454	75630	74994	74489
		50%	76015	69105	65782	63843	62575	61681	61018	60506	60100

A Modified Equation for Expected Maximum Shear Strength of the Special Segment for Design of Special Truss Moment Frames

SHIH-HO CHAO and SUBHASH C. GOEL

Seismic behavior of the special truss moment frame (STMF) system has been studied both analytically and experimentally by Goel and Itani (1994) and Basha and Goel (1995) at the University of Michigan during the past 15 years and has been incorporated into the AISC *Seismic Provisions for Structural Steel Buildings* (AISC, 2005), hereafter referred to as the AISC Seismic Provisions. This system consists of a truss girder with a special segment designed to behave inelastically under severe earthquakes while the other members, including girder-to-column connections, outside the special segment remain essentially elastic. The special segment can be made with X-diagonal or Vierendeel web members, as shown in Figure 1. When an STMF is subjected to lateral seismic forces, the induced shear force in the middle of the joist girder is resisted primarily by the chord members and the web diagonals of the special segment. After yielding and buckling of the diagonal members, plastic hinges will form at the ends of the chord members as shown in Figure 2. The yield mechanism of the frame is a combination of yielding of all special segments in the frame plus the plastic hinges at the column bases (Figure 2). The plastic hinges at the base may be in the columns or in the base connection, whichever is practically feasible. Design of STMFs starts with designing the special segment. Based on a capacity design approach, other elements are then designed to remain elastic under the shear forces in the middle of the truss girder generated by fully yielded and strain hardened special segments (in other words, the expected vertical shear strength, V_{ne}), along with other external forces.

The expected maximum shear strength of the special segment, V_{ne}, is given in the current AISC Seismic Provisions [Equation 12-1 in AISC (2005)] as:

$$V_{ne} = \frac{3.75 R_y M_{nc}}{L_s} + 0.075 E_s I \frac{\left(L - L_s\right)}{L_s^3} + R_y \left(P_{nt} + 0.3 P_{nc}\right) \sin\alpha \quad (1)$$

where

R_y = yield stress modification factor
M_{nc} = nominal flexural strength of the chord members of the special segment
$E_s I$ = flexural elastic stiffness of the chord members of the special segment
L = span length of the truss
L_s = length of the special segment, center-to-center of supports
P_{nt} = nominal axial tension strength of diagonal members of the special segment
P_{nc} = nominal axial compression strength of diagonal members of the special segment
α = angle of diagonal members with the horizontal

The first two terms of Equation 1 were derived based on a study of a Vierendeel special segment (without X-braces) (Basha and Goel, 1994). One of the assumptions made in the derivation was that the elastic moment at the ends of

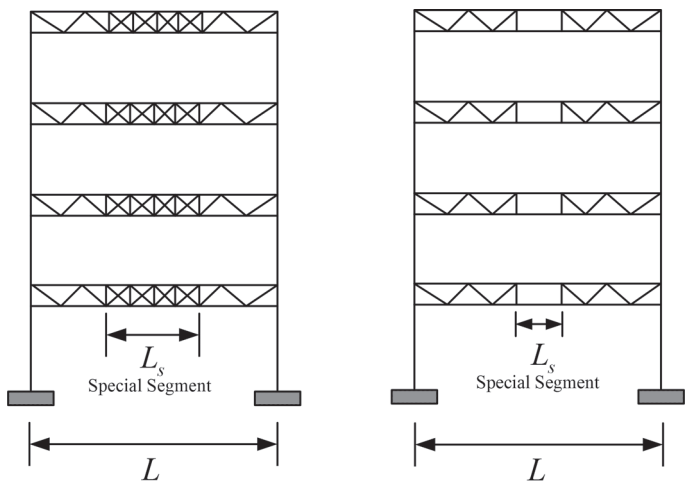

Fig. 1. STMF with different configurations of special segment.

Subhash Goel is professor, department of civil and environmental engineering, University of Michigan, Ann Arbor, MI.

Shih-Ho Chao is assistant professor, department of civil and environmental engineering, University of Texas, Arlington, TX.

chord members of the special segment results from vertical translation only, in other words, the effect of end rotation is neglected as shown in Figure 3a. This assumption leads to overestimation of the elastic stiffness of the chord members, which in turn results in a higher coefficient, 0.075, in the second term of Equation 1. Nevertheless, this overestimation has a small influence on V_{ne} if the moment of inertia of the chord member is small. However, for heavier chord members the overestimation can be quite large because of their large moment of inertia and the second term of Equation 1 is directly related to the member's moment of inertia. Because the members outside the special segment, such as vertical members, diagonal members, connections and columns are designed based on V_{ne}, any overestimation would result in an overly conservative design of those members.

PROPOSED MODIFICATION

A remedy to the aforementioned problem is to use a more realistic flexural elastic stiffness of the chord members. This is done by the approach that follows.

If the chord member has no end rotation (fixed end condition), the elastic moment at the chord end can be given by:

$$M = \frac{6E_s I\theta}{L_s} \tag{2}$$

where

θ = relative vertical displacement at chord ends divided by the length of special segment

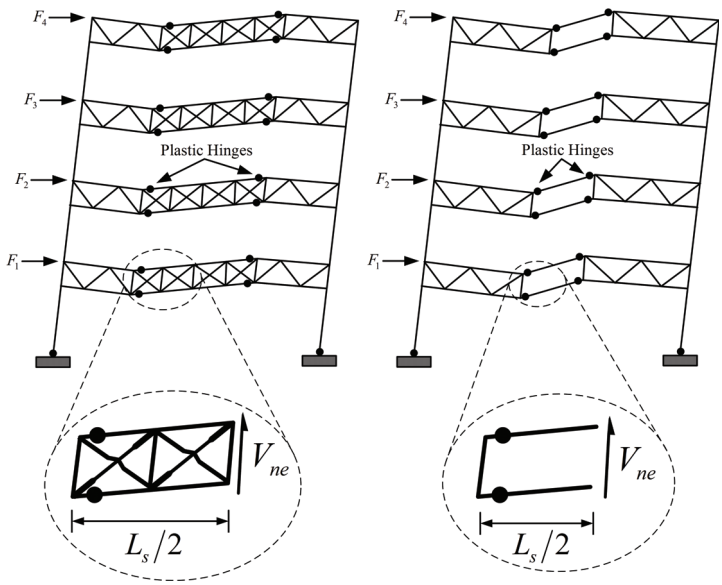

Fig. 2. Mechanism of STMF with different special segments.

Hence, the elastic stiffness is:

$$\frac{M}{\theta} = \frac{6E_s I}{L_s} = k \tag{3}$$

This elastic stiffness will decrease by allowing the end rotation to occur. For the extreme case, in other words, when the chord member has pinned ends as shown in Figure 3b, the elastic stiffness is equal to zero. True elastic stiffness is somewhere between these two extreme cases. It is assumed here that the true elastic stiffness can be approximated by:

$$k = \frac{3E_s I}{L_s} \tag{4}$$

By using this formulation, the maximum chord end moment is determined as follows:

Referring to Figure 4, the chord moment-rotation relation can be modeled by a bilinear curve, in which the inelastic stiffness is ηk. From Equation 4, the maximum elastic rotation is:

$$\theta_e = \frac{M_p L_s}{3E_s I} \tag{5}$$

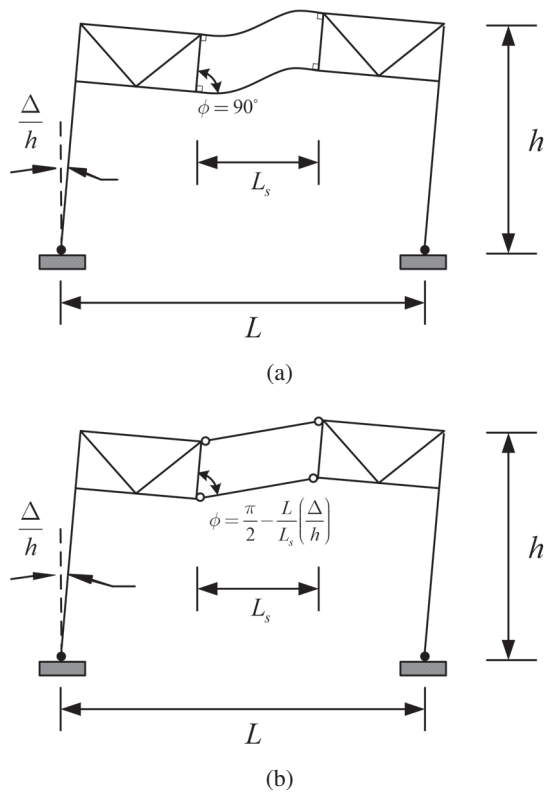

Fig. 3. Deformation of chord of the Vierendeel special segment: (a) no chord end rotation; (b) free chord end rotation.

The maximum rotation of the chord member can be obtained by using the geometric relation. Thus,

$$\theta_u = \frac{L}{L_s}\left(\frac{\Delta}{h}\right) \tag{6}$$

where

(Δ/h) = story drift

Hence the plastic rotation is:

$$\theta_p = \theta_u - \theta_e = \frac{L}{L_s}\left(\frac{\Delta}{h}\right) - \frac{M_p L_s}{3E_s I} \tag{7}$$

The expression for maximum moment can be written as (see Figure 4):

$$\begin{aligned} M_{max} &= M_p + \eta k \theta_p \\ &= (1-\eta) R_y M_{nc} + 3E_s I \eta \left(\frac{L}{L_s^2}\right)\left(\frac{\Delta}{h}\right) \end{aligned} \tag{8}$$

where

η = ratio of the post-yield slope to the elastic slope of the assumed bilinear moment-rotation model of the chord member

The expected maximum shear strength of the special segment, V_{ne}, is then calculated as:

$$V_{ne} = \frac{4M_{max}}{L_s} \tag{9}$$

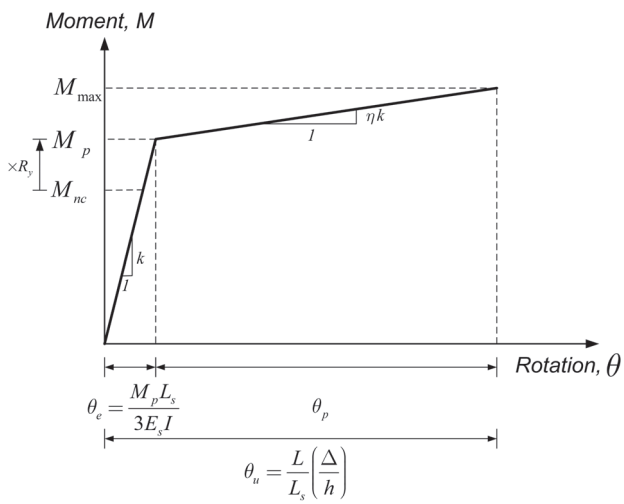

Fig. 4. Moment-rotation relationship of chord member.

It is noted that the slope, η, only accounts for strain hardening; that is, the expected plastic moment, M_p, was used instead of the nominal strength, M_{nc}, as shown in Figure 4. Based on tests on STMF subassemblages in which the special segment was composed of double-angle sections, Basha and Goel (1994) found that a value of η equal to 10% was adequate for the post-yield slope (see Figure 5). This value was also found adequate for double-channel sections based on tests conducted by Parra-Montesinos, Goel and Kim (2006). Figure 6 shows the backbone curve of hysteretic loops for a typical double-channel element, as well as the corresponding bilinear model. By using η = 10%, and Δ/h = 0.03 in Equation 8, Equation 9 becomes:

$$V_{ne} = \frac{3.6 R_y M_{nc}}{L_s} + 0.036 E_s I \frac{L}{L_s^3} \tag{10}$$

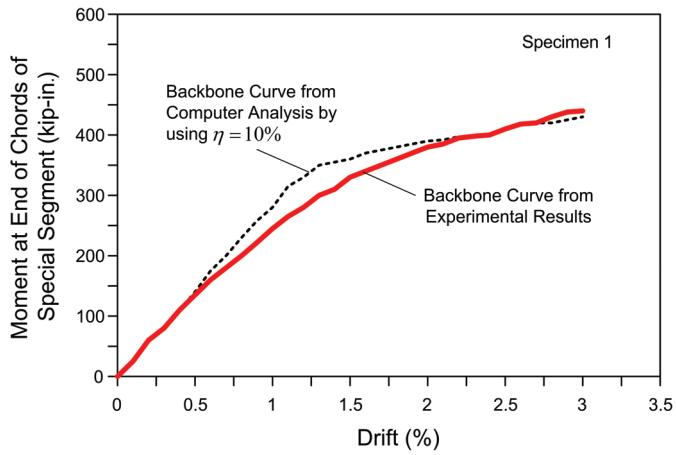

(a)

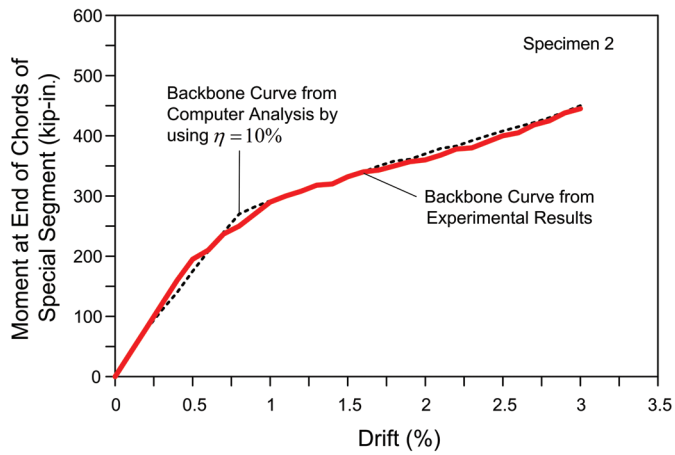

(b)

Fig. 5. Moment versus drift plots of subassemblage tested, chord member was a built-up section composed of double-angles and plate (Basha and Goel, 1994).

The value of $\Delta/h = 0.03$ was chosen because current design practice is generally based on a limiting drift ratio of around 0.02. If the maximum rotation capacity, θ_p, of a chord member is available, Equation 9 can also be expressed by:

$$V_{ne} = \frac{4R_y M_{nc}}{L_s} + 1.2E_s \frac{I}{L_s^2}\theta_p \qquad (11)$$

The second term in Equation 11 accounts for the contribution of strain-hardening in the chord members. It is noted that Dusicka, Itani and Sahai (2002) derived a similar equation for V_{ne}. Their expression, however, did not account for strain-hardening effects.

VERIFICATION OF THE MODIFIED EQUATION

The proposed modification was verified by previous test results as well as nonlinear static and dynamic analyses as described in the following.

Previous Test Results

Equation 10 was first verified by the test results (Parra-Montesinos et al., 2006) on double-channel (2C10×25, I = 182.2 in.^{4}, Z = 46.2 in.^{3}, F_y = 50 ksi) elements used for chord members of STMF, in which the maximum shear capacity was measured at 150 kips when the corresponding story drift reached 3%. The value of V_{ne} calculated from Equation 10, by using R_y = 1.1, gives the same exact value, in other words, 150 kips.

Equation 10 was further verified using the test results of a subassemblage STMF (Basha and Goel, 1994), in which the chord members of the Vierendeel special segment were made of a built-up section composed of double angles and a plate (2L3×3×½ and PL1×2¼). The built-up section had a rather small moment of inertia (I = 5.87 in.^{4}). The maximum end moment at the story drift of 3% was 440 kip-in., which corresponds to V_{ne} = 26.2 kips. The estimated value from Equation 10 is 24.4 kips, which is about 7.3% lower than the experimental value. On the other hand, the AISC equation (Equation 1) gives a value of 28.4 kips, about 8.5% higher than the testing data.

Nonlinear Static Analysis

Equation 10 was then verified by investigating the maximum developed shears in the Vierendeel special segments of a seven-story STMF (Chao and Goel, 2006). The chord member at the fifth floor of this frame was made of 2C10×25. Modeling of the moment-rotation relation for the chord members was based on that shown in Figure 6. Pushover analysis was performed until the interstory drift at the fifth level reached 3%, as shown in Figure 7. It was found that the average V_{ne} was about 143 kips, which is close to the predicted value, 150 kips. While the proposed equation gives good agreement with the test and analysis results, the V_{ne} as calculated by using the AISC expression (Equation 1) is 177.3 kips, about 20% higher than that obtained from Equation 10. It should be noted that both the AISC

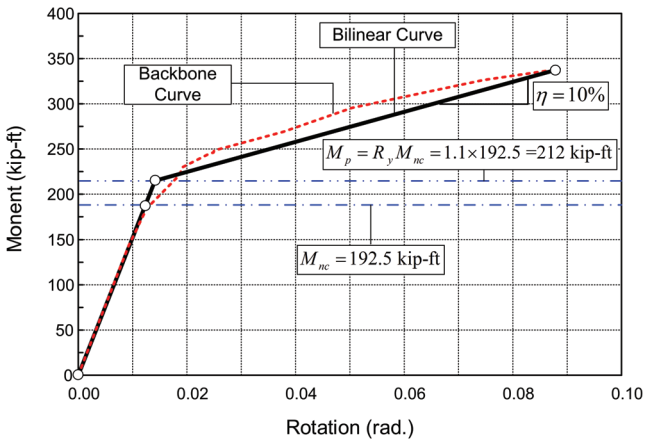

Fig. 6. Modeling of the backbone curve of double-channel element using bilinear curve.

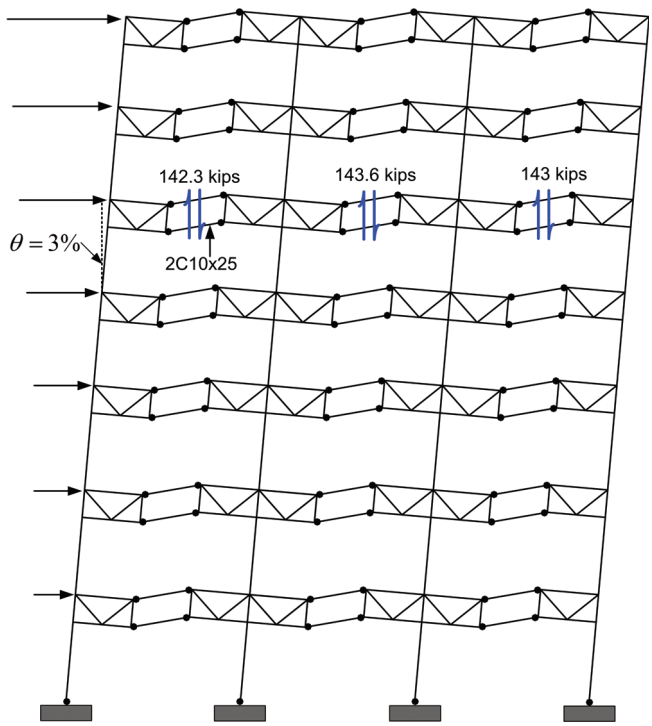

Fig. 7. Maximum developed shears in the fifth-floor special segments when the study STMF was statically pushed until the fifth floor reached 3% story drift.

expression and Equation 10 are based on a story drift equal to 3%. If the expected maximum story drift is well below 3%, the AISC expression would be even more conservative.

It should also be noted that the L_s used in Equation 10 is taken as center-to-center distance of the vertical members at the ends of the special segment. In reality, the distance between the plastic hinges, L_p, will be smaller than L_s. This length in the University of Michigan double-channel tests was formed to be about $0.82L_s$ and the V_{ne} in the seven-story STMF analysis was calculated based on $0.85L_s$. Both of them have almost the same V_{ne} as that obtained from Equation 10. This suggests that Equation 10 is still slightly conservative even when L_s is used instead of L_p in the denominator of Equation 10.

Nonlinear Dynamic Analysis

Two nine-story STMFs with Vierendeel type special segments (Figure 8), representing the class of essential facilities (in other words, hospital buildings) as well as ordinary office/residential occupancy type, were designed for evaluating the proposed modification (Chao and Goel, 2006). Double-channel sections were used for chord members. For ordinary building types, the design target drifts of 2% and 3% for 10% in 50 years and 2% in 50 years design hazard levels, respectively, were chosen. The corresponding numbers for essential facilities were 1.5% and 2.25%. Design spectral values were based on NEHRP Provisions (FEMA, 2001) for the San Francisco site. After the final design work was completed, nonlinear dynamic analyses were conducted to study the responses. Nine, 10% in 50 years, and five, 2% in 50 years, SAC Los Angeles region ground motions representing the two design hazard levels were used for the nonlinear response history analyses.

The results showed that yielding was limited to the special segments only, while the other elements remained elastic. This suggests that the proposed expression for V_{ne} was quite adequate to ensure elastic performance of the elements outside the special segments. Figures 9 and 10 show the maximum developed shears in the special segments for the ordinary and essential STMFs, respectively. It can be seen that the AISC equation significantly overestimates the expected shear strength, which would lead to undue over-design of elements outside the special segments. On the other hand,

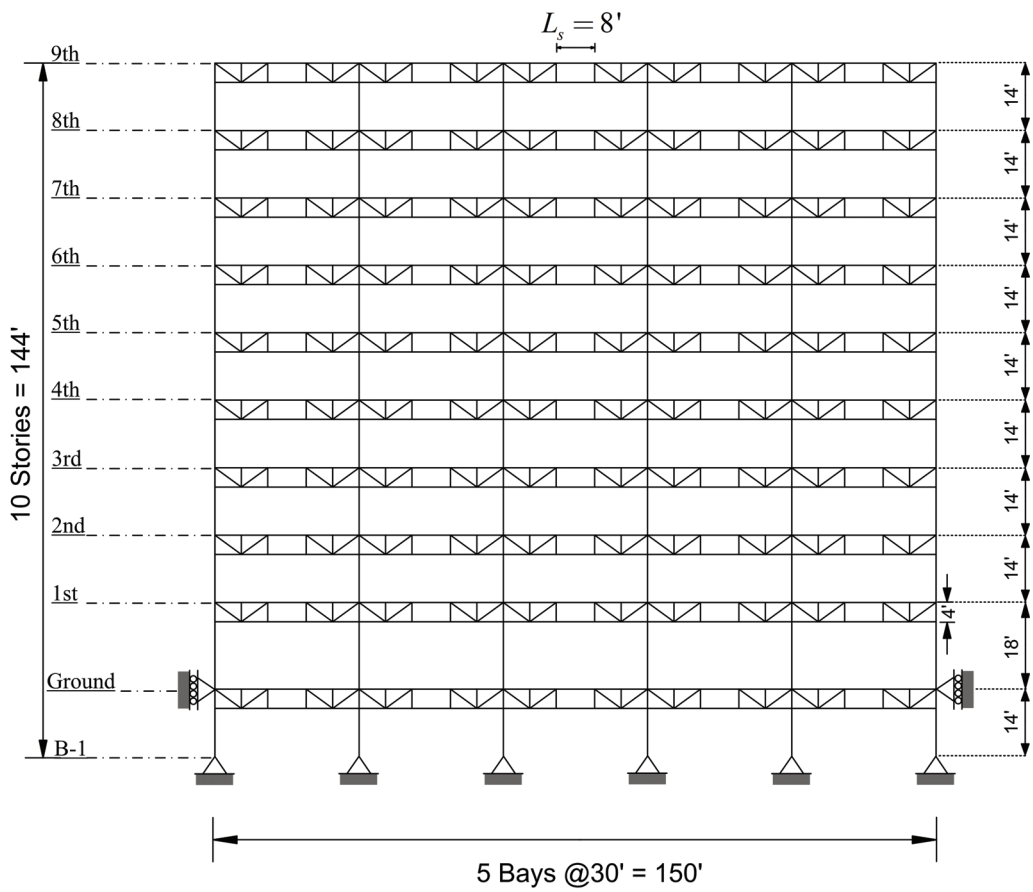

Fig. 8. Elevation of study nine-story STMFs.

the proposed expression (Equation 10) is closer to the actual developed shears while maintaining some safety margin.

Therefore, based on the preceding discussion, it is suggested that the current AISC expression (with the web diagonals also included in the special segment) can be modified as:

$$V_{ne} = \frac{3.6R_yM_{nc}}{L_s} + 0.036E_sI\frac{L}{L_s^3} + R_y\left(P_{nt} + 0.3P_{nc}\right)\sin\alpha \quad (12\text{-}1)$$

or

$$V_{ne} = \frac{4R_yM_{nc}}{L_s} + 1.2E_s\frac{I}{L_s^2}\theta_p + R_y\left(P_{nt} + 0.3P_{nc}\right)\sin\alpha \quad (12\text{-}2)$$

VIERENDEEL SPECIAL SEGMENTS WITH INTERMEDIATE VERTICAL MEMBERS

A special segment can contain multiple Vierendeel panels by adding intermediate vertical members, as shown in Figure 11. One benefit of using multiple Vierendeel panels is that the redundancy of the seismic energy dissipation mechanism increases. It also has the advantages of allowing more flexibility in mechanical and architectural layout, as well as reducing the rotational ductility demands on special segment chords (Valley and Hooper, 2002). It is very likely that during minor to moderate earthquake events, inelastic deformation would only occur in the intermediate vertical members, which could be replaced relatively easily. In addition, the size of chord members can be reduced because of additional

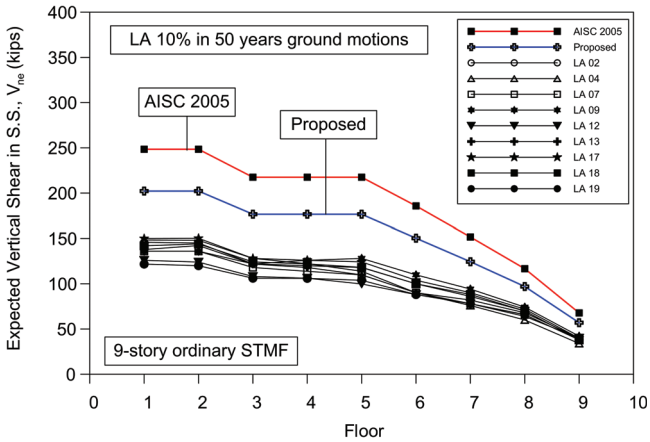

(a)

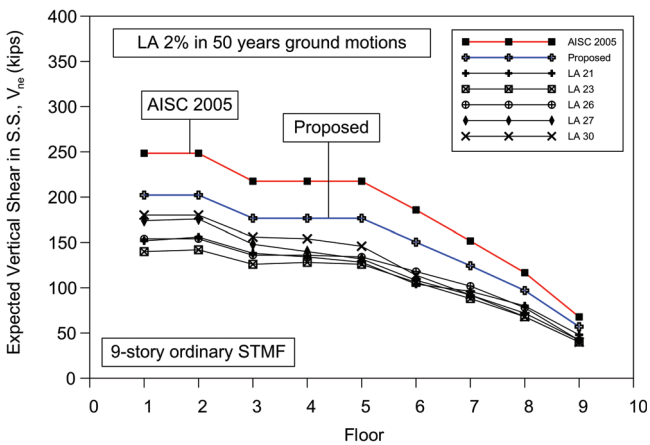

(b)

Fig. 9. Maximum developed shears in special segments in the nine-story ordinary STMF subjected to 10%/50 and 2%/50 ground motions.

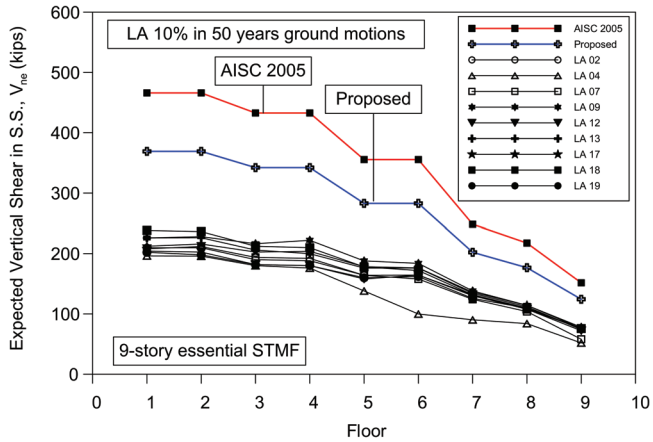

(a)

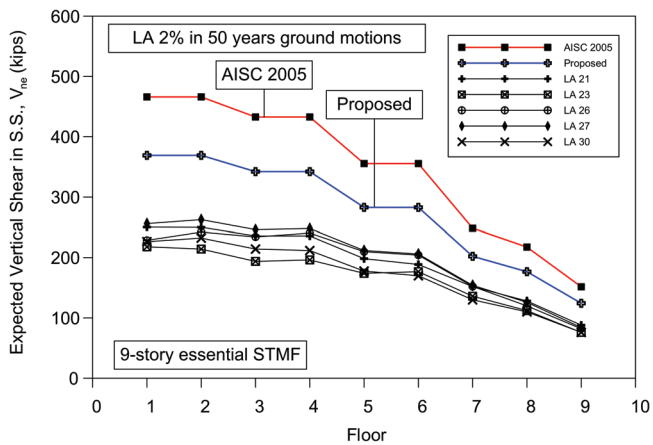

(b)

Fig. 10. Maximum developed shears in special segments in the nine-story essential STMF subjected to 10%/50 and 2%/50 ground motions.

strength due to those intermediate vertical members. In the case where multiple Vierendeel panels are present, the calculation of V_{ne} should include the contribution from intermediate vertical members. It can be shown that both the chord member and the intermediate vertical member have the same plastic rotation when the yield mechanism is reached (Figure 11). Thus the maximum moment developed in the chord members and intermediate vertical members can be obtained from Equation 8, as follows:

$$\left(M_c\right)_{max} = \left(1-\eta\right) R_y M_{nc} + 3E_s I_c \eta \left(\frac{L}{L_s^2}\right)\left(\frac{\Delta}{h}\right) \tag{13}$$

$$\left(M_v\right)_{max} = \left(1-\eta\right) R_y M_{nv} + 3E_s I_v \eta \left(\frac{L}{L_s^2}\right)\left(\frac{\Delta}{h}\right) \tag{14}$$

where

$(M_c)_{max}$, $(M_v)_{max}$ = maximum expected developed moments in the chord member and intermediate vertical member, respectively

I_c = moment of inertia of the chord member

I_v = moment of inertia of the intermediate vertical member

It should be noted that the strain-hardening ratio tends to increase when the member length decreases (Engelhardt and Popov, 1989). For a typical chord member, a 10% strain-hardening ratio may be reasonable but the strain-hardening ratio for the vertical member might be actually higher due to its much shorter length. In this study, the chord and intermediate vertical members were assumed to have the same strain-hardening ratio.

The expected maximum shear strength of the special segment with one intermediate vertical member is then calculated as (Figure 12):

$$V_{ne} = \frac{4\left(M_c\right)_{max}}{L_s} + \frac{2\left(M_v\right)_{max}}{L_s} \tag{15}$$

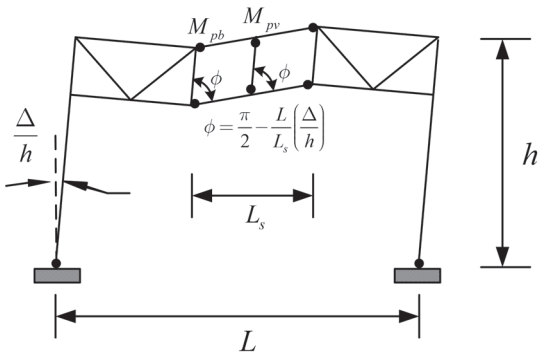

Fig. 11. Yield mechanism of STMF with multiple Vierendeel panels.

For a special segment with two intermediate vertical members (Figure 13):

$$V_{ne} = \frac{4\left(M_c\right)_{max}}{L_s} + \frac{4\left(M_v\right)_{max}}{L_s} \tag{16}$$

In general, the expected maximum shear strength of a special segment with intermediate vertical members can be expressed as:

$$V_{ne} = \frac{4\left(M_c\right)_{max}}{L_s} + \left(\frac{m}{2}\right)\frac{4\left(M_v\right)_{max}}{L_s} \tag{17}$$

where

m = number of intermediate vertical members

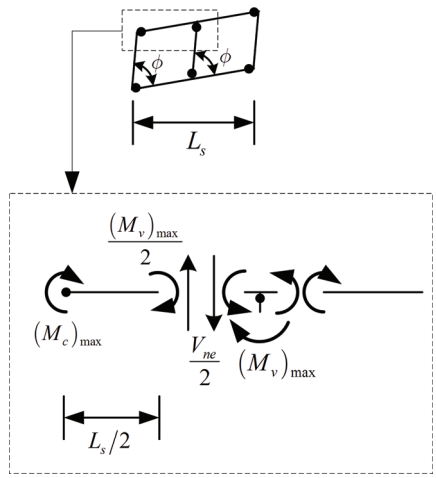

Fig. 12. Calculation of V_{ne} *for two Vierendeel panels.*

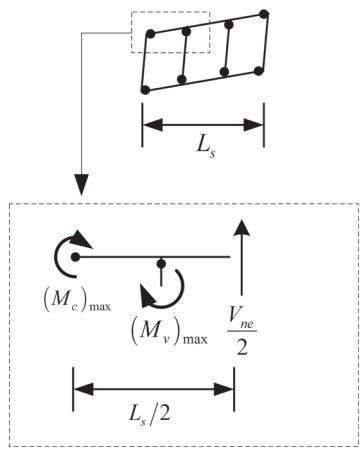

Fig. 13. Calculation of V_{ne} *for three Vierendeel panels.*

By using $\eta = 0.1$, and $\Delta/h = 0.03$, V_{ne} will be given by:

$$V_{ne} = \left(\frac{3.6R_yM_{nc}}{L_s} + 0.036E_sI_c\frac{L}{L_s^3} \right) + \frac{m}{2}\left(\frac{3.6R_yM_{nv}}{L_s} + 0.036E_sI_v\frac{L}{L_s^3} \right) \quad (18\text{-}1)$$

or

$$V_{ne} = \left(\frac{4R_yM_{nc}}{L_s} + 1.2E_s\frac{I_c}{L_s^2}\theta_{pc} \right) + \frac{m}{2}\left(\frac{4R_yM_{nv}}{L_s} + 1.2E_s\frac{I_v}{L_s^2}\theta_{pv} \right) \quad (18\text{-}2)$$

where

θ_{pc} and θ_{pv} = maximum rotation capacity of the chord and intermediate vertical members, respectively

A NOTE ON THE DESIGN OF MULTIPLE VIERENDEEL PANELS

It should be noted that, as illustrated in Figure 11, while the vertical members generally have smaller length than the chord members, the vertical members experience the same plastic rotation with the chord members when the yield mechanism forms. As pointed out by Engelhardt and Popov (1989), as member length decreases, flexural yielding tends to be confined to a smaller region at the ends of the member leading to larger curvature and bending strain demands for the same plastic rotation. This higher demand on bending strains in turn results in a higher possibility of fracture at welded connections at the member ends. In addition, the reduced length of the plastic region can cause problems of flange buckling and lateral-torsional buckling in flexural yielding members. As a consequence, until further experimental results are available, it is suggested that the intermediate vertical members should be treated as secondary members to prevent possible instability of the frame in case premature failure occurs in the vertical members. The term "secondary members" is used here in the sense that most of the truss strength and energy dissipation capacity should be provided by the chord members. In addition, plastic hinges must be avoided in the chord members except at chord ends; therefore, the moment capacity of vertical members has to be limited so that the moment in the chord members at sections adjacent to the vertical members is less than the moment capacity of chord members after the vertical members yield.

Therefore, to design intermediate vertical members as secondary members, it is suggested at this time that at least 70% of the input energy be dissipated by the chord members and the remainder by intermediate vertical members, unless further research can show that yielding of intermediate vertical members is not detrimental to the overall performance of an STMF. Therefore, the following equation can be applied at a given floor level (Chao and Goel, 2006):

$$\frac{30\%}{70\%} = \frac{\left(2m_iM_{pvi}\right)\left(\pi/2 - \phi\right)}{\left(4M_{pbi}\right)\left(\pi/2 - \phi\right)} \quad (19)$$

$$M_{pvi} \approx \frac{M_{pbi}}{m_i} \quad (20)$$

where

M_{pvi} = required plastic moment capacity of the intermediate vertical members at the ith level

M_{pbi} = required plastic moment capacity of the chord members at the ith level

m_i = number of intermediate vertical members at the ith level

The term $\pi/2 - \phi$ represents the rotation of the chord and intermediate vertical members (see Figure 11). It should also be mentioned that the design of chord and intermediate vertical members can be easily implemented by using the plastic design method (Chao and Goel, 2006). In that case, the internal work stored in a special segment can be expressed by:

$$\left(4M_{pbi} + 2m_iM_{pvi}\right)\theta = \left(4M_{pbi} + 2m_i\frac{M_{pbi}}{m_i}\right)\theta \quad (21)$$

$$= 6M_{pbi}\theta$$

$$= \text{External Work}$$

If the design of chord members is performed based on Equation 21, then the design of intermediate vertical members should follow Equation 20.

SUMMARY AND CONCLUSION

A revised equation for maximum expected shear strength, V_{ne}, was derived by using a more realistic assumption and validated by experimental results as well as nonlinear static and dynamic analyses. Based on extensive nonlinear dynamic analyses, it was found that the current AISC equation for V_{ne} in the special segments can significantly overestimate the expected shear strength, which in turn leads to undue overdesign of members outside the special segments, such as vertical members, diagonal members, connections and columns. The values given by the proposed equation were closer to the actual developed shears while maintaining some safety margin. A design equation of V_{ne} for STMF using multiple Vierendeel panels in the special segments was also proposed.

ACKNOWLEDGMENTS

The authors gratefully acknowledge partial financial support provided by Nabih Youssef & Associates Structural Engineers, and NUCOR Research and Development for this study. The senior author also received a stipend from the G.S. Agarwal Fellowship Fund at the Department of Civil and Environmental Engineering while working on this project. The opinions and views expressed in the paper are solely those of the authors.

REFERENCES

AISC (2005), *Seismic Provisions for Structural Steel Buildings*, ANSI/AISC 341-05, American Institute of Steel Construction, Chicago, IL.

Basha, H.S. and Goel, S.C. (1994), "Seismic Resistant Truss Moment Frames with Ductile Vierendeel Segment," *Report No. UMCEE 94-29*, Department of Civil and Environmental Engineering, University of Michigan, Ann Arbor, MI.

Basha, H.S. and Goel, S.C. (1995), "Special Truss Moment Frames with Vierendeel Middle Panel," *Engineering Structures*, Vol. 17, No. 5, pp. 352–358.

Chao, S.-H. and Goel, S.C. (2006), "Performance-Based Plastic Design of Seismic Resistant Special Truss Moment Frames," *Report No. UMCEE 06-03*, Department of Civil and Environmental Engineering, University of Michigan, Ann Arbor, MI.

Dusicka, P., Itani, A.M. and Sahai, R. (2002), "Advances in the Seismic Design of Special Truss Moment Frames," *Proceedings*, 71st Annual Convention of Structural Engineers of California, Santa Barbara, CA, pp. 185–196.

Engelhardt, M.D. and Popov, E.P. (1989), "Behavior of Long Links in Eccentrically Braced Frames," *Report No. UCB/EERC-89/01*, Earthquake Engineering Research Center, University of California at Berkeley.

Goel, S.C. and Itani, A.M. (1994), "Seismic-Resistant Special Truss-Moment Frames," *Journal of Structural Engineering*, ASCE, Vol. 120, No. 6, pp. 1781–1797.

NEHRP (2001), "Recommended Provisions for the Development of Seismic Regulations for New Buildings (FEMA 368)," Federal Emergency Management Agency, Washington, DC.

Parra-Montesinos, G.J., Goel, S.C. and Kim, K.Y. (2006), "Behavior of Steel Double-Channel Built-Up Chords of Special Truss Moment Frames under Reversed Cyclic Bending," *Journal of Structural Engineering*, ASCE, Vol. 132, No. 9, pp. 1343–1351.

Valley, M. and Hooper, J. (2002), "Issues in the Design of Special Truss Moment Frames in High-Seismic Regions," *Proceedings*, 7th U.S. National Conference on Earthquake Engineering, Boston, MA, July 21–25, pp. 1177–1185.

Performance-Based Plastic Design of Special Truss Moment Frames

SHIH-HO CHAO and SUBHASH C. GOEL

The special truss moment frame (STMF) is a relatively new type of steel framing system suitable for high seismic areas. The frames dissipate earthquake energy through ductile special segments located near the mid-span of truss girders. STMFs generally have higher structural redundancy compared to other systems because four plastic hinges can form in the chords of one truss girder. The redundancy can be further enhanced if web members are used in the special segments. Simple connection details are needed for the girder-to-column connections. One other advantage of using STMF systems is that the truss girders can be used over longer spans, and greater overall structural stiffness can be achieved by using deeper girders. In addition, the open webs can easily accommodate mechanical and electrical ductwork. As a consequence, this system is gaining popularity in the United States, especially for hospital and commercial buildings. Research work carried out at the University of Michigan led to the formulation of design code provisions (Goel and Itani, 1994; Basha and Goel, 1995; AISC, 2005a). Current design practice generally follows elastic analysis procedures to proportion the frame members. Therefore, it is possible that story drifts and yielding in the special segments may not be uniformly distributed along the height of the structure and may be concentrated in a few floors causing excessive inelastic deformations at those levels. Thus, the intended deformation limits and yield mechanism may not be achieved when an STMF is subjected to strong earthquakes.

Shih-Ho Chao is assistant professor, department of civil and environmental engineering, University of Texas, Arlington, TX.

Subhash Goel is professor, department of civil and environmental engineering, University of Michigan, Ann Arbor, MI.

In recent years, seismic design has been gradually moving toward a more direct performance-based design approach, which is intended to produce structures with predictable and controlled seismic performance. To achieve this goal, knowledge of the ultimate structural behavior, such as nonlinear relationships between forces and deformations, and the yield mechanism of structural systems are essential. Therefore, the desired global yield mechanism needs to be built into the design process. In current practice, the performance-based seismic design for a new structure is carried out in a somewhat indirect manner. It usually starts with an initial design according to conventional elastic design procedures using applicable design codes, followed by a nonlinear static pushover assessment (ATC, 1996; ASCE, 2000). Usually, an iterative process between design and assessment follows. Moreover, as mentioned in FEMA 440 (ATC, 2004), this procedure still has difficulty in predicting reasonably accurate structural behavior during a major earthquake when compared with the results from nonlinear response history analyses.

While further refinement is needed in current practice to move toward more reliable performance-based design methodologies, this paper presents a direct performance-based design approach that basically requires no assessment such as nonlinear static (pushover) or dynamic analysis after design. Based on an energy (work) concept (Leelataviwat, Goel and Stojadinović, 1999; Lee, Goel and Chao, 2004; Chao and Goel, 2005), the proposed approach determines the design base shear by using the code-specified elastic design spectral value for a given hazard level, a preselected global structural yield mechanism, and a target drift. In addition, the design lateral force distribution employed in the proposed method is based on nonlinear dynamic analysis results using a large number of ground motions (Somerville, Smith, Punyamurthula and Sun, 1997). The chord members in the special segments are designed according to the plastic design method (Chao and Goel, 2006), while the members outside the special segments are designed by using a capacity design approach. A complete detailed design procedure was developed and the design steps are summarized in a flowchart in Figures 10 and 11, which could be easily applied to develop a computer program.

PROPOSED PERFORMANCE-BASED PLASTIC DESIGN PROCEDURE

Design Lateral Forces

Unlike in the current design codes, the design lateral force distribution in the proposed method is determined based on maximum story shears that are obtained from extensive nonlinear time-history analyses. The proposed design lateral force distribution was found suitable for moment frames (MFs), eccentrically braced frames (EBFs), concentrically braced frames (CBFs), and special truss moment frames (STMFs) (Chao, Goel and Lee, 2007). This lateral force distribution is expressed as:

$$F_i = (\beta_i - \beta_{i+1})F_n \qquad \text{when } i = n,\ \beta_{n+1} = 0 \tag{1}$$

$$F_n = V\left(\frac{w_n h_n}{\sum_{j=1}^{n} w_j h_j}\right)^{0.75T^{-0.2}} \tag{2}$$

$$\beta_i = \frac{V_i}{V_n} = \left(\frac{\sum_{j=i}^{n} w_j h_j}{w_n h_n}\right)^{0.75T^{-0.2}} \tag{3}$$

where

β_i = shear distribution factor at level i
V_i, V_n = story shear forces at level i and at the top (nth) level, respectively
w_i = seismic weight at level j
h_j = height of level j from the ground
w_n = seismic weight of the structure at the top level
h_n = height of roof level from ground
T = fundamental natural period
F_i, F_n = lateral forces applied at level i and top level n, respectively
V = design base shear

Design Base Shear

Design base shear in current seismic codes is commonly obtained by reducing the elastic strength demands to the inelastic strength demands by using response modification factors. These inelastic strength demands are further increased according to the importance of specific structures using an occupancy importance factor. Generally, the design base shear is determined from the code prescribed design acceleration spectrum and expressed in the following form:

$$V = C_s W = S_a\left(\frac{I}{R}\right)W \tag{4}$$

where

C_s = seismic response coefficient calculated based on specified design spectrum
S_a = spectral response acceleration
I = occupancy importance factor
R = response modification factor [= 7.0 for STMF (NEHRP, 2000)]
W = total seismic weight

After selecting the member sizes for required strengths (which is generally done by elastic analysis), the calculated drift using elastic analysis is multiplied by a deflection amplification factor, C_d, given in the building code, and kept within specified drift limits (on the order of 2%). It should be noted that the response modification factors, R, specified in design codes for various structural systems are based on a number of factors including engineering judgment. Moreover, conventional design procedures are based on elastic force-based analysis methods rather than displacement-based methods. Thus, the inelastic response beyond the elastic limit for a structure cannot be reliably predicted.

A more rational design approach to overcome the aforementioned shortcomings was proposed based on energy equation and plastic design concepts (Leelataviwat et al., 1999; Lee et al., 2004). In this approach, the design base shear is determined by pushing the structure monotonically up to a target drift after the formation of a selected yield mechanism. The choice of target drift will generally be based on acceptance criteria, such as damage or life safety. For example, a maximum transient story drift ratio of 2.5% is specified in FEMA 356 (FEMA, 2000) to meet the life safety performance level for steel moment frames. The amount of work needed to do that is assumed as a factor γ times the elastic input energy $E = \frac{1}{2}MS_v^2$ for an equivalent single degree of freedom (SDOF). It should be noted that this amount of work assumes no relationship with the energy dissipated during earthquake excitation. In the proposed method it is simply used as a means to calculate the required design base shear by establishing a tie between the intended yield mechanism, target drift, force-displacement characteristics of the structure, and elastic input energy from the design ground motion. Thus, the energy equation can be written as:

$$\left(E_e + E_p\right) = \gamma E = \gamma\left(\frac{1}{2}MS_v^2\right) \tag{5}$$

where

E_e, E_p = elastic and plastic components of the energy (work) needed to push the structure up to the target drift, respectively
S_v = design spectral pseudo-velocity
M = total mass of the system

The modification factor, γ, depends on the structural ductility factor, μ_s, and the ductility reduction factor, R_μ, which is related to the period of the structure. Figure 1 shows the relationship between the base shear, CW, and the corresponding drift, Δ, of the elastic and corresponding elastic-plastic

SDOF systems. From the geometric relationship, Equation 5 can be written as:

$$\gamma\left(\frac{1}{2}C_{eu}W\Delta_{eu}\right) = \frac{1}{2}C_yW\left(2\Delta_{max} - \Delta_y\right) \quad (6)$$

where

C_{eu} = seismic response coefficient corresponding to the maximum base shear when the structure behaves essentially elastically

C_y = seismic response coefficient corresponding to the maximum base shear when the structure demonstrates elastic-perfect-plastic behavior

Δ_y = yield drift

Using the expression for drifts, Δ, Equation 6 can be rewritten as:

$$\gamma\frac{\Delta_{eu}}{\Delta_y} = \frac{\left(2\Delta_{max} - \Delta_y\right)}{\Delta_{eu}} \quad (7)$$

where

Δ_{eu} = $R_\mu\Delta_y$ from Figure 1

Δ_{max} = $\mu_s\Delta_y$ from Figure 1

Substituting these terms into Equation 7, the energy modification factor, γ, can be determined as:

$$\gamma = \frac{2\mu_s - 1}{R_\mu^2} \quad (8)$$

where

μ_s = ductility factor equal to target drift divided by yield drift = Δ_{max}/Δ_y

R_μ = ductility reduction factor = C_{eu}/C_y

It can be seen from Equation 8 that the energy modification factor, γ, is a function of the ductility reduction factor, R_μ, and the structural ductility factor, μ_s. In this study, the method by Newmark and Hall (1982) is adopted to relate the ductility reduction factor and the structural ductility factor as shown in Figure 2. Plots of calculated energy modification factor, γ, from Equation 8 are shown in Figure 3.

The design elastic energy demand, E, can be determined from the elastic design pseudo-acceleration spectra as typically given in the building codes. The design pseudo-acceleration based on the selected design spectrum for elastic systems can be specified as:

$$A = S_a g \quad (9)$$

where

A = design pseudo-acceleration

g = acceleration due to gravity

S_a = spectral response acceleration as defined in Equation 4

Note that no occupancy importance factor is included in the design pseudo-acceleration for the proposed approach. The occupancy importance factor, I, increases the design force level in an attempt to lower the drift and ductility demands for the structure for a given level of ground shaking (SEAOC, 1999; NEHRP, 2000). However, that cannot be considered as a direct method to achieve the intended purpose such as

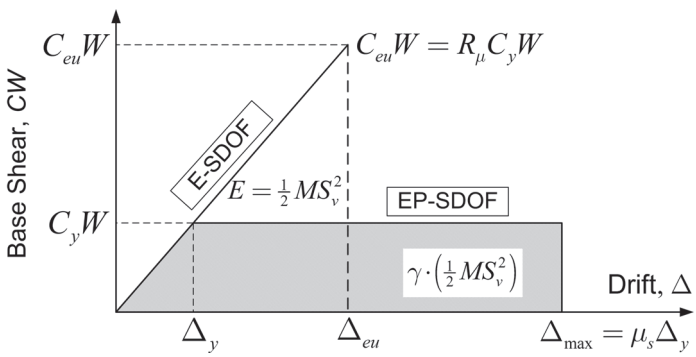

Fig. 1. Structural idealized response and energy balance concept.

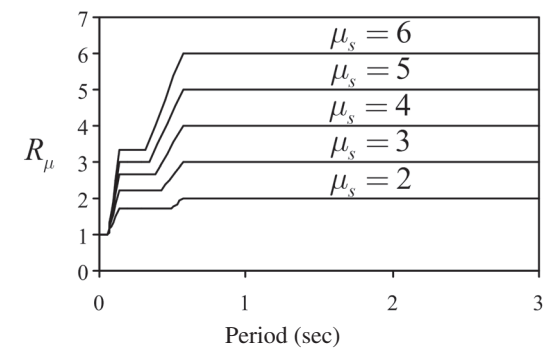

Fig. 2. Ductility reduction factors proposed by Newmark and Hall (1982).

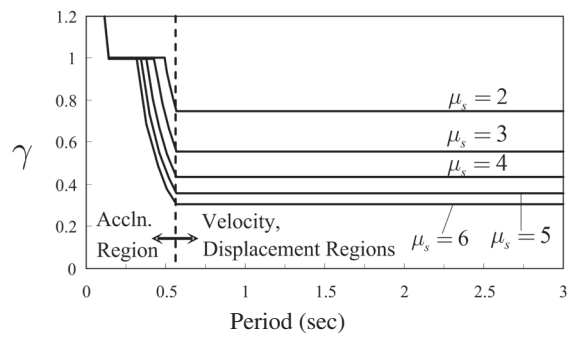

Fig. 3. Modification factors for energy equation vs. period.

damage control. The reduction of potential damage could better be handled by using appropriate drift limitations. In this regard, the approach of calculating the design base shear proposed in this study uses the target drift as the governing parameter. It is assumed that the selected target drift will have the occupancy importance factor built into it. In any case, S_a can be modified or increased in order to account for factors such as near-fault effect, redundancy consideration, or possible torsion in the global structural system.

The energy (work) equation can be rewritten as:

$$\left(E_e + E_p\right) = \gamma\left(\frac{1}{2}MS_v^2\right) = \frac{1}{2}\gamma M\left(\frac{T}{2\pi}S_a g\right)^2 \tag{10}$$

Akiyama (1985) showed that the elastic vibrational energy, E_e, can be calculated by assuming that the entire structure can be reduced into an SDOF system, in other words,

$$E_e = \frac{1}{2}M\left(\frac{T}{2\pi}\frac{V}{W}g\right)^2 \tag{11}$$

where

V = yield base shear
W = total seismic weight of the structure = Mg

Substituting Equation 11 into Equation 10 and rearranging the terms gives:

$$E_p = \frac{WT^2 g}{8\pi^2}\left(\gamma S_a^2 - \left(\frac{V}{W}\right)^2\right) \tag{12}$$

Using a preselected yield mechanism for the STMF configurations shown in Figure 4 and equating the plastic energy term, E_p, to the external work done by the design lateral forces gives:

$$E_p = \sum_{i=1}^{n} F_i h_i \theta_p \tag{13}$$

where

θ_p = inelastic drift of the global structure, which is the difference between the selected target drift, θ_u, and yield drift, θ_y

Based on nonlinear analyses, the yield drift for STMF can be taken as 0.75% for design purposes (Chao and Goel, 2006). Substituting Equations 1 and 12 into Equation 13, and solving for V/W gives:

$$\frac{V}{W} = \frac{-\alpha + \sqrt{\alpha^2 + 4\gamma S_a^2}}{2} \tag{14}$$

where

V = design base shear
α = dimensionless parameter, which depends on the stiffness of the structure, the modal properties, and the intended drift level, and is given by:

$$\alpha = \left(\sum_{i=1}^{n}(\beta_i - \beta_{i+1})h_i\right)\left(\frac{w_n h_n}{\sum_{j=1}^{n} w_j h_j}\right)^{0.75T^{-0.2}}\left(\frac{\theta_p 8\pi^2}{T^2 g}\right) \tag{15}$$

It should be noted that the required design base shear given by Equation 14 is related to the lateral force distribution, the target plastic drift, θ_p, and preselected yield mechanism. Also note that in Equation 15 when $i = n$, $\beta_{n+1} = 0$.

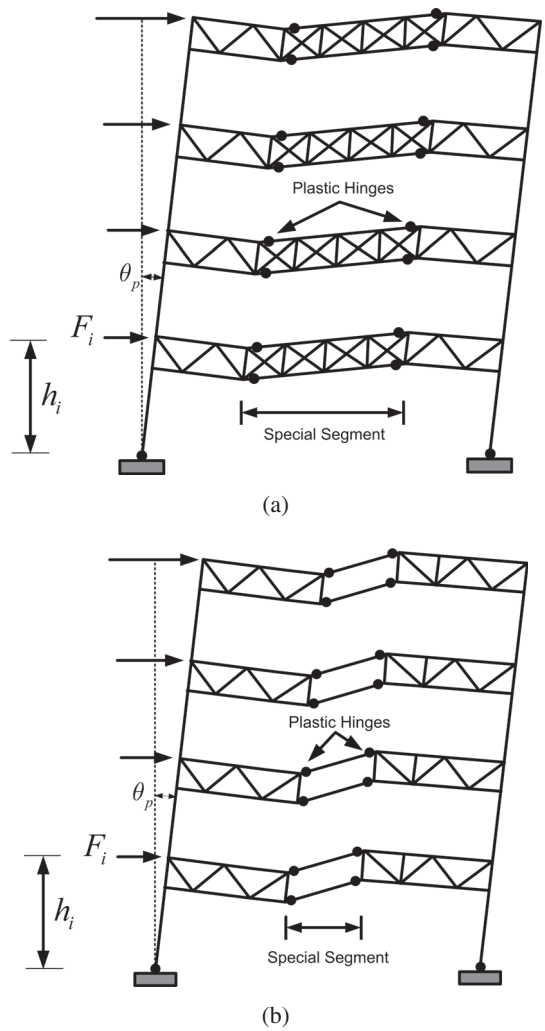

Fig. 4. Preselected yield mechanism of STMF with various geometries: (a) with X-diagonal web members in special segment; (b) without web members in special segment (Vierendeel type).

It can be seen that the proposed method for determining the lateral design forces is based on principles of structural dynamics, while ensuring formation of selected yield mechanism and drift control simultaneously. There is no need for using a response modification factor, R, an occupancy importance factor, I, or a displacement amplification factor (such as C_d), as required in current practice and largely based on engineering judgment. It should also be noted that the design base shear in the proposed method as given by Equation 14 represents the ultimate yield force level (in other words, $C_y W$ in Figure 1) at which a complete mechanism is expected to form. In contrast, the code design base shear as given by Equation 4 represents the required strength at the first significant yield point for use in design by elastic methods.

Preselected Yield Mechanism

Figure 4 shows STMFs subjected to design lateral forces and pushed to its target drift limit state. All the inelastic deformations are intended to be confined within the special segments in the form of plastic hinges (and yielding and buckling of the diagonal web members when they are used). Because the plastic hinges at column bases generally form during a major earthquake, the desired global yield mechanism of STMF is achieved through yielding (due to shear force) of the special segments plus the plastic hinges at the column bases.

Proportioning of Chord Members of the Special Segments

In this study, STMFs with a Vierendeel-type special segment (see Figure 4b) are used to demonstrate the proposed plastic design approach. The primary aim of using a plastic design procedure is to ensure the formation of the intended yield mechanism. For STMFs, the plastic hinges are intended to occur only in the special segments and column bases. Earlier studies have shown that it is desirable to have the distribution of chord member strength along the building height closely follow the distribution of story shears, in other words, the shear distribution factor, β_i, which was obtained and calibrated by nonlinear response history analysis results. This helps to distribute the yielding more evenly along the height, thereby, preventing yielding from concentrating at a few levels. Referring to Figure 5, only one bay of an STMF is shown for illustration of the design procedure. It should be noted that using all the bays gives the same required chord strength.

By using the principle of virtual work and equating the external work to the internal work, as is commonly done in plastic analysis by the mechanism method, the required chord member strength at each level can be determined as:

$$\sum_{i=1}^{n} F_i h_i \theta_p = 2M_{pc}\theta_p + 4\sum_{i=1}^{n} \beta_i M_{pbr} \frac{L}{L_s}\theta_p \qquad (16)$$

where

L = span length of truss girders
L_s = length of special segment (see Figure 5)
M_{pbr} = required plastic moment of chord members at the top level and the only unknown variable in Equation 16

The required chord member strength (plastic moment capacity) at level i can be determined by multiplying M_{pbr} by the shear distribution factor β_i at level i, namely, $\beta_i M_{pbr}$. M_{pc} is the required plastic moment of columns in the first story as shown in Figure 5. Note that due to the selected deformation mechanism of the truss girder (as shown in Figures 4 and 5) and assuming uniformly distributed gravity loads, the external work done by the gravity loads is zero, and thus not included in Equation 16.

M_{pc} is the required plastic moment of columns in the first story, which can be selected in such a way that no soft-story mechanism would occur when a factor of 1.1 times the design lateral forces are applied on the frame (Leelataviwat et al., 1999), as shown in Figure 6:

$$M_{pc} = \frac{1.1V'h_1}{4} \qquad (17)$$

where

V' = base shear (for an equivalent one-bay frame), which is equal to V divided by the number of bays
h_1 = height of the first story

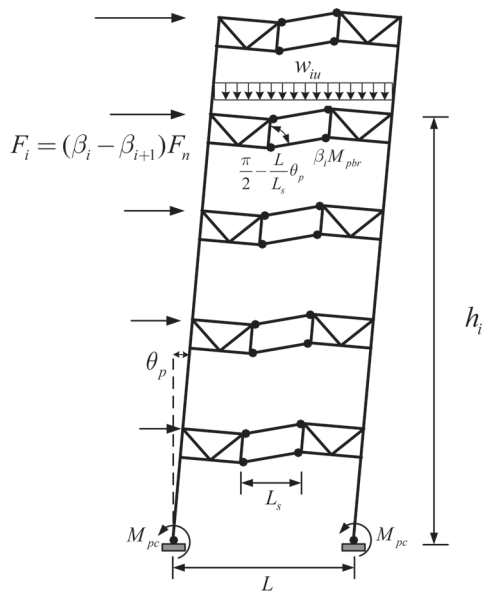

Fig. 5. One-bay STMF with preselected yield mechanism for calculating required strength of chord member. Note that the values of F_i and F_n are for one bay only.

The factor 1.1 is the overstrength factor accounting for possible overloading due to stain hardening and uncertainty in material strength.

By using Equations 16 and 17, the required chord member strength at level *i* can be determined as:

$$\beta_i M_{pbr} = \beta_i \frac{\left(\sum_{i=1}^{n} F_i h_i - 2M_{pc}\right)}{4\frac{L}{L_s}\sum_{i=1}^{n}\beta_i} \tag{18}$$

The design of the chord member is performed using:

$$\phi M_{nci} = \phi Z_i F_y \geq \beta_i M_{pbr} \tag{19}$$

where

ϕ = resistance factor = 0.90
Z_i = plastic section modulus
F_y = specified minimum yield stress (taken equal to 50 ksi in this study)

Chord members should also satisfy the specified width-thickness limitations as listed in the AISC *Seismic Provisions for Structural Steel Buildings* Table I-8-1 (AISC, 2005a), hereafter referred to as the AISC Seismic Provisions. Design recommendations on Vierendeel special segments with intermediate vertical members can be found elsewhere (Chao and Goel, 2006).

Design of Members Outside the Special Segments

The design of elements outside the special segments, including truss members and columns, is performed based on the capacity design approach. That is, elements outside the special segments should have a design strength to resist the combination of factored gravity loads and the maximum expected vertical shear strength, V_{ne}, developed at the midpoint of the special segments. The expression for V_{ne}, as specified in the AISC Seismic Provisions [Equation 12-1, (AISC, 2005a)], was originally derived based on a somewhat conservative chord deformation assumption. For members with a larger moment of inertia, such as the double-channel sections employed in this study, the AISC expression generally leads to quite a conservative design for members outside the special segments. In view of this, a modification has been proposed by Chao and Goel (2006) and was used in this study. For STMF with a special segment of the Vierendeel configuration:

$$V_{ne} = \frac{3.6R_y M_{nc}}{L_s} + 0.036E_s I_s \frac{L}{L_s^3} \tag{20}$$

where

R_y = yield overstrength factor (taken as 1.1)
M_{nc} = nominal flexural strength of the chord members of the special segment
E_s = Young's modulus (= 29,000 ksi)
I_s = moment of inertia of the chord members of the special segment

Once the maximum expected vertical shear strength is determined, the frame can be broken into free-body diagrams of exterior and interior columns with associated truss girders as shown in Figures 7, 8 and 9.

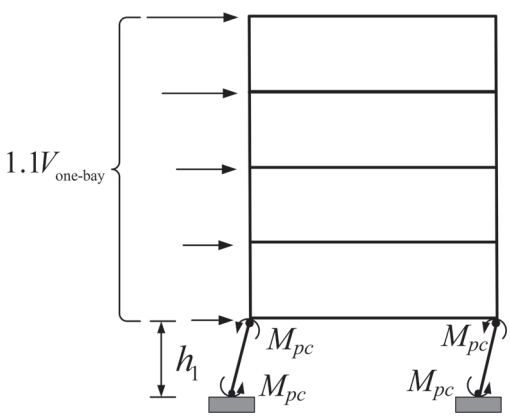

Fig. 6. One-bay equivalent frame with soft-story mechanism (Leelataviwat et al., 1999).

Design of Columns with Associated Truss Girders

Referring to Figure 7a, when the frame reaches its target drift, the vertical shear force in the middle of the special segment at all levels is assumed to reach the maximum expected strength, $(V_{ne})_i$. The column at the base is also assumed to have reached its maximum capacity, M_{pc}. At this stage, the required balancing lateral forces applied on this free body are assumed to maintain the distribution as used earlier and can be easily calculated by using equilibrium of the free body. For the case when the lateral forces are acting to the right, the sum of those forces, $(F_R)_{ext}$, can be obtained as:

$$(F_R)_{ext} = \frac{\frac{L}{2}\sum_{i=1}^{n}(V_{ne})_i - \frac{L^2}{8}\sum_{i=1}^{n} w_{iu} + M_{pc}}{\sum_{i=1}^{n}\alpha_i h_i} \tag{21}$$

where

w_{iu} = factored uniformly distributed gravity load on the truss girders = $1.2DL + 0.5LL$ in this study

and

$$\alpha_i = \frac{F_i}{\sum_{i=1}^{n} F_i} = \frac{(\beta_i - \beta_{i+1})}{\sum_{i=1}^{n}(\beta_i - \beta_{i+1})} \text{ when } i = n,\ \beta_{n+1} = 0 \tag{22}$$

For the case when the lateral forces are directed to the left (Figure 7b), the sum of the applied lateral forces, $(F_L)_{ext}$, can be obtained as:

$$(F_L)_{ext} = \frac{\frac{L}{2}\sum_{i=1}^{n}(V_{ne})_i + \frac{L^2}{8}\sum_{i=1}^{n} w_{iu} + M_{pc}}{\sum_{i=1}^{n}\alpha_i h_i} \quad (23)$$

For the case where the gravity loading on truss girders consists of concentrated loads, Equation 21 can be replaced by Equation 24 (see Figure 8):

$$(F_R)_{ext} = \frac{\frac{L}{2}\sum_{i=1}^{n}(V_{ne})_i - L_1\sum_{i=1}^{n} p_{iu} + M_{pc}}{\sum_{i=1}^{n}\alpha_i h_i} \quad (24)$$

where

p_{iu} = factored concentrated gravity loads on the truss girders = $1.2DL + 0.5LL$, as shown in Figure 8

Also Equation 23 can be replaced by:

$$(F_L)_{ext} = \frac{\frac{L}{2}\sum_{i=1}^{n}(V_{ne})_i + L_1\sum_{i=1}^{n} p_{iu} + M_{pc}}{\sum_{i=1}^{n}\alpha_i h_i} \quad (25)$$

It should be mentioned that although the column design has been carried out by using column trees, the overturning of the entire frame is accounted for through beam shear forces applied on the column trees.

For the case of interior columns with associated truss girders, both directions of lateral forces lead to the same result;

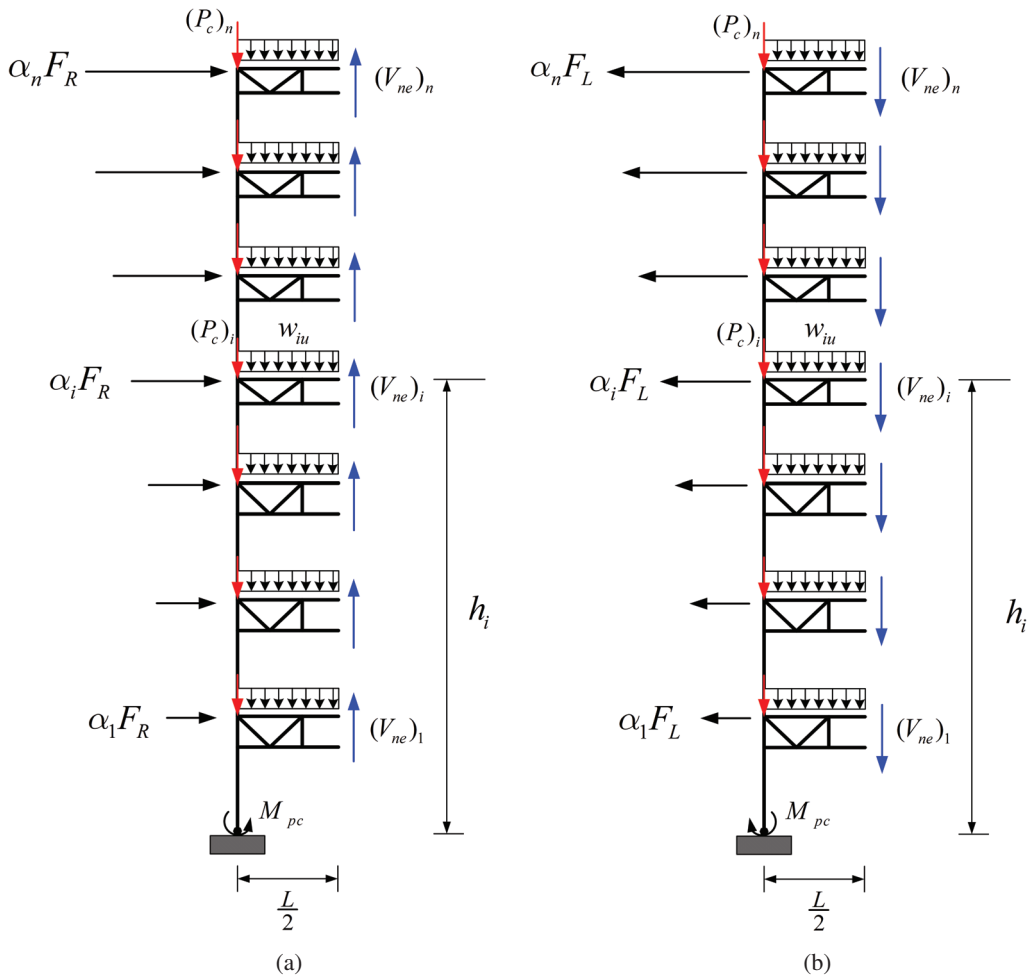

Fig. 7. Free-body diagram of an exterior column and associated truss girder branches: (a) lateral forces acting to right side; (b) lateral forces acting to left side.

hence only the lateral forces acting to the right are shown in Figure 9. The sum of lateral forces, $(F_R)_{int}$, can be calculated as:

$$(F_R)_{int} = \frac{L\sum_{i=1}^{n}(V_{ne})_i + 2M_{pc}}{\sum_{i=1}^{n}\alpha_i h_i} \quad (26)$$

After the lateral forces required for equilibrium are calculated as described earlier, the required strength of individual members (diagonals, chord members, columns and vertical members, if any) can be easily computed by using an elastic structural analysis program. Preliminary sections can be assumed in the beginning and revised later. The terms $\alpha_i F_R$, $\alpha_i F_L$, $(V_{ne})_i$, $(P_c)_i$, p_{iu} and w_{iu}, which appear in the preceding equations and in Figure 9, are treated as applied loads. Design of these elements is performed in accordance with the AISC *Specification for Structural Steel Buildings*, ANSI/AISC 360-05 (AISC, 2005b) through conventional elastic design procedures. For STMF with hinged bases, the column-truss models may be structurally unstable when loaded because they are basically determinate cantilever beams. Nevertheless, the hinge support can be replaced with a fixed support for computing the element forces without affecting the results because all the external forces are already balanced and moment at the column base will automatically be zero (because of hinged supports). The vertical members adjacent to the special segment are recommended to have the same section as the chord member in the special segment without performing any design calculations (Basha and Goel, 1994). However, a stronger section can be used, if needed. Flowcharts are given in Figures 10 and 11 to illustrate the entire design procedure.

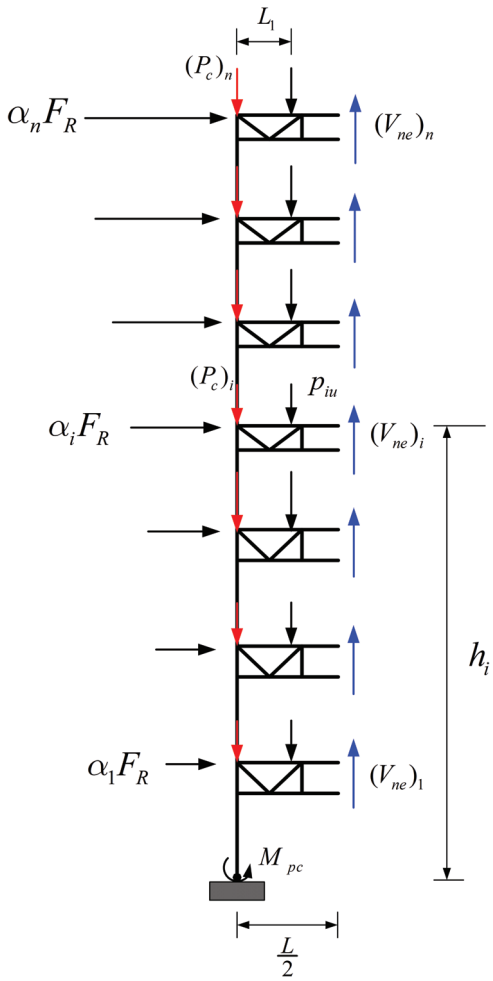

Fig. 8. Free-body diagram of an exterior column and associated truss girder branches with concentrated gravity loadings on truss girders (lateral forces acting to right side).

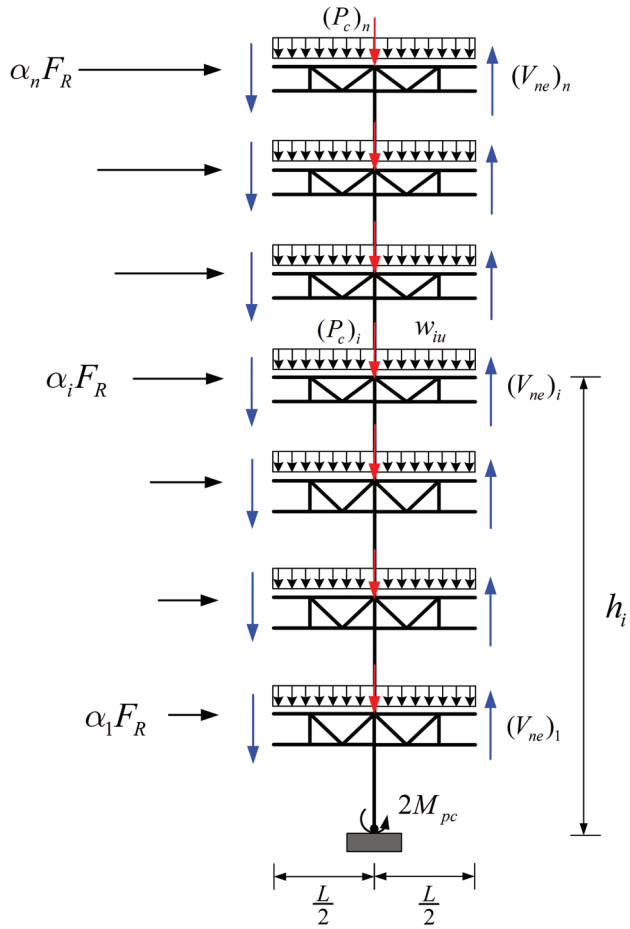

Fig. 9. Free-body diagram of an interior column and associated truss girder branches subjected to lateral forces to right.

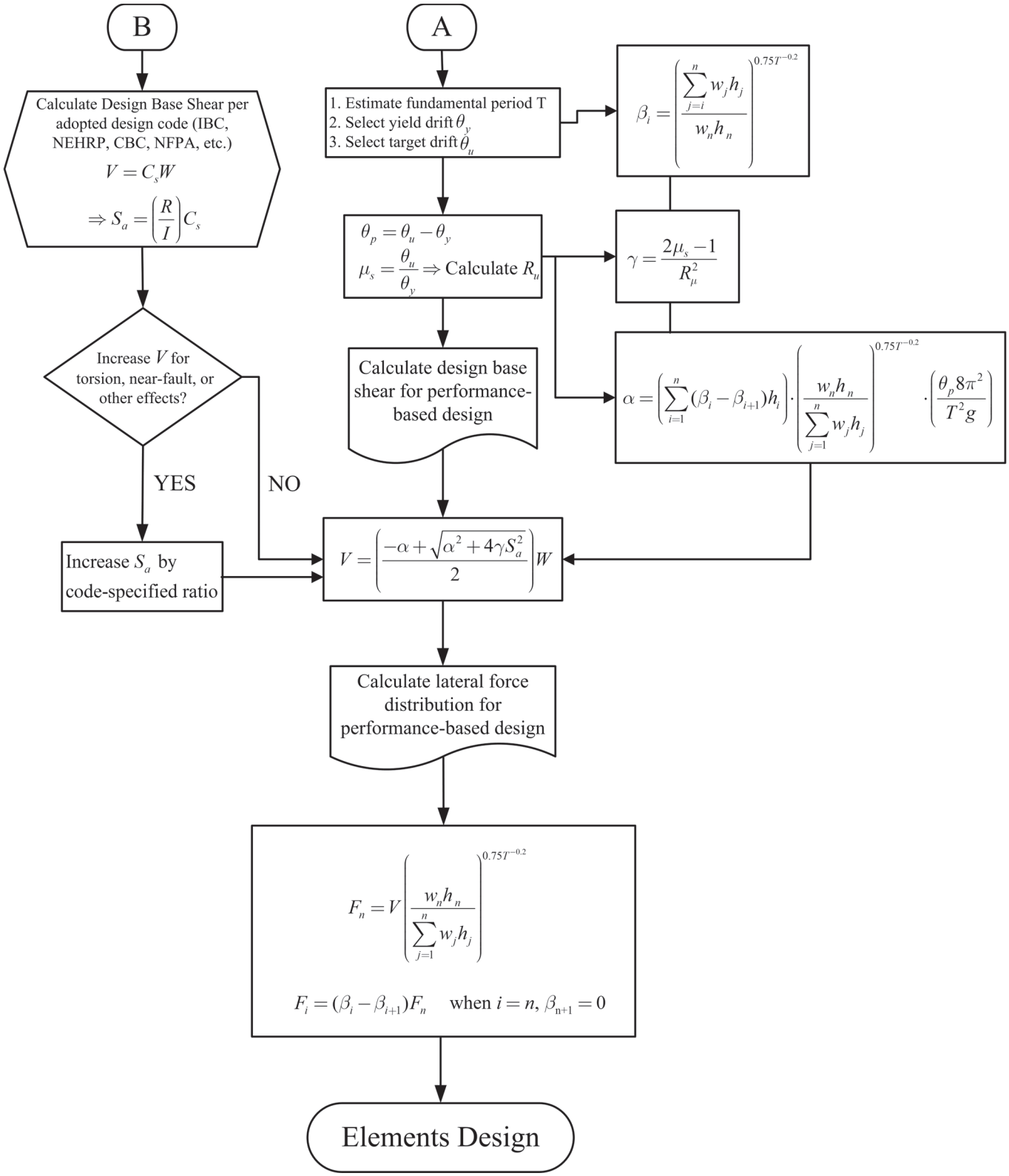

Fig. 10. Performance-based plastic design flowchart for STMF: determine design base shear and lateral force distribution.

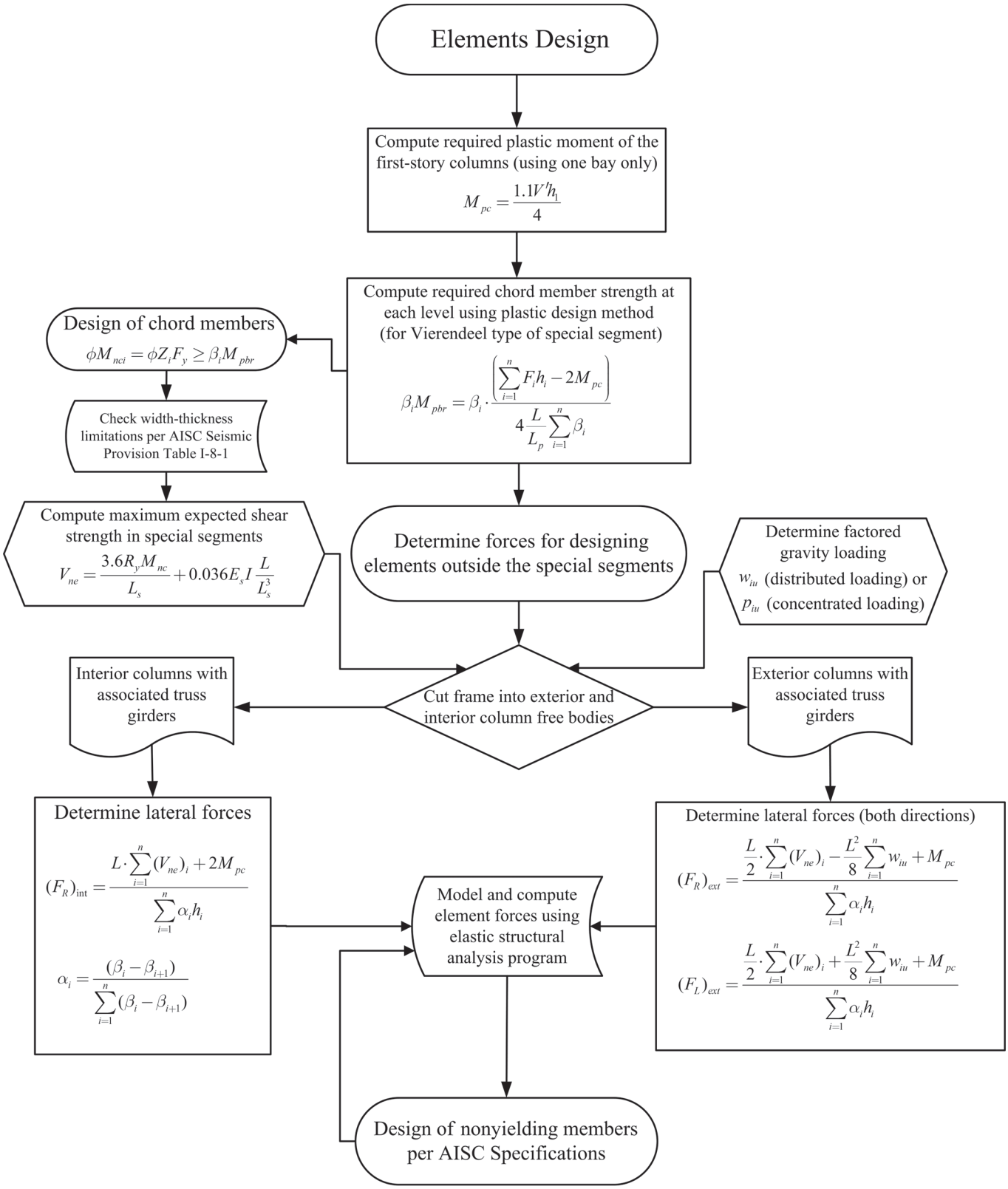

Fig. 11. Performance-based plastic design flowchart for STMF: element design.

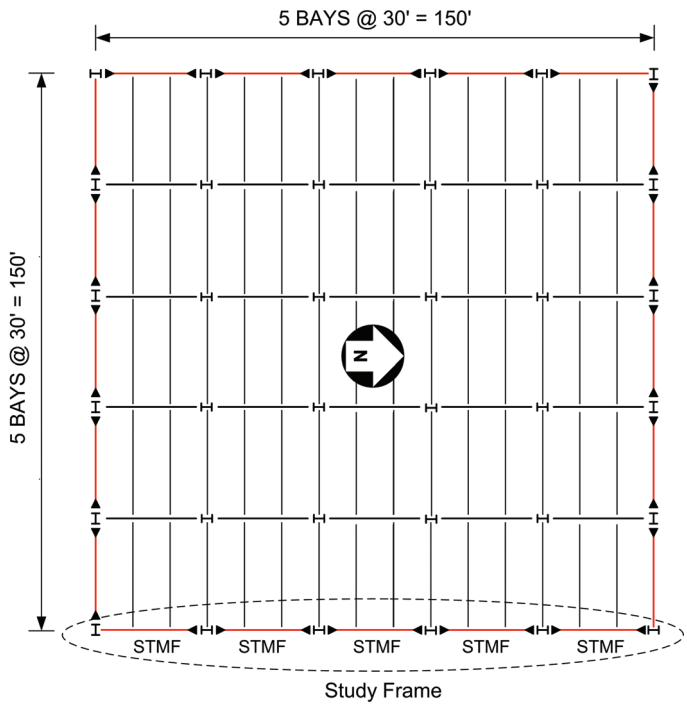

(a)

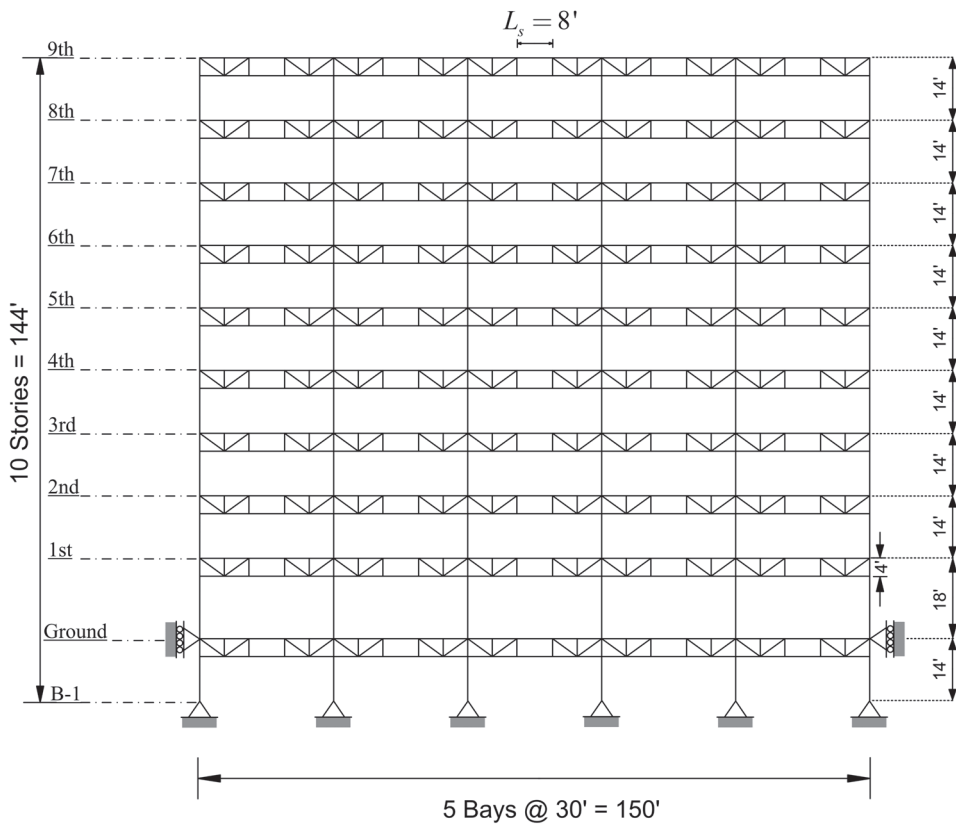

(b)

Fig. 12. Building plan and elevation of study STMFs.

DESIGN AND ANALYSIS OF THE STUDY FRAMES

Two nine-story STMFs, representing essential facilities (in other words, hospital buildings) and ordinary occupancy (office/residential) type, were designed by using the proposed procedure. The building plan and elevation are shown in Figure 12. For an ordinary occupancy building, the target drifts of 2% and 3% for 10% in 50 years [2/3 maximum considered earthquake (MCE)] and 2% in 50 years (MCE) design hazard levels, respectively, were chosen. These values were chosen to be consistent with the current design practice. The corresponding numbers for essential buildings were 1.5% and 2.25%. Design spectral values were based on NEHRP Provisions for the San Francisco site (NEHRP, 2000). The final member sections for the two study frames are shown in Figures 13 through 16. In this study, the column sizes were changed at every floor for study purposes. In practice, column sizes can be changed every two or three floors instead of every floor. This would somewhat increase the material weight but reduce the fabrication cost, due to the reduction of column splices. It is also noted that, to avoid biaxial bending in the exterior columns, the lower chord member adjacent to the exterior column bending about the weak axis is not connected to the column (see Figures 13 and 15).

After the final design work was completed, nonlinear response history analyses were conducted to study the response and ductility demands of the frames. Nine 10% in 50 years,

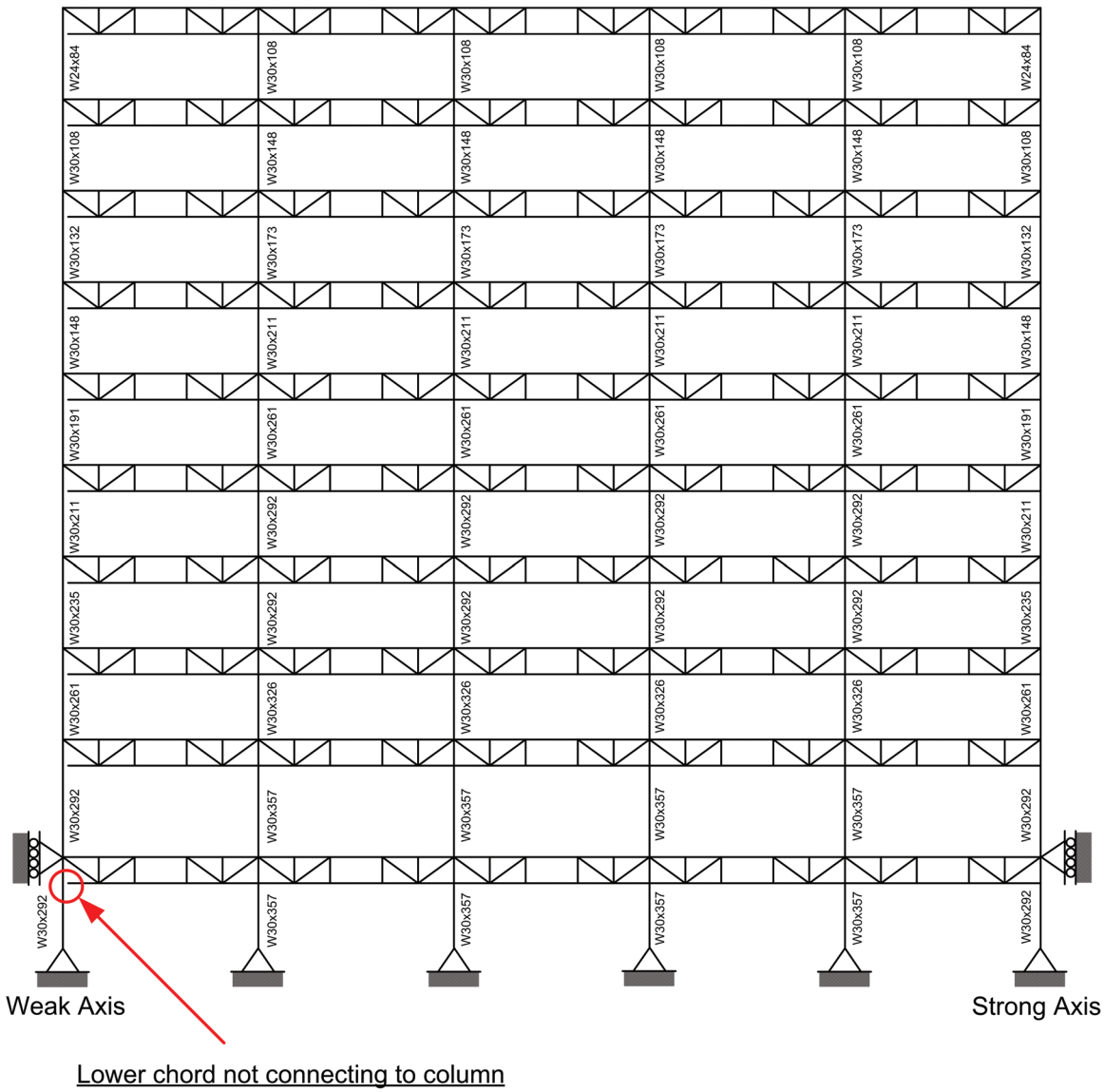

Fig. 13. Design column sections for the nine-story ordinary STMF.

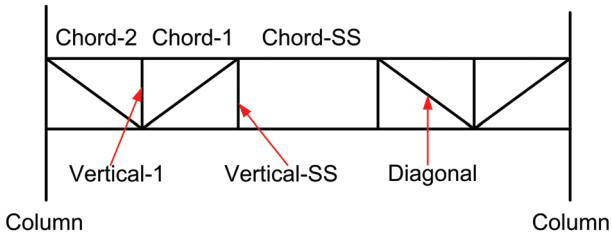

FLR	Chord-SS	Chord-1	Chord-2	Vertical-SS	Vertical-1	Diagonal
9	C7×12.25	C7×12.25	C7×12.25× (0.25-in. plate)	C7×12.25	MC6×12	MC6×12
8	C8×18.75	C8×18.75	C8×18.75× (0.5-in. plate)	C8×18.75	MC6×12	MC6×16.3
7	C9×20	C9×20	C9×20× (0.75-in. plate)	C9×20	MC6×12	MC7×22.7
6	C10×20	C10×20	C10×20× (1.0-in. plate)	C10×20	MC6×12	MC7×22.7
5	C10×25	C10×25	C10×25× (1.25-in. plate)	C10×25	MC6×12	MC9×25.4
4	C10×25	C10×25	C10×25× (1.25-in. plate)	C10×25	MC6×12	MC9×25.4
3	C10×25	C10×25	C10×25× (1.25-in. plate)	C10×25	MC6×12	MC9×25.4
2	C10×30	C10×30	C10×30× (1.5-in. plate)	C10×30	MC6×16.3	M10×C25
1	C10×30	C10×30	C10×30× (1.5-in. plate)	C10×30	MC6×16.3	M10×C25
B-1	C10×30	C10×30	C10×30× (1.5-in. plate)	C10×30	MC6×16.3	M10×C25

Note 1: All sections are double channels.
Note 2: B-1 Level uses the same sections as at Level 1.
Note 3: Web plates are extended over the whole length of the corresponding panel, i.e., 5.5 ft.

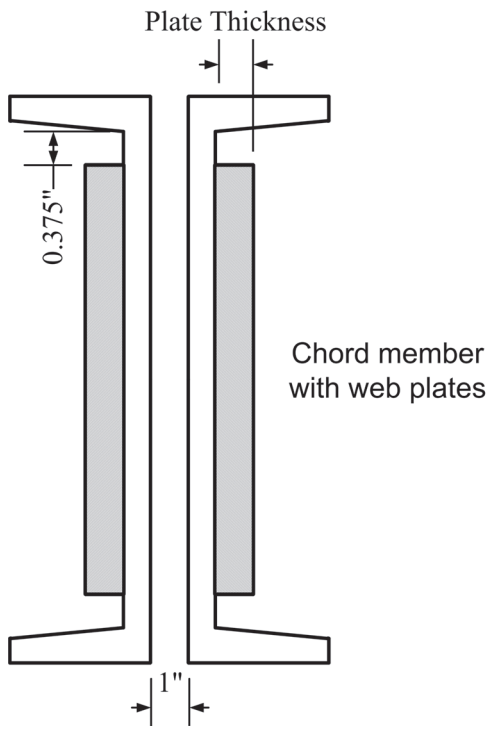

Fig. 14. Design special segment and truss member sections for the nine-story ordinary STMF.

and five 2% in 50 years SAC* Los Angeles region ground motions representing the two design hazard levels were used (Somerville et al., 1997). The results of the analyses were studied to validate the design procedure, and to compare the chord member ductility demands with the capacities as determined from the testing work on built-up double-channel specimens (Parra-Montesinos, Goel and Kim, 2006). The seismic performance of the study frames was examined in terms of location of yielding, maximum plastic rotation in chord members, maximum interstory drift, peak floor accelerations, and maximum relative story shear distribution. The analyses were performed using the Perform-2D (RAM, 2003) program. $P - \delta$ effect was accounted for in the analysis. However, the "leaning columns" with vertical loading from gravity frames were not included in this study because the interstory drifts were not large enough to induce significant P–Δ effect. At the same time, the beneficial effect of the "leaning columns" to provide additional lateral strength was ignored. These two assumptions should be offsetting each other's influence on the response. Detailed modeling for the nonlinear analyses can be found elsewhere (Chao and Goel, 2006).

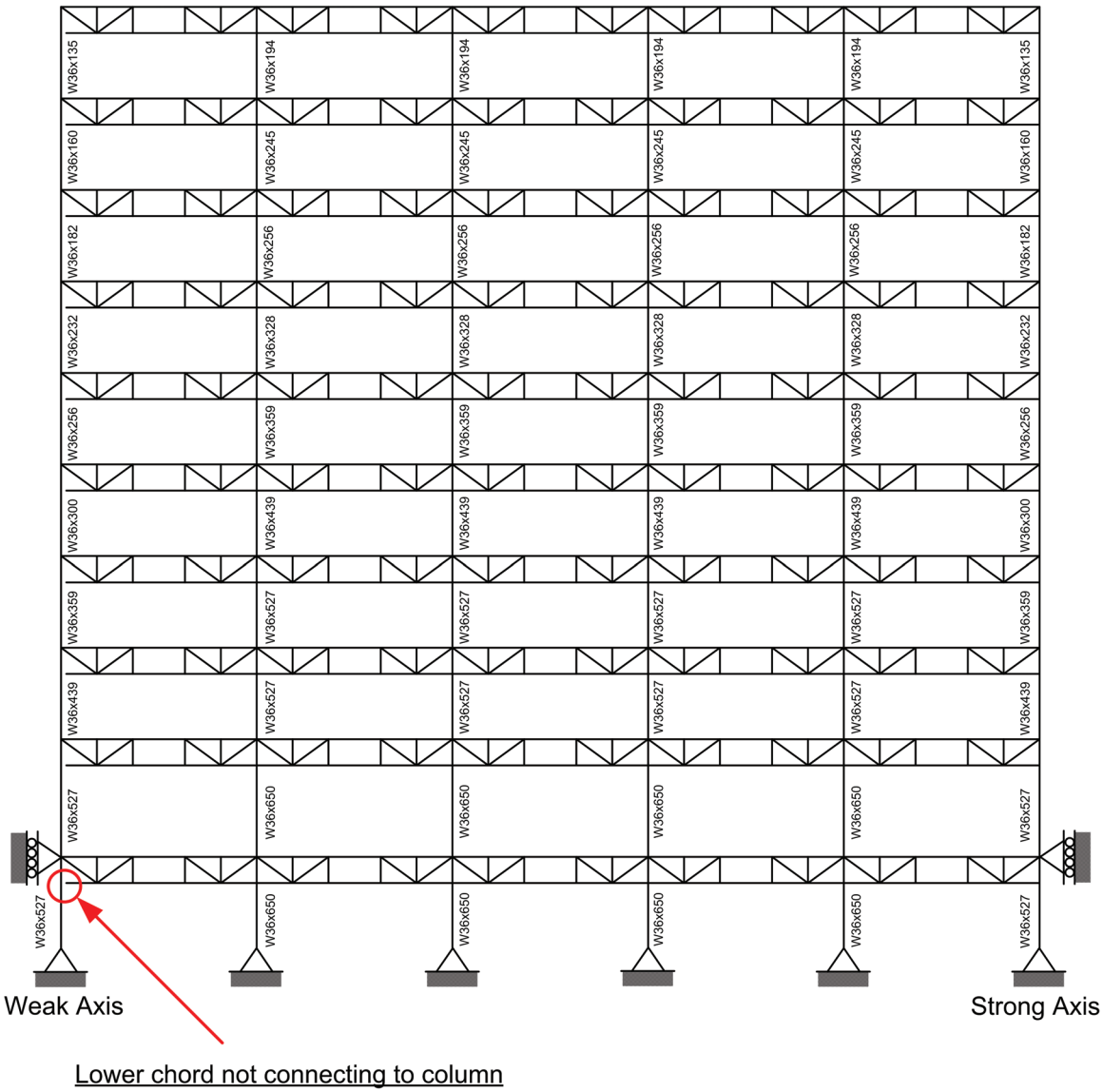

Fig. 15. Design column sections for the nine-story essential STMF.

*A joint venture partnership of Structural Engineers Association of California, Applied Technology Council, and California Universities for Research in Earthquake Engineering

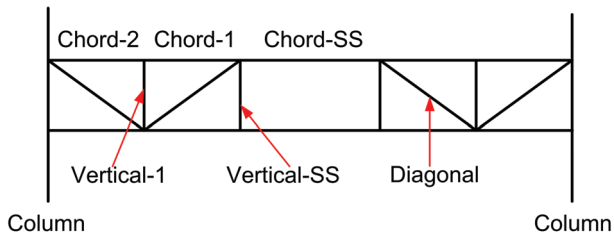

FLR	Chord-SS	Chord-1	Chord-2	Vertical-SS	Vertical-1	Diagonal
9	C9×20	C9×20	C9×20× (0.25-in. plate)	C9×20	MC6×12	MC9×25.4
8	C10×25	C10×25	C10×25× (0.5-in. plate)	C10×25	MC6×12	MC9×25.4
7	C10×30	C10×30	C10×30× (0.75-in. plate)	C10×30	MC6×12	MC9×25.4
6	C12×30	C12×30× (0.25-in. plate)	C12×30× (1.0-in. plate)	C12×30	MC6×12	MC10×41.1
5	C12×30	C12×30× (0.25-in. plate)	C12×30× (1.0-in. plate)	C12×30	MC7×22.7	MC10×41.1
4	MC12×31	MC12×31× (0.25-in. plate)	MC12×31× (1.25-in. plate)	MC12×31	MC7×22.7	MC10×41.1
3	MC12×31	MC12×31× (0.25-in. plate)	MC12×31× (1.25-in. plate)	MC12×31	MC7×22.7	MC10×41.1
2	MC12×35	MC12×35× (0.25-in. plate)	MC12×35× (1.5-in. plate)	MC12×35	MC7×22.7	MC10×41.1
1	MC12×35	MC12×35× (0.25-in. plate)	MC12×35× (2.0-in. plate)	MC12×35	MC8×22.8	MC10×41.1
B-1	MC12×35	MC12×35× (0.25-in. plate)	MC12×35× (2.0-in. plate)	MC12×35	MC8×22.8	MC10×41.1

Note 1: All sections are double channels.
Note 2: B-1 Level uses the same sections as at Level 1.
Note 3: Web plates are extended over the whole length of the corresponding panel, i.e., 5.5 ft.

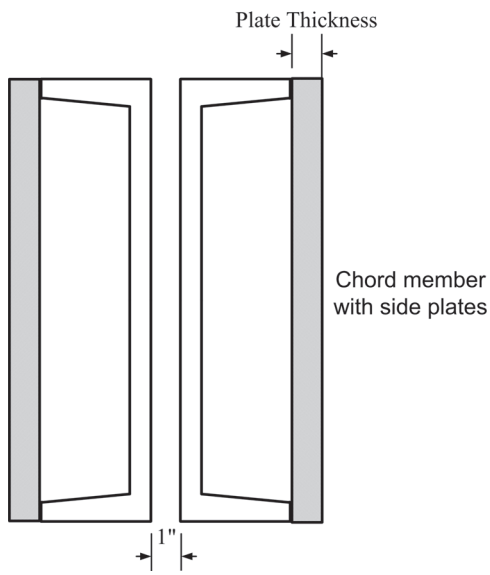

Fig. 16. Design special segment and truss member sections for the nine-story essential STMF.

PERFORMANCE EVALUATION OF THE STUDY FRAMES

Maximum Plastic Rotation in the Special Segments

Analysis results showed that plastic hinges occurred mainly at the ends of the chord members in the special segments, while the other elements remained elastic. It can be concluded that STMFs designed by the proposed performance-based plastic design (PBPD) approach resulted in the formation of a mechanism as intended. Maximum plastic hinge rotations at all levels for the two study frames are shown in Figures 17 and 18, along with their mean values from all ground motions.

As can be seen, the maximum plastic hinge rotation is about 0.04 rad when subjected to 10% in 50 years ground motions and 0.08 rad when subjected to 2% in 50 years ground motions. The peak mean values of the rotations are about 0.022 rad and 0.055 rad for 10% in 50 years and 2% in 50 years ground motions, respectively. It should be mentioned that tests of double-channel sections for STMF showed plastic rotation capacity on the order of 0.07 rad (Parra-Montesinos et al., 2006). The plastic rotations are generally uniformly distributed along the height of the frames, which is thought to be primarily due to the design lateral force distribution used in this study.

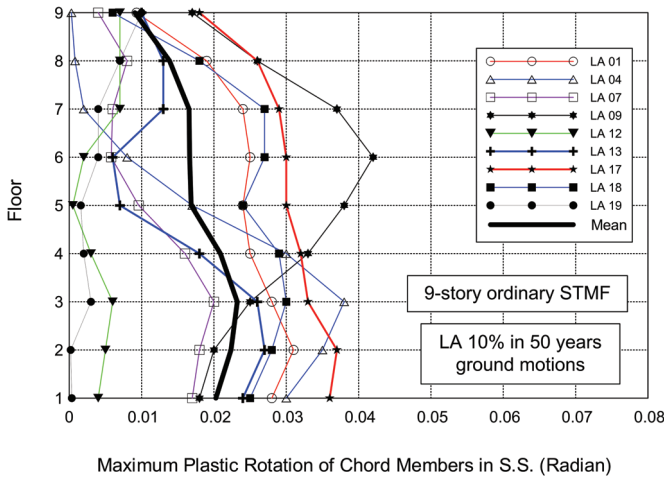

(a)

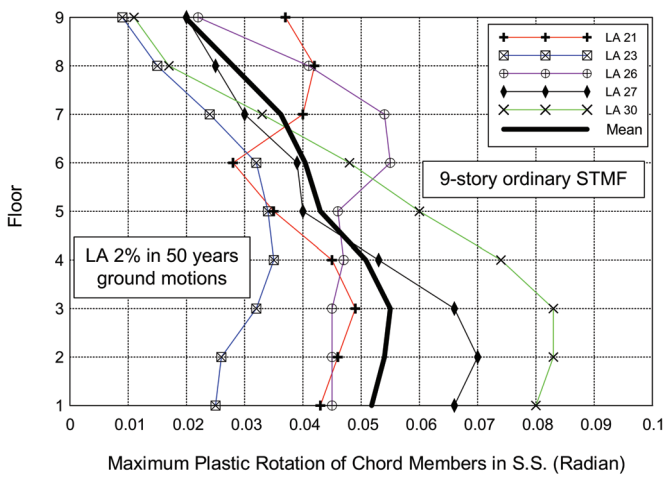

(b)

Fig. 17. Maximum plastic hinge rotations in chord members for nine-story ordinary STMF subjected to 10%/50 and 2%/50 ground motions.

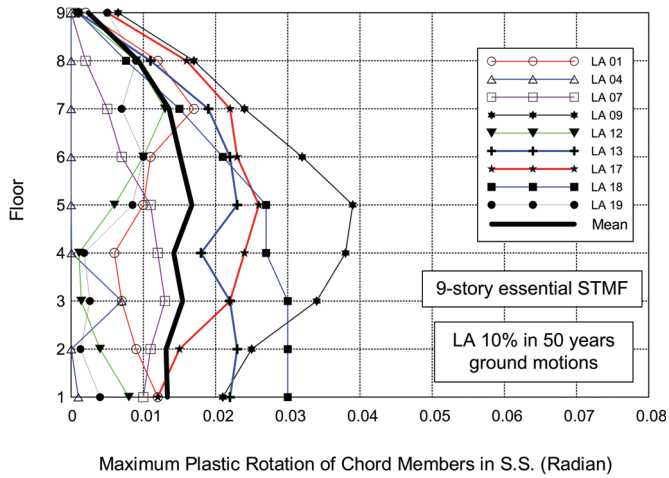

(a)

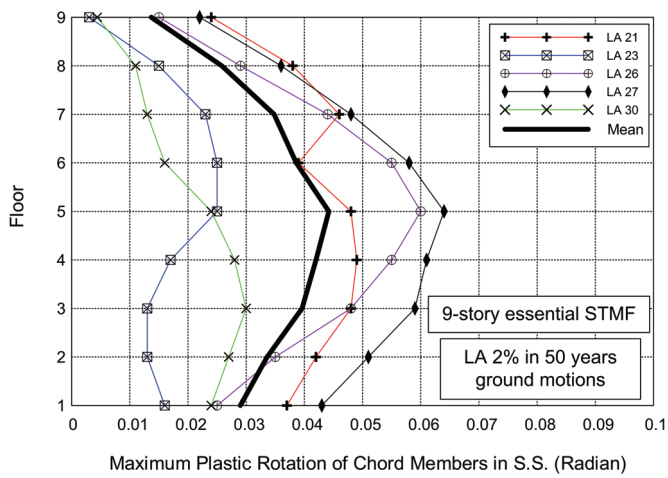

(b)

Fig. 18. Maximum plastic hinge rotations in chord members for nine-story essential STMF subjected to 10%/50 and 2%/50 ground motions.

Maximum Interstory Drifts

Figures 19 and 20 show the maximum interstory drifts for the ordinary and essential STMFs, respectively. The mean values of maximum story drifts and corresponding target drifts are also shown. It can be noticed that all the maximum interstory drifts of the PBPD frames were within the pre-selected target drift limits for the hazard levels, signifying that the seismic performance of the deformation-sensitive components (such as cladding, partitions, interior veneers, and glazing systems), as well as the chord member damage can be kept within target limits by the proposed design procedure.

Maximum Absolute Floor Accelerations

As seen in Figure 21, the maximum absolute floor accelerations of the two study STMFs are generally below the code-specified floor design acceleration except at a few lower levels, indicating that the seismic performance of the acceleration-sensitive components (such as mechanical equipment, piping systems, and storage vessels) can also be expected to be satisfactory. Higher floor accelerations in the essential STMF are primarily the result of higher stiffness of the essential STMF, which is known to cause greater floor accelerations (Mayes, Goings, Naguib, Harris, Lovejoy, Fanucci, Bystricky and Hayes, 2004).

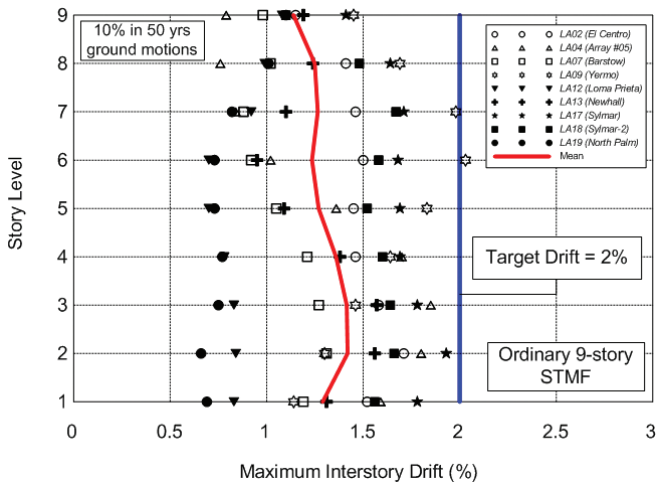

(a)

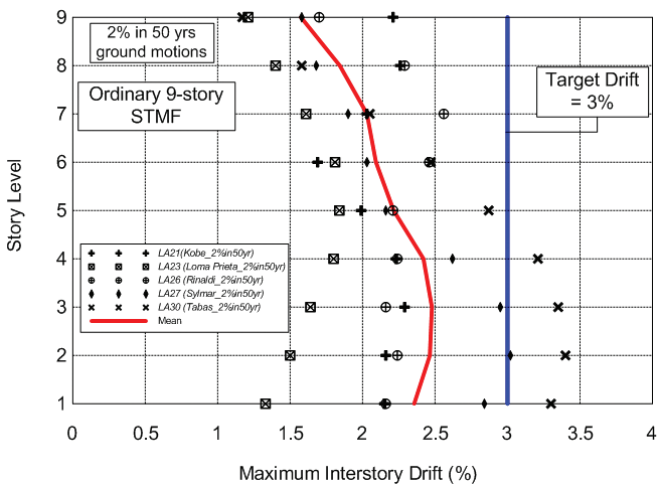

(b)

Fig. 19. Mean value of maximum interstory drifts and corresponding target drifts for the nine-story ordinary STMF.

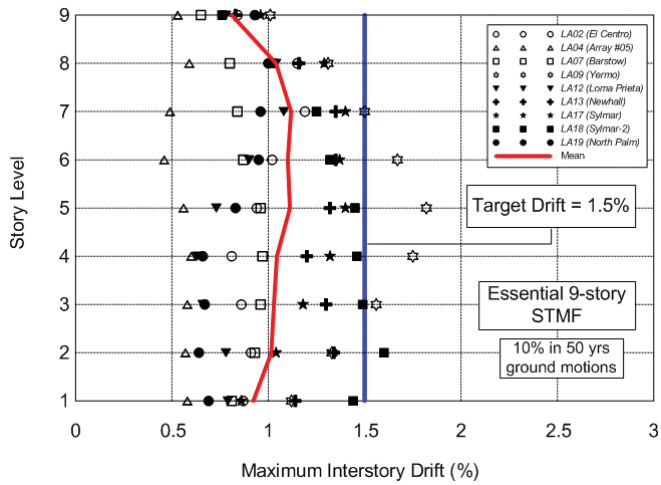

(a)

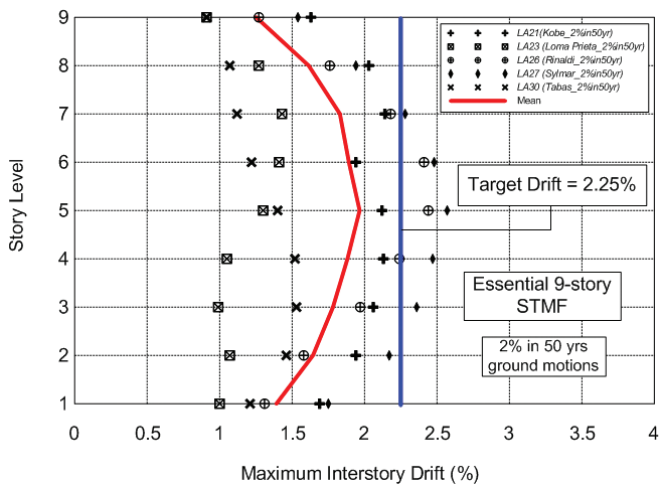

(b)

Fig. 20. Mean value of maximum interstory drifts and corresponding target drifts for the nine-story essential STMF.

Maximum Relative Story Shear Distributions

The maximum relative story shear distributions (namely, the story shear in any story divided by the story shear in the top story) obtained from nine 10% in 50 years, and five 2% in 50 years response histories for the nine-story ordinary STMF are shown in Figure 22. It can be seen that the proposed design story shear distribution well represents the mean story shear distribution of the structure due to the ground motion records used in this study. Relative story shear distributions according to NEHRP (NEHRP, 2000) and the *Uniform Building Code* (UBC 97) (ICBO, 1997) expressions are also plotted. It can be seen that while the NEHRP distribution shows significant deviation from those obtained from nonlinear dynamic analyses the UBC distribution gives better prediction. This may be attributed to the additional concentrated force applied at the top floor by using the UBC expression. The results suggest that the NEHRP distribution (also the distribution used by current IBC Provisions), which is generally based on the first mode elastic story shear distribution including some higher mode effects, does not predict the realistic maximum story shear distribution during major earthquakes (Chao et al., 2007). The proposed design force distribution does it much better because it is based on inelastic response results.

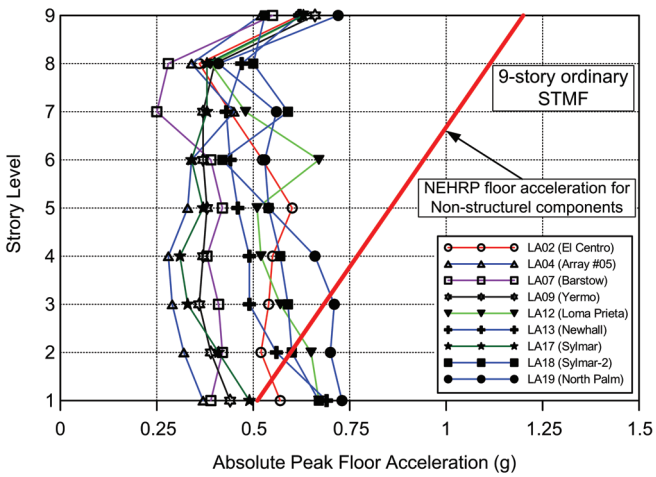

(a)

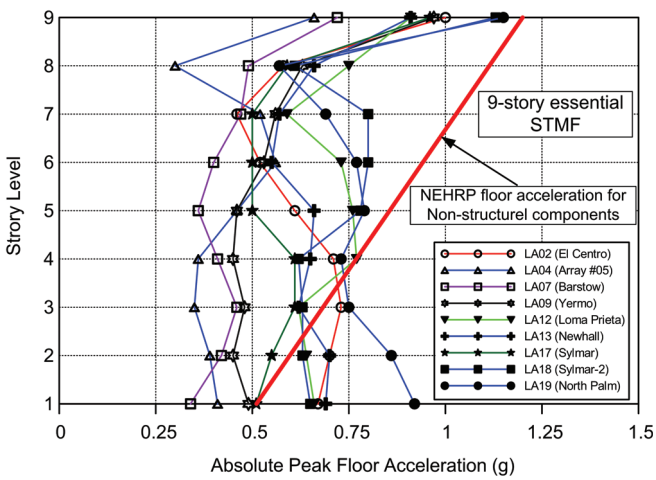

(b)

Fig. 21. Peak floor accelerations (10% in 50 years) and the NEHRP-specified design acceleration for acceleration-sensitive nonstructural components: (a) ordinary STMF; (b) essential STMF.

DESIGN EXAMPLE

The proposed performance-based plastic design (PBPD) procedure is summarized in the flowcharts given in Figures 10 and 11 using the nine-story ordinary STMF example. The main steps in the procedure are:

1. The basic design parameters are first obtained from NEHRP 2000 as summarized in Table 1.

2. The design base shear is determined for a two-level performance criteria: (a) a 2% maximum story drift for a ground motion hazard with 10% probability of exceedance in 50 years (10/50 and 2/3 MCE) and (b) 3% maximum story drift for 2/50 event (MCE). Then the modified design parameters are calculated and listed in Table 2. The design base shear is obtained from Equations 3, 14, and 15. After knowing the design base shear, the lateral forces are calculated by using Equations 1, 2 and 3 as shown in Tables 3 and 4. It is seen from Tables 1 and 2 that for this example the PBPD design base shear is 1.77 times that obtained from NEHRP 2000. This is explained as follows: (1) the drift control is built into the PBPD design base shear expression, and (2) the base shear in the proposed method corresponds to the global yield mechanism while that from NEHRP is intended for use with elastic design methods.

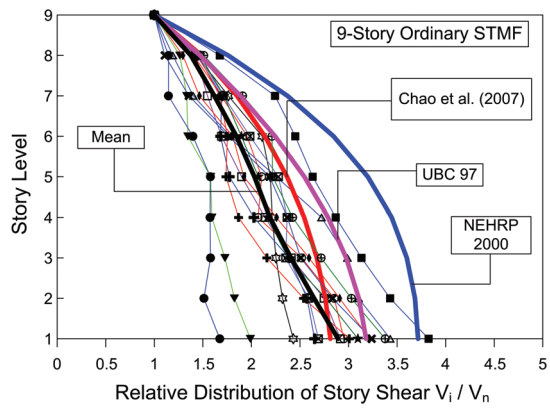

Fig. 22. Relative story shear distributions obtained from nonlinear dynamic analyses.

Table 1. Design Parameters for Nine-Story Ordinary STMF Calculated According to NEHRP 2000	
Parameters	**Nine-Story STMF**
S_S	1.50 g
S_1	0.78 g
S_{MS}	1.50 g
S_{M1}	1.01 g
F_a	1.000
F_v	1.3
S_{DS}	1.00 g
S_{D1}	0.68 g
Site Class	*C*
Occupancy Importance Factor, *I*	1.0 (Ordinary Building)
Seismic Design Category	*E*
Building Height	130 ft (above the base)
T_a	1.375 sec
C_U	1.4
T	1.925 sec
Response Modification Factor, *R*	7
Total Building Weight, *W*	19839 kips
$C_s = V/W$	0.056

Table 2. Design Parameters for the PBPD Procedure		
Parameters	**10% in 50-Year Hazard**	**2% in 50-Year Hazard**
S_a	0.39 g	0.525 g
T	1.925	1.925
Yield Drift, θ_y	0.75%	0.75%
Target Drift, θ_u	2%	3%
Inelastic Drift, θ_p	1.25%	2.25%
$\mu_s = \theta_u/\theta_y$	2.67	4
R_μ	2.67	4
γ	0.609	0.438
α	0.841	1.515
V/W	0.099	0.076
Design Base Shear, *V*	1956.1 kips (governs)	1504.3 kips

Table 3. Shear Distribution Factor for the Nine-Story Ordinary STMF						
Floor	h_j (ft)	w_j (kips)	$w_j h_j$ (kip-ft)	$\sum_{j=i}^{n} w_j h_j$	β_i (= V_i / V_n)	$(\beta_i - \beta_{i+1})h_i$
9	130	2357	306410	306410	1.000	130.00
8	116	2180	252880	559290	1.486	56.34
7	102	2180	222360	781650	1.852	37.34
6	88	2180	191840	973490	2.139	25.31
5	74	2180	161320	1134810	2.367	16.80
4	60	2180	130800	1265610	2.543	10.57
3	46	2180	100280	1365890	2.673	6.02
2	32	2180	69760	1435650	2.762	2.85
1	18	2222	39996	1475646	2.813	0.91

Table 4. Design Lateral Forces for the Nine-Story Ordinary STMF (for Two Frames)		
Floor	$\beta_i - \beta_{i+1}$	F_i, kips
9	1.000	695.4
8	0.486	337.8
7	0.366	254.6
6	0.288	200.1
5	0.227	157.9
4	0.176	122.5
3	0.131	91.0
2	0.089	61.9
1	0.050	35.1

Table 5. Required Chord Member Strength and Selected Chord Member Sections						
Floor	Require Moment Strength $\beta_i M_{pbr}$, kip-ft	Required Z, in.^{3}	Section* (Double Channels)	Z, in.^{3}	M_{nc}, kip-in.	I_x, in.^{4}
9	61.0	16.3	C7×12.25	16.92	846	48.4
8	90.6	24.2	C8×18.75	27.8	1390	87.8
7	112.9	30.1	C9×20	33.8	1690	121.8
6	130.5	34.8	C10×20	38.8	1940	157.8
5	144.3	38.5	C10×25	46.2	2310	182.2
4	155.1	41.4	C10×25	46.2	2310	182.2
3	163.0	43.5	C10×25	46.2	2310	182.2
2	168.5	44.9	C10×30	53.4	2670	206
1	171.6	45.7	C10×30	53.4	2670	206

*Section sizes taken from the 3rd Ed. AISC *Load and Resistance Factor Design Manual of Steel Construction*.

Table 6. Compactness Check for Chord Member Sections per AISC *Seismic Provisions* Table I-8-1

Floor	Width-Thickness Ratio $\frac{b_f}{t_f}$	Limiting Width-Thickness Ratio $0.3\sqrt{\frac{E_s}{F_y}}$	Width-Thickness Ratio $\frac{d}{t_w}$	Limiting Width-Thickness Ratio* $1.12\sqrt{\frac{E_s}{F_y}}\left(2.33-\frac{P_u}{\phi_b P_y}\right)$
9	5.98	7.22	22.3	35.87
8	6.49	7.22	16.4	35.87
7	6.42	7.22	20.1	35.87
6	6.28	7.22	26.4	35.87
5	6.63	7.22	19.0	35.87
4	6.63	7.22	19.0	35.87
3	6.63	7.22	19.0	35.87
2	6.95	7.22	14.9	35.87
1	6.95	7.22	14.9	35.87

*Note: Conservatively $P_u = \phi_b P_y$ was assumed even though the chord members in the special segment are generally subjected to small axial forces.

3. The required plastic moment of the first-story columns is computed as (Equation 17):

$$M_{pc} = \frac{1.1V'h_1}{4}$$
$$= \left(1.1 \times \frac{1956.1 \text{ kips}}{(2)(5)} \times 18 \text{ ft}\right)/4$$
$$= 968.3 \text{ kip-ft}$$

Note that V' is the base shear for one bay (in each direction of the building there are two STMFs and each STMF has five bays, see Figure 12).

4. The required chord member strength at each level is determined by using Equation 18. ASTM A992 steel with 50-ksi nominal yield strength is used. The selected chord sections for each level are given in Table 5 and the compactness check is shown in Table 6.

5. Design of members (chords, verticals, diagonals and columns) outside the special segment is based on the capacity design approach (see Figure 11 for design flowchart). It should be noted that the lateral forces at each level are those needed to develop the expected ultimate strength of the special segments, in other words, V_{ne}. The applied forces on the interior and exterior column free-bodies are shown in Table 7. Figure 23 shows the forces acting on the interior column free-body. The required elastic moment and axial force for each element outside the special segment can be easily obtained by using an elastic structural analysis. All the elements are designed as beam-column elements, according to the AISC *Specification for Structural Steel Buildings* (AISC, 2005b). The final sections are shown in Figures 13 and 14.

SUMMARY AND CONCLUSIONS

A direct performance-based plastic design (PBPD) approach, which requires no iterative evaluation or refinement such as by nonlinear static (pushover) or dynamic analysis after the initial design, has been presented. Based on an energy (work) concept and plastic design method, the proposed approach gives the design base shear by using the elastic design spectral value for a given hazard level, a preselected global structural yield mechanism, and a preselected target drift. The design lateral force distribution employed in the proposed method is based on nonlinear response history analysis results using a number of ground motions. The chord members are designed according to the AISC Seismic Provisions, while the members outside the special segment are designed by using a capacity design approach. The following conclusions can be drawn from this study:

1. All inelastic activity was confined to the special segments and the column bases in the study frames; that is, STMFs designed by the proposed PBPD method resulted in the formation of a yield mechanism as intended.

Table 7. Design Forces for Elements Outside Special Segments					
Floor	$(V_{ne})_i$ kips	Concentrated Factored Gravity Loading @ 10 ft Spacing in Each Bay, kips	Lateral Forces at Ultimate Drift Level for Exterior Column Free Body, kips		Lateral Forces at Ultimate Drift Level for Interior Column Free Body, kips
			$\alpha_i F_R$	$\alpha_i F_L$	F_i
9	55.5	16	68.5	78.0	146.4
8	94.6	15	33.3	37.9	71.1
7	121.5	15	25.1	28.5	53.6
6	147.1	15	19.7	22.4	42.1
5	172.7	15	15.5	17.7	33.2
4	172.7	15	12.1	13.7	25.8
3	172.7	15	9.0	10.2	19.2
2	197.6	15	6.1	6.9	13.0
1	197.6	15	3.4	3.9	7.4
∑	1332.0		192.6	219.3	411.9

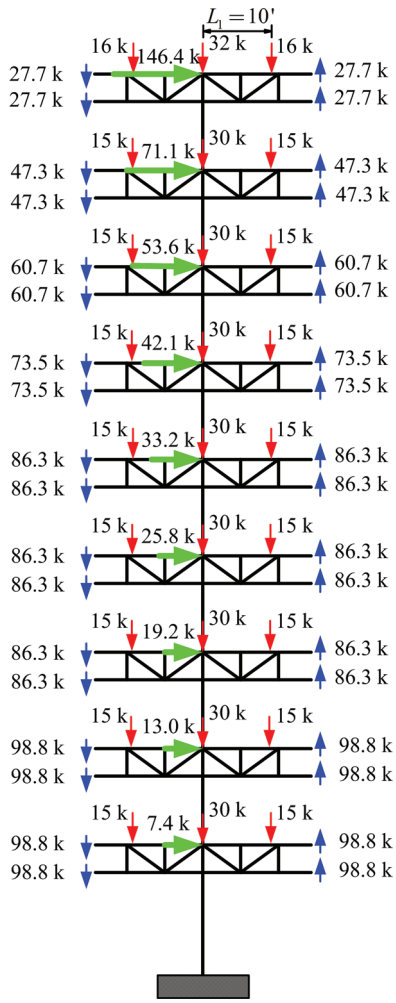

Fig. 23. Forces acting on the interior column free body (nine-story ordinary STMF).

2. The maximum plastic hinge rotations of chord members in the study frames were within the available rotation capacity for all 10% in 50 years ground motions used in this study. Moreover, the study frames generally showed quite uniformly distributed plastic rotations along the height, due to the use of the proposed lateral force distribution. This also leads to more even distribution of dissipated energy along the height.

3. It was observed that all interstory drifts of the study frames were within the 1.5% and 2% preselected target drift when the structure was subjected to the 2/3 MCE ground motions (first level hazard) for the ordinary and essential buildings, respectively. Also, most interstory drifts were within the 2.25% and 3% preselected target drift when the structure was subjected to the MCE ground motions (second level hazard) for the ordinary and essential buildings, respectively. This suggests that satisfactory seismic performance of the deformation-sensitive nonstructural components can also be achieved by the proposed design procedure.

4. The maximum absolute floor accelerations were generally within the code-specified values, suggesting that the seismic performance of the acceleration-sensitive components can also be assumed to be satisfactory.

5. Based on 14 time-history nonlinear dynamic analyses, the suggested design story shear distribution (lateral force distribution) represents the mean story shear distributions of the structure very well because it is based on inelastic behavior. On the contrary, the NEHRP (IBC) force distribution does not represent the expected maximum story shear distributions during strong earthquakes. The UBC expression, by providing an additional force at the top level, gave a more realistic relative story shear distribution than the NEHRP expression.

6. Overall, STMFs designed by the proposed performance-based plastic design (PBPD) method can be expected to satisfy the required performance objectives when subjected to a major earthquake. This is because the selected performance objectives in terms of the yield mechanism and maximum drift are explicitly built into the determination of design lateral forces and design of the frame members.

ACKNOWLEDGMENTS

The financial support for this study was provided by Nabih Youssef & Associates Structural Engineers, NUCOR Research and Development, and the G.S. Agarwal Fellowship Fund in the Department of Civil and Environmental Engineering at the University of Michigan. The opinions and views expressed in this paper are solely those of the authors and do not necessarily reflect those of the sponsors.

REFERENCES

AISC (2005a), *Seismic Provisions for Structural Steel Buildings*, ANSI/AISC 341-05, American Institute of Steel Construction, Chicago, IL.

AISC (2005b), *Specification for Structural Steel Buildings,* ANSI/AISC 360-05, American Institute of Steel Construction, Chicago, IL.

Akiyama, H. (1985), "Earthquake-Resistant Limit-State Design of Buildings," University of Tokyo Press, Japan.

ASCE (2000), "Prestandard and Commentary for the Seismic Rehabilitation of Buildings," *FEMA 356 Report*, prepared by the American Society of Civil Engineers, published by Federal Emergency Management Agency, Washington, DC.

ATC (1996), "Seismic Evaluation and Retrofit of Concrete Buildings," *ATC-40 Report*, Vol. 1 & 2, Applied Technology Council, Redwood City, CA.

ATC (2004), "Improvement of Nonlinear Static Seismic Analysis Procedures (Draft)," *FEMA 440 Report*, Applied Technology Council, Redwood City, California and Federal Emergency Management Agency, Washington, DC.

Basha, H.S. and Goel, S.C. (1994), "Seismic Resistant Truss Moment Frames with Ductile Vierendeel Segment," *Report No. UMCEE 94-29*, Department of Civil and Environmental Engineering, University of Michigan, Ann Arbor, MI.

Basha, H.S. and Goel, S.C. (1995), "Special Truss Moment Frames with Vierendeel Middle Panel," *Engineering Structures*, Vol. 17, No. 5, pp. 352–358.

Chao, S.-H. and Goel, S.C. (2005), "Performance-Based Seismic Design of EBF Using Target Drift and Yield Mechanism as Performance Criteria," *Report No. UMCEE 05-05*, Department of Civil and Environmental Engineering, University of Michigan, Ann Arbor, MI.

Chao, S.-H. and Goel, S.C. (2006), "Performance-Based Plastic Design of Seismic Resistant Special Truss Moment Frames," *Report No. UMCEE 06-03*, Department of Civil and Environmental Engineering, University of Michigan, Ann Arbor, MI.

Chao, S.-H., Goel, S.C., and Lee, S.S. (2007), "A Seismic Design Lateral Force Distribution Based on Inelastic State of Structures," *Earthquake Spectra,* Earthquake Engineering Research Institute, Vol. 23, No. 3, August, pp. 547–569.

FEMA (2000), "Prestandard and Commentary for the Seismic Rehabilitation of Buildings," FEMA 356, Federal Emergency Management Agency, Washington, DC.

Goel, S.C. and Itani, A.M. (1994), "Seismic-Resistant Special Truss-Moment Frames," *Journal of Structural Engineering*, ASCE, Vol. 120, No. 6, pp. 1781–1797.

ICBO (1997), *Uniform Building Code*, International Conference of Building Officials, Whittier, CA.

Lee, S.S., Goel, S.C. and Chao, S.-H. (2004), "Performance-Based Design of Steel Moment Frames Using Target Drift and Yield Mechanism," *Proceedings,* 13th World Conference on Earthquake Engineering, Paper No. 266, Vancouver, BC, Canada.

Leelataviwat, S., Goel, S.C. and Stojadinović, B. (1999), "Toward Performance-Based Seismic Design of Structures," *Earthquake Spectra*, Vol. 15, No. 3, pp. 435–461.

Mayes, R.L., Goings, C., Naguib, W. Harris, S., Lovejoy, J., Fanucci, J.P., Bystricky, P. and Hayes, J.R. (2004), "Comparative Performance of Buckling-Restrained Braces and Moment Frames," *Proceedings,* 13th World Conference on Earthquake Engineering, Paper No. 2887, Vancouver, BC, Canada.

NEHRP (2000), "Recommended Provisions for the Development of Seismic Regulations for New Buildings (FEMA 368) and Commentary (FEMA 369)," Federal Emergency Management Agency, Washington, DC.

Newmark, N.M. and Hall, W. J. (1982), "Earthquake Spectra and Design," Earthquake Engineering Research Institute, El Cerrito, CA.

Parra-Montesinos, G.J., Goel, S.C. and Kim, K.Y. (2006), "Behavior of Steel Double-Channel Built-Up Chords of Special Truss Moment Frames under Reversed Cyclic Bending," *Journal of Structural Engineering*, ASCE, Vol. 132, No. 9, pp. 1343–1351.

RAM International (2003), "Perform-2D User Guide."

SEAOC (1999), "Recommended Lateral Force Requirements and Commentary," Seismology Committee of Structural Engineers Association of California, Sacramento, California, 7th Edition.

Somerville, P.G., Smith, M., Punyamurthula, S. and Sun, J. (1997), "Development of Ground Motion Time Histories for Phase 2 of the FEMA/SAC Steel Project," *Report No. SAC/BD-97/04*, SAC Joint Venture, Sacramento, CA.

Current Steel Structures Research

REIDAR BJORHOVDE

Structural steel research touches a number of closely related and sometimes maybe not so closely related subjects. For example, columns are connected to concrete footings by anchor rods, the joint action of which affect the response of the steel member and the steel frame. Steel beams may be connected to a concrete shear wall or to a glulam rafter, all of which require special considerations because of the use of significantly different materials. And the material response characteristics must be taken into account, both with respect to short- and long-term behavior aspects. Conditions such as humidity (for example) affects the steel for corrosion, but it may play a major role at all times during the service life of the structure, because wood and concrete both shrink and/or expand as a function of humidity. How do façade attachments influence the response of the spandrels or other steel members to which they are connected? What about the use of cold-formed steel elements or stainless steel? Standards are certainly available, but practical and intelligent designs go well beyond computations in accordance with structural code requirements.

The preceding observations reflect some real conditions for the constructed project, and the designers and fabricators and general contractors have to be able to address the diverse needs of the structure. And what must be done about loading conditions that come at the designer in literally hundreds of combinations? What about floor vibrations, which can be a serious issue, even though they may not endanger the stability or strength of the structure? What about roof deflections or strength needs under the conditions of ponding? Numerous questions of these kinds arise every year, and it is the engineer's responsibility to ensure that all realistic conditions have been addressed.

It is interesting and most useful to note that the Canadian Institute of Steel Construction (CISC) is currently undertaking an effort to examine the issues surrounding steel and other materials as used in combination in buildings. The first two articles have been published (Leckie, 2007a, 2007b); the third will appear in 2008. Design and construction practices in Canada are extremely similar to what is used in the United States, and American practitioners will clearly benefit from these evaluations.

The findings that are presented in this paper reflect a broad range of state-of-the-art work. A recent project in Spain is one of the first to examine the tested behavior of two-dimensional (2D) versus three-dimensional (3D) connections and how they compare and influence each other. A Canadian study focuses on connections to rectangular hollow sections (RHS), using various plate attachments. An unusual project in Finland examines a novel approach to optimization of steel beam design, attempting to cover all feasible parameter ranges and limit states. Fatigue in tubular structures is a major, long-term effort in Switzerland, as part of an intensive bridge design and construction program. The study discussed here examines micro- and macro-structural size effects. Orthotropic bridge decks are used extensively in Europe; the French "Orthoplus Project" applies advanced concepts to these types of bridge decks, including surfacing solutions. Finally, a multi-year major effort in the Netherlands dealing with the numerous issues of ponding of roof structures has come to fruition, and a detailed analysis and design report has now been published.

References are provided throughout the paper, whenever such are available in the public domain. However, much of the work is still in progress, and reports or publications have not yet been prepared for public dissemination.

CONNECTION BEHAVIOR AND STRENGTH

Three-Dimensional Behavior of Semi-Rigid Connections: This project has been conducted at the University of Navarra in Pamplona, Spain, with Professor Eduardo Bayo as the director (Cabrero and Bayo, 2007a, 2007b).

The most common approach to steel frame analysis and design is based on planar (2D) modeling, although realistic assessments should reflect 3D behavior. Further, most, if not all connections are semi-rigid (Type PR), and the effect on frame response can be significant. Unfortunately, most analyses have focused on 2D behavior with perfectly pinned or rigid connections, and almost all physical tests have been conducted in various forms of 2D representation.

Using extended end-plate beam-to-column connections for the strong as well as the weak axis of the column, Figure 1 shows the test specimen that was developed by the researchers in collaboration with several fabricators. The joints into the column are all bolted, but the end plates are welded to the beam ends. It is noted that the weak-axis connection is

Reidar Bjorhovde is the Research Editor of the AISC *Engineering Journal*.

not framed into the column web, but rather to plates that are welded to the column flange tips. The researchers observe that this solution means that the weak- and strong-axis connections will not interact, and the design can therefore be done individually for the connections. Finally, the weak axis plates are partial end plates, as can be seen in Figure 1. This was done to allow for easier tightening of the bolts.

The member dimensions are somewhat smaller than what is typical North American practice. The column shape for all specimens was an HEB 160 (160 mm = 5½ in. deep). The *x*-axis beam was an IPE 330 (330 mm = 13 in. deep); the *y*-axis beam was an IPE 240 (240 mm = 9½ in. deep). The shape steel grade was S350 (yield stress 350 MPa = 50 ksi); all plate material was grade S275 (yield stress 275 MPa = 40 ksi). Two end plate thicknesses were used: 16 mm (⅝ in.) and 10 mm (⅜ in.).

Figure 2 shows two of the connections following testing, with the one on the left having the thicker (16 mm) end plates and the one on the right with the thinner (10 mm) plates.

As would be expected, the connection strengths and stiffnesses were reduced when the smaller end plate thickness was used. Interestingly, the connections in both axes exhibited higher initial stiffness when 3D proportional loading was applied, meaning that there is a certain amount of coupling effects between the *x*- and *y*-directions. The stiffness increase due to coupling was about 15% for the *x*-axis connections; it was 8 to 23% for the *y*-axis connections.

The project has also provided an analytical component model for these connections, in line with the typical approach of Eurocode 3 (CEN, 2005). An extensive parametric study used a finite element evaluation with different loading conditions and geometric configurations, giving good correlation with the experimental results.

Behavior of Longitudinal Double Plates-to-RHS Connections: This project has been conducted at the University of British Columbia in Vancouver, BC, Canada, with Professor Siegfrid Stiemer as the director.

The aim of the project has been to evaluate the response characteristics of T-connections with longitudinal double plates connected to a rectangular hollow structural section. Seven double-plate and two single-plate connections were tested in a setup as shown in Figure 3. The primary test parameters were (1) the ratio of the width of the plates to the width of the RHS and (2) the type or number of plates.

As expected, the strength of the double-plate connection increased as the spacing between the plates was increased, and the double-plate connection had higher strength than the design using single plates with the same plate area. This is attributed to the fact that the width ratio for the double-plate connections is larger than that of the single-plate case. Further, the double plates are welded to the RHS in locations where the stiffness is greater than at the centerline of the section.

Yield-line analyses were performed for different locations of the plastic hinges that typically developed in the RHS, including in the wall next to the plate fillet welds and close to the corner radius. An example of such plastic hinge locations is shown in Figure 4. The connection strengths predicted by the yield-line model are in good agreement with the experimental data.

Continuing project work will address the effect of a range of width-to-thickness ratios for the main chord, and for double-plate connection width ratios larger than 0.80.

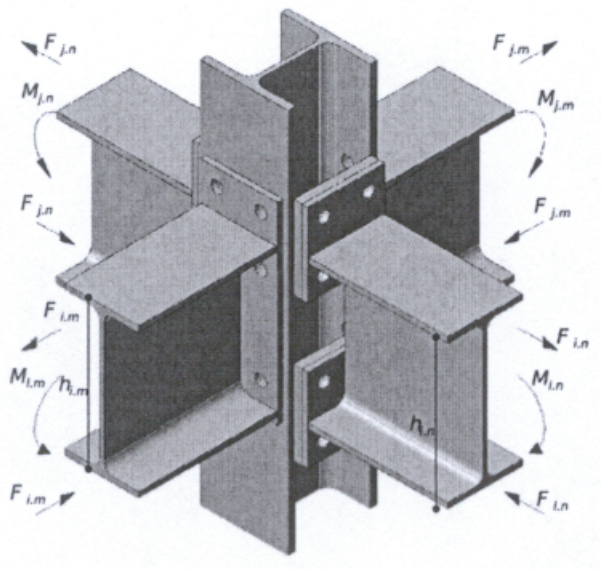

Fig. 1. Three-dimensional type PR connection (figure courtesy of Eduardo Bayo).

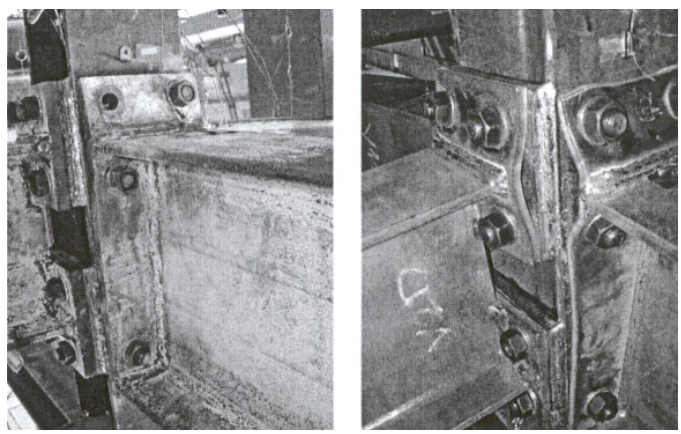

Fig. 2. Two specimens after testing (photo courtesy of Eduardo Bayo).

OPTIMIZATION OF WELDED BUILT-UP BEAM DESIGN

Welded Steel Beam Design Using Particle Swarm Analysis: This research project has been conducted at Tampere University in Tampere, Finland, in collaboration with Cardiff University in Cardiff, United Kingdom, as well as with two Finnish companies. Professor Markku Heinisuo has been the project director.

Particle swarm analysis or particle swarm optimization (PSO) is a relatively new approach to optimization, which has not found many applications in engineering at this time. However, it offers significant potential for analysis and design situations where there are a great many variables that control the final solution. Part of the problem is clearly that although it is feasible to arrive at acceptable solutions in terms of engineering theory, practice-oriented designs may not have come from the PSO algorithm.

The researchers first solved a carefully structured example, using a comprehensive search. On this basis the optimum design solution was found *a priori*, with the aim of examining the PSO approach through a scientifically valid test. At this stage of the research work it is noted that PSO does not perform well unless it is used as part of a multilayer procedure.

The study will be expanded to include comprehensive structural and fabrication features, as well as parameters that reflect design, transportation, erection, building use, life cycle costs and other relevant issues. The focus will be on the development of efficient search engines that can handle extremely large numbers of variables. Only time can tell whether the PSO approach will produce solutions that can be used in practice.

CONSTRUCTION AND PERFORMANCE OF BRIDGE STRUCTURES

Modeling of Micro- and Macro-Structural Size Effects for Fatigue of Welded Tubular Structures: This project reflects part of a major, long-time effort that has been carried out at the Federal Polytechnic University of Lausanne (EPFL) in Lausanne, Switzerland, under the direction of Professor Manfred Hirt and Senior Scientist Dr. Alain Nussbaumer.

The focus of this study has been the development of an accurate probabilistic fatigue crack growth model for tubular joints, and large-scale fatigue tests of relevant tubular connections with multiple possible crack sites have also been conducted (Walbridge and Nussbaumer, 2008). A novel approach to crack monitoring has been utilized—the researchers believe it is the first time it has been applied to a large-scale tubular truss beam. The method is known as the alternative current potential drop (ACDP), and it has proven to be very accurate and efficient. Fatigue cracks were found both in tension chords as well as in compression joints, and residual stresses were therefore incorporated into the ABAQUS finite element model. The approach also included sizing effects for different geometric parameters, to arrive at suitable stress intensity factors for different basic load cases. Further, proportional and nonproportional sizing effects were developed from the experimental database.

The research work is continuing, and emphasis will now be placed on various residual stress (RS) effects. This will include RS measurements on tubular truss beams and will

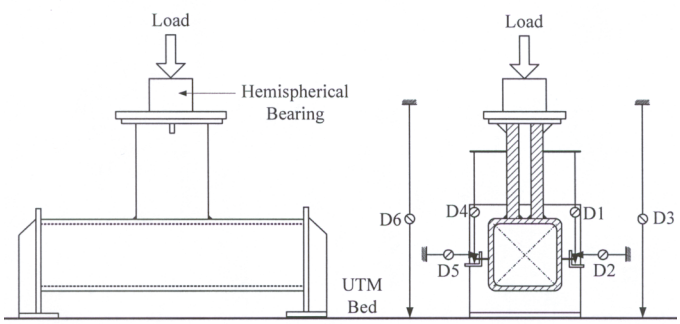

Fig. 3. Double plates to RHS connection test setup (figure courtesy of Siegfrid Stiemer).

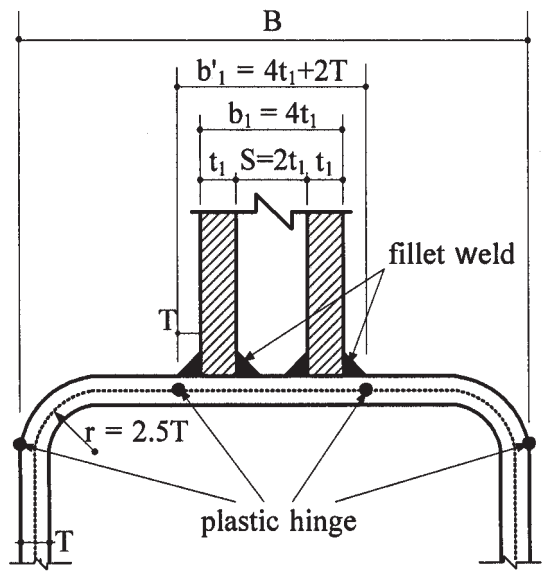

Fig. 4. Plastic hinge locations in RHS walls (figure courtesy of Siegfrid Stiemer).

eventually be extended to incorporate welding and post-weld treatment influences, to allow for scaling effects. It is expected that the design of a wide range of tubular structures will be significantly enhanced as a result of this project.

Advanced Engineering for Orthotropic Bridge Decks and Surfacing Solutions: This is a three-year research project now under way in France, known by the name Orthoplus. It is funded by the French national research agency (ANR) and involves efforts by seven public and private partners. The project director is Dr. Claude Le Quéré of the bridge organization Sétra.

The primary aim of Orthoplus is to provide criteria for the optimization of the design of orthotropic bridge decks (Le Quéré, 2007). Figure 5 shows a typical example from such decks, using the solution that was utilized for the famous bridge Viaduc de Millau south of Clermont-Ferrand. The modeling includes the composite action of the surface layer of the deck as well as the steel deck plate, including the fatigue mechanism in the steel plate.

New orthotropic plate theoretical approaches will be developed, along with tools of analysis that will give practical and realistic assessments of the duration (life) of the deck. The methodology will incorporate the influence of the type and thickness of the surfacing material.

PONDING OF ROOF STRUCTURES

Ponding of rain water can be a major problem for flat or near-flat roof structures (or even not so flat roofs if the drains are clogged), and most design codes include some form of criteria for the analysis and design for such loads. Appendix 2 of the AISC *Specification for Structural Steel Buildings* contains simplified and more advanced recommendations for ponding (AISC, 2005). The basis for these criteria were developed by Marino (1966), and they have functioned adequately since their introduction in the late 1960s.

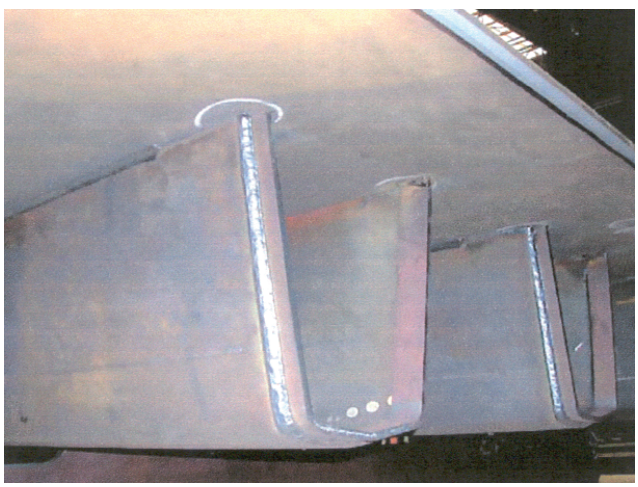

Fig. 5. Troughs of the deck of the Viaduc de Millau (photo courtesy of André Colson).

However, work at Delft University of Technology in Delft, the Netherlands, has resulted in a major report with case studies, failure analyses, and recommendations for improved design checks and methods of evaluation. The 200-page report has been published as part of the university's long-standing HERON report series (Heron, 2006), and it contains analyses and practical design suggestions on the following subjects:

- "Roof failures due to ponding—a symptom of underestimated development," by J.N.J.A. Vambersky
- "Ponding collapse analyses of light weight roof structures by water raising capacity," by S.N.M. Wijte
- "Structural design for ponding of rainwater on roof structures," by F. van Herwijnen, H.H. Snijder and H.J. Fijneman
- "Ponding on flat roofs: a different perspective," by J. Blaauwendraad
- "Evaluation of ponding analysis methods using 3-D finite element modeling," by A. Schouten, J. Locht and J.P.B.N. Derks

REFERENCES

AISC (2005), *Specification for Structural Steel Buildings*, American Institute of Steel Construction, Chicago, IL.

Cabrero, J.M. and Bayo, E. (2007a), "The Semi-Rigid Behaviour of Three-Dimensional Steel Beam-to-Column Joints Subjected to Proportional Loading. Part I: Experimental Evaluation," *Journal of Constructional Steel Research*, Vol. 63, No. 9, pp. 1241–1253.

Cabrero, J.M. and Bayo, E. (2007b), "The Semi-Rigid Behaviour of Three-Dimensional Steel Beam-to-Column Joints Subjected to Proportional Loading. Part II: Theoretical Model and Validation," *Journal of Constructional Steel Research*, Vol. 63, No. 9, pp. 1254–1267.

CEN (2005), *Eurocode 3: Design of Steel Structures—EN 1993*, Comité Européen de Normalisation, Brussels, Belgium.

Heron (2006), "Ponding of Roof Structures," *HERON*, Publication of the Delft University of Technology, L.J. Sluys, Editor-in-Chief, Vol. 51, No. 2/3, 200 pp.

Leckie, J. (2007a), "Steel and Other Materials—Part One: Steel and Glass," *Advantage Steel*, No. 29, pp. 8–12, CISC, Willowdale, Ontario, Canada.

Leckie, J. (2007b), "Steel and Other Materials—Part Two: Steel and Wood," *Advantage Steel*, No. 30, pp. 8–12, CISC, Willowdale, Ontario, Canada.

Le Quéré, C. (2007), "Projet Orthoplus: Ingénierie et de Leur Revêtement," *Travaux*, No. 843, July–August, pp. 26–29.

Marino, F.J. (1966), "Ponding of Two-Way Roof Systems," *Engineering Journal*, AISC, Vol. 3, 3rd Quarter, pp. 93–100.

Walbridge, S. and Nussbaumer, A. (2008), "Probabilistic Fatigue Analysis of Shop and Field Treated Tubular Truss Bridges," *Journal of Constructional Steel Research*, Vol. 64, No. 2, pp. 156–166.

ACKNOWLEDGMENTS

Special thanks are due the following members of the International Structural Steel Research Advisors (ISSRA) who provided input to this paper:

Eduardo Bayo, University of Navarra, Pamplona, Spain

Frans Bijlaard, Delft University of Technology, Delft, the Netherlands

André Colson, FNTP, Paris, France

Michael Gilmor, CISC, Toronto, Ontario, Canada

Manfred Hirt, EPFL, Lausanne, Switzerland

Jouko Kouhi, Finnish Constructional Steelwork Association, Helsinki, Finland

Additional assistance has been provided by Sylvie Boulanger, CISC, Montreal, Canada; S.F. Stiemer, University of British Columbia, Vancouver, BC, Canada; and Alain Nussbaumer, EPFL, Lausanne, Switzerland.

Suggested Reading from Other Publishers

The following abstracts summarize papers published by others on the subject of steel design and construction that may be of interest to *Engineering Journal* readers.

From the December 2007 (Volume 133, No. 12) issue of *Journal of Structural Engineering,* published by the American Society of Civil Engineers:

Fatigue Strength of End-Coped Crane Runway Girders
Xiaoli Tong, Christopher Y. Tuan, Jianping Yang, Jiaqi Zhang and Qingrui Yue

Fatigue cracks were found on a series of end-coped crane runway girders after 14 years of service in a steel mill building in China. Two typical crane runway girders with different spans were studied in this paper. Finite element analyses were conducted to investigate the stress concentration at the coped ends. Analytical results showed the stress concentration effect was highly localized and the stress concentration factor decreased with increasing cope radius and decreasing total depth. The analytical results agreed well with the field measured data. Fatigue tests were conducted to determine the fatigue strength using eight ⅕-scaled end-coped girder specimens. Based on the analytical results and limited test data, the fatigue strength for a maximum principal stress range of 103 MPa at 2 million cycles may serve as a possible design guideline for end-coped crane runway girders using the conventional *S-N* curves. Procedures for design and evaluation of the fatigue life of end-coped crane runway girders are suggested.

Large-Scale Testing of a Replaceable "Fuse" Steel Coupling Beam
Patrick J. Fortney, Bahram M. Shahrooz and Gian A. Rassati

When coupled core wall (CCW) systems are built in regions of high seismicity, the ductility demands on the coupling beams can be of critical concern. Steel coupling beams, whether encased in concrete or not, offer a very high degree of ductility relative to common concrete coupling beams. Hybrid core wall systems, in other words, CCW systems with steel or steel/concrete composite coupling beams, provide excellent lateral stiffness from the walls and coupling action, while providing excellent energy dissipation and ductility characteristics of steel coupling beams. Previous research pertaining to steel coupling beams has made great strides in furthering the understanding of the behavior of steel coupling beams, and recommendations regarding design methodologies have been established. However, as steel coupling beam ends are embedded in the wall piers, postdamage repair can be costly. This paper presents the results of large-scale cyclic tests of a steel coupling beam designed and detailed based on the writers' previous recommendations and an innovative "fuse" steel coupling beam, which provides an added feature to the steel coupling beam in that postdamage repair/replacement difficulties and expenses are minimized.

From the January 2008 (Volume 134, No. 1) issue of *Journal of Structural Engineering,* published by the American Society of Civil Engineers:

Seismic Response of Multistory Buildings with Self-Centering Energy Dissipative Steel Braces
Robert Tremblay, M. Lacerte and C. Christopoulos

This paper examines the seismic response of 2-, 4-, 8-, 12-, and 16-story steel framed buildings with self-centering energy dissipative (SCED) bracing members. The structures are assumed to be located in Los Angeles, California. Identical buildings equipped with buckling restrained braces (BRB) are also studied for comparison purposes. Incremental static analysis and nonlinear dynamic analysis under ground motion ensembles corresponding to three hazard levels were performed. The SCED frames generally experienced smaller peak story drifts, less damage concentration over the building height, and smaller residual lateral deformations compared to the BRB system. Higher floor acceleration peaks were observed in the SCED frames due to the sharper transitions between elastic and inelastic response assumed in the analysis. The study also indicated that higher design seismic loads may be needed for low-rise SCED and BRB frames in order to improve their collapse prevention performance.

Seismic Analysis of Concentrically Braced Frame Systems with Self-Centering Friction Damping Braces
Songye Zhu and Yunfeng Zhang

This paper presents a special type of bracing element, termed self-centering friction damping brace (SFDB), for use in seismic-resistant concentrically braced frame (CBF) systems. The SFDB is a passive energy dissipation device with its core recentering component made of stranded superelastic Nitinol wires, while enhanced energy dissipation mechanism of the SFDB is achieved through friction. Compared with conventional braces for steel frame buildings, SFDB has a few desirable performance characteristics, such as minimized residual drifts of the CBF system and its ability to withstand several design level earthquakes without the need for replacement. The mechanical configuration of the SFDB is first described. A comparative study of SFDB frame and buckling restrained braced (BRB) frame was carried out, which is based on nonlinear dynamic analysis of two prototype CBF buildings—a three- and a six-story steel frame. Two suites of earthquake ground motions, which represent the frequent and design basis earthquakes for Los Angeles, were considered in the nonlinear time-history analysis. The results of the nonlinear time-history and pushover analysis show that the SFDB frame can achieve a seismic response level comparable to that of the BRB frame while having significantly reduced residual drifts. The SFDB thus has a potential to establish a new type of CBF system with self-centering capability.

From the February 2008 (Volume 134, No. 2) issue of *Journal of Structural Engineering,* published by the American Society of Civil Engineers:

Strength and Reliability of Steel Frames with Random Properties
Stephen G. Buonopane

This paper studies the effects of random properties on the strength and reliability of two steel frames. Monte Carlo simulation is used to analyze the behavior of a low-rise industrial frame and a grain storage bin. Both structures exhibit significant second-order effects with their strength limited by loss of frame stability. Both frames have been previously studied for the development of the direct analysis provisions of the 2005 AISC *Specification for Structural Steel Buildings*. The analyses consider randomness in yield strength, elastic modulus, residual stresses, and out-of-plumb (*P*–Delta) and out-of-straightness (*P*–delta) imperfections. The effects of spatial correlation of these properties are also studied. The simulation results are used to estimate probability distributions of frame strength and reliability, or probability of failure. The results provide probabilistic relationships between material and geometric properties of steel frames and the overall strength of the frames. Randomness in elastic modulus and residual stresses are shown to have a significant impact on strength and reliability of the frames by increasing lateral deflections and thereby second-order forces. The results confirm the importance of including geometric imperfections for proper assessment of frame stability.

From the March 2008 (Volume 25, No. 3) issue of *Journal of Protective Coatings and Linings,* published by SSPC:

High-Heat Coatings: An Overview of Coating Performance and Product Characteristics
Orville Brown

This article reviews high-heat coating technology, including the chemistry of high-heat binder systems, the wide range in continuous service temperature of high-heat coatings available, and the unique coating properties in the different technologies presently used in high-heat coatings.

Contracting Issues: Are Owners Getting What They Ask For?
Brandon & Damiano

This article is the third in a series about quality management systems and tools for contract administration. Here, the authors discuss the appropriate relationship between quality assurance and quality control.

From the February 5, 2008 (Volume 86, No. 3) issue of *The Structural Engineer,* published by The Institution of Structural Engineers (United Kingdom):

An Analytical Method for the Design of Steel Frames with Semi-Continuous Connections
John Graham

An analytical method for the design of steel frames is presented that allows for semi-continuous, extended end plate joints, calculable rotational stiffnesses to be included in the procedure. A steel frame and its elasto-plastic connections may be accurately modeled to achieve almost full joint rigidity, acceptable sway movements, and a global elastic stress solution at service load levels. Increased loading up to factored load values produces more flexible and ductile joint behavior, which is taken into consideration during the analysis, as is the formation of plastic hinges within the frame members and ultimately, where achievable, instability and the development of a collapse mechanism.

GUIDE FOR AUTHORS

SCOPE: The ENGINEERING JOURNAL is dedicated to the improvement and advancement of steel construction. Its pages are open to all who wish to report on new developments or techniques in steel design, research, the design and/or construction of new projects, steel fabrication methods, or new products of significance to the uses of steel in construction. Only original papers should be submitted.

GENERAL: Papers intended for publication must be submitted by mail to the Editor, Cynthia J. Duncan, ENGINEERING JOURNAL, AMERICAN INSTITUTE OF STEEL CONSTRUCTION, One East Wacker Drive, Suite 700, Chicago, IL, 60601-1802.

The articles published in the *Engineering Journal* undergo peer review before publication for (1) originality of contribution; (2) technical value to the steel construction community; (3) proper credit to others working in the same area; (4) prior publication of the material; and (5) justification of the conclusion based on the report.

All papers within the scope outlined above will be reviewed by engineers selected from among AISC, industry, design firms, and universities. The standard review process includes outside review by an average of three reviewers, who are experts in their respective technical area, and volunteers in the program. The maximum number of papers sent to a single reviewer is three per year, with a frequency of not more than one per quarter. Papers not accepted will be returned to the author. Published papers become the property of the American Institute of Steel Construction, Inc. and are protected by appropriate copyrights. No proofs will be sent to authors. Each author receives three copies of the issue in which his contribution appears.

MANUSCRIPT PREPARATION: Manuscripts must be provided on PC-formatted media, such as a CD-ROM, in Microsoft Word format. A laser-quality proof must accompany your submittal. Fonts and spacing must be suitable for easy reading and reproduction (for the peer-review process). Do not embed photographs, diagrams, illustrations, charts or graphs within the electronic manuscript files. Only equations may be embedded within the flow of the text. Specific requirements for electronic graphics are outlined below. *Engineering Journal* reserves the right not to publish a submittal if suitable graphics cannot be provided by the author.

Title and By-Line: Exact name, title and affiliation of the author or authors are required to appear on the first page of the manuscript.

Body Text: Please restrict font usage to Times, Helvetica, Times New Roman, Arial, and Symbol (for Greek and mathematical characters.)

Headings: All headings should be typed flush left, using upper and lower case, with two line spaces above.

Tables: Each table should appear on its own page. Footnotes to tables should appear below the table, identified by superscripted lower case letters (a, b, c, etc.).

Equations: Whenever possible, equations should be set using Microsoft Equation Editor or MathType (www.mathtype.com). Please set equations using Times New Roman, Times, and/or Symbol fonts.

Captions: Captions should be typed, double-spaced, and located at the end of the electronic manuscript. All photos and graphics must be clearly marked to indicate their corresponding caption.

References: Should be noted clearly in the text and listed, double-spaced, on a separate page in the following sample format.

In text: (Doe, 1992)

In Reference List:

Doe, J.H. (1992), "Structural Steel," *Engineering Journal*, AISC, Vol. 100, No. 1, 1st Quarter, pp. 2–10.

Footnotes: Footnotes should be noted clearly in the text with a superscript asterisk, and should appear at the bottom of the text page, in the following style:

*For a detailed discussion, see...

Graphics (other than photographs): Provide a clear $8\frac{1}{2}$ in. × 11 in. laser-quality proof of each graphic element. Graphics should reproduce cleanly in black-and-white format. Graphics may be submitted and reproduced in color at the Editor's discretion. Please restrict font usage to Helvetica, Arial or Symbol, in sizes suitable for at least 50% reduction (12 pt. minimum). Line weights must be suitable for 50% reduction. When possible, provide each graphic element in a separate electronic file. TIF or EPS file formats are preferred, with a minimum resolution of 300 dots per inch.

Photographs: Provide either original photographs or high-quality electronic files and laser-quality proofs. Electronic photographs may be submitted as grayscale TIF or JPG images, one photograph per file. Photographs may be submitted and reproduced in color at the Editor's discretion. Minimum image resolution is 300 dots per inch. Photographs should be a minimum of 4 in. wide, so the minimum image width is 1200 pixels. Detailed photographs may require resolutions up to 1200 dots per inch. Photos embedded in word-processing documents are not acceptable.

There's always a solution in steel.

ENGINEERING JOURNAL
American Institute of Steel Construction
One East Wacker Drive, Suite 700
Chicago, IL 60601